uOttawa

L'Université canadienne
Canada's university

FACULTÉ DES ÉTUDES SUPÉRIEURES ET POSTOCTORALES

uOttawa

L'Université canadienne
Canada's university

FACULTY OF GRADUATE AND POSDOCTORAL STUDIES

Sheryn Kirkpatrick
AUTEUR DE LA THÈSE / AUTHOR OF THESIS

M.Sc. (Cellular and Molecular Medicine)
GRADE / DEGREE

Department of Cellular and Molecular Medicine
FACULTÉ, ÉCOLE, DÉPARTEMENT / FACULTY, SCHOOL, DEPARTMENT

Characterization of the Binding Properties of ^{11}C-Laveled Candesartan Derivatives as Potential Angiotensin II AT_1 Receptor Radioligands for Pet Imaging

TITRE DE LA THÈSE / TITLE OF THESIS

Jean Da Silva
DIRECTEUR (DIRECTRICE) DE LA THÈSE / THESIS SUPERVISOR

Rob Beanlands
CO-DIRECTEUR (CO-DIRECTRICE) DE LA THÈSE / THESIS CO-SUPERVISOR

EXAMINATEURS (EXAMINATRICES) DE LA THÈSE / THESIS EXAMINERS

Glenn Wells

Rhian Tonyz

Gary W. Slater
Le Doyen de la Faculté des études supérieures et postdoctorales / Dean of the Faculty of Graduate and Postdoctoral Studies

CHARACTERIZATION OF THE BINDING PROPERTIES OF ^{11}C-LABELED CANDESARTAN DERIVATIVES AS POTENTIAL ANGIOTENSIN II AT_1 RECEPTOR RADIOLIGANDS FOR PET IMAGING

BY

SHERYN KIRKPATRICK

This thesis is submitted as a partial fulfillment of the Master of Science program in Cellular and Molecular Medicine

Your file Votre référence
ISBN: 978-0-494-61215-6
Our file Notre référence
ISBN: 978-0-494-61215-6

CHARACTERIZATION OF THE BINDING PROPERTIES OF ^{11}C-LABELED CANDESARTAN DERIVATIVES AS POTENTIAL ANGIOTENSIN II AT_1 RECEPTOR RADIOLIGANDS FOR PET IMAGING

MSc Thesis 2006, Sheryn Kirkpatrick,
Department of Cellular and Molecular Medicine, University of Ottawa
Ottawa, Ontario, Canada

ABSTRACT

The renin-angiotensin system (RAS) has been implicated in the pathophysiology of heart failure, hypertension and diabetic nephropathy. Positron emission tomography (PET), a non-invasive imaging modality, can provide information on cellular function and receptor density. Based on previous structure-activity studies, two ^{11}C-labeled analogues of the clinically used AT_1 receptor antagonist candesartan were developed, [^{11}C]methyl-candesartan and [^{11}C]TH4, and characterized for binding specificity and selectivity. [^{11}C]Methyl-candesartan was further tested to determine the presence of labeled metabolites and potential for small animal PET. [^{11}C]Methyl-candesartan displayed higher specific binding and selectivity to angiotensin II type 1 (AT_1) over angiotensin II type 2 (AT_2), Mas (Ang(1-7)), β-adrenergic and α_2-adrenergic receptors in kidney regions in *ex vivo* studies. Selectivity for AT_1 over Mas receptors was not observed for [^{11}C]TH4. Renal binding selectivity over AT_2 was confirmed in [^{11}C]methyl-candesartan microPET imaging studies. Metabolite analysis of [^{11}C]methyl-candesartan detected a labeled metabolite in the rat kidney, although the identity has not been determined. The work presented here supports the potential of [^{11}C]methyl-candesartan for *in vivo* imaging of AT_1 receptors.

TABLE OF CONTENTS

LIST OF TABLES

LIST OF FIGURES

List of Abbreviations

%ID/g	Percent of injected dose per gram of tissue
$[^{11}C]CH_3I$	$[^{11}C]$methyl iodide
$[^{11}C]CH_3O^-$	$[^{11}C]$methanide ion
$[^{11}C]CH_4$	$[^{11}C]$methane
$[^{11}C]CO_2$	$[^{11}C]$carbon dioxide
ACE	Angiotensin converting enzyme
Ang I	Angiotensin I
Ang II	Angiotensin II
ANOVA	Analysis of variance
ARB	Angiotensin II type 1 receptor blocker
Arg	Arginine
Asn	Asparagine
Asp	Aspartate
AT_1	Angiotensin II type 1 receptor
AT_{1A}	Angiotensin II type 1 receptor subtype A
AT_{1B}	Angiotensin II type 1 receptor subtype B
AT_2	Angiotensin II type 2 receptor
AUC	Area under the curve
BBB	Blood-brain barrier
cAMP	Cyclic adenosine monophosphate
CPM	Counts per minute
DAG	Diacylglycerol
DN	Diabetic nephropathy
DNA	Deoxyribonucleic acid
DV	Distribution volume
ED	Effective dose
EDE	Effective dose equivalent
EGF	Endothelial growth factor
ERK	Extracellular signal-related kinase
GPCR	G protein-coupled receptor
GRK	G protein-coupled receptor kinase
GTP	Guanosine triphosphate
HF	Heart failure
His	Histidine
HPLC	High performance liquid chromatography

IC_{50}	Half maximal inhibitory concentration
ID_{50}	Half maximal inhibitory dose
IP_3	Inositol 1,4,5-triphosphate
ip	Intraperitoneal; intraperitoneally
iv	Intravenous; intravenously
JAK2	Janus kinase 2
LA	Left atrium
LDL	Low-density lipoproteins
LLI	Lower large intestine
LV	Left ventricle
Lys	Lysine
MAPK	Mitogen-activated protein kinase
MI	Myocardial infarction
mRNA	Messenger ribonucleic acid
NE	Norepinephrine
PET	Positron emission tomography
Phe	Phenylalanine
PKC	Protein kinase C
PLC	Phospholipase C
PLD	Phospholipase D
RA	Right atrium
RAS	Renin-angiotensin system
ROI	Region of interest
RT-PCR	Real-time polymerase chain reaction
RV	Right ventricle
SHP-2	Src homology phosphatase-2
SI	Small intestine
SNA	Sympathetic nerve activity
SNS	Sympathetic nervous system
STAT	Signal transducer and activator of transcription
TH4	2-oxo-3-[[2'-(1H-tetrazol-5-yl)-biphenyl-4-yl] methyl]-2,3-dihydro-1H-benzoimidazole-4-carboxylic acid
Trp	Tryptophan
Tyr	Tyrosine
ULI	Upper large intestine
YIPP	Tyrosine-Isoleucine-Proline-Proline motif

ACKNOWLEDGMENTS

There are many people that I need to thank for their assistance, guidance, support and love, all of which were instrumental in the creation of this thesis...

I would first like to thank the Radiochemistry staff, without whom none of these studies would have been possible: Dr. Tayebeh Hadizad, Sam Mason, Jeff Collins, and Paul Coletta. I am grateful also to Rawad Antoun, Adam Thomas, Marika Kolajova, the Animal Care staff, Myra Kordos and Julia Lockwood for technical assistance with studies and scanning.

I am eternally grateful as well to Stephanie Thorn, Miran Kenk, and James Thackeray, for the guidance, mentorship, and training, they so good-naturedly provided. I also need to thank my supervisors, Dr. Jean DaSilva and Dr. Rob Beanlands for the invaluable direction, guidance, and leadership they bestowed with the utmost care and patience. I thank them as well for their constructive comments in the creation and amelioration of this thesis.

Thank you to my family for loving me always and inspiring me to challenge and expand myself, at times even more than I had imagined. To my parents, you instilled in me a thirst for knowledge and a need to have an impact – thank you for both, they have served me well. To my sister, a constant surprise, delight and amazement, I hope I made you proud.

To my husband Joshua, I cannot possibly describe how much your unwavering support has aided me in the pursuit of my goals. Thank you seems so inappropriate compared to the gift of the foundation you created for me. I love you to the ends of the earth and back and dedicate this thesis to you.

1. INTRODUCTION

1.1. Renin Angiotensin System

1.1.1. General

The renin-angiotensin system (RAS) exerts control over several physiological parameters including regulation of blood pressure, electrolyte and water balance, thirst, hormone secretion, and renal function (de Gasparo et al., 2000). Angiotensin II (Ang II) is the primary signal peptide of the RAS (Figure 1.1). The formation of Ang II begins with the prohormone angiotensinogen (Figure 1.2). Angiotensinogen is expressed predominantly in the liver but also by other tissues (Danser et al., 1994). Angiotensinogen is secreted into the systemic circulation, where it is cleaved by renin between the two leucine residues in positions 10 and 11 (de Gasparo et al., 2000). Renin, a carboxypeptidase, is secreted by the kidneys in the classical RAS, but is also expressed in other tissues (Danser et al., 1994; Dzau et al., 1988; Dzau et al., 1986; Mento et al., 1998). The cleavage of angiotensinogen by renin produces angiotensin I (Ang I), a 10 amino acid peptide. Hydrolysis of Ang I by angiotensin-converting enzyme (ACE) produces Ang II, which can then bind to its cell surface receptors. To transduce the signal and initiate the intracellular effects, Ang II binds to two types of 7 transmembrane domain G protein-coupled receptors (GPCRs), type 1 (AT_1) and type 2 (AT_2). Stimulation of the AT_1 receptor promotes the classical effects of the RAS, namely: vasoconstriction, cell growth and proliferation, while AT_2 activation generally opposes these classical responses, namely: inhibition of growth and promotion of apoptosis and differentiation (Allen et al., 2000; Ardaillou, 1999).

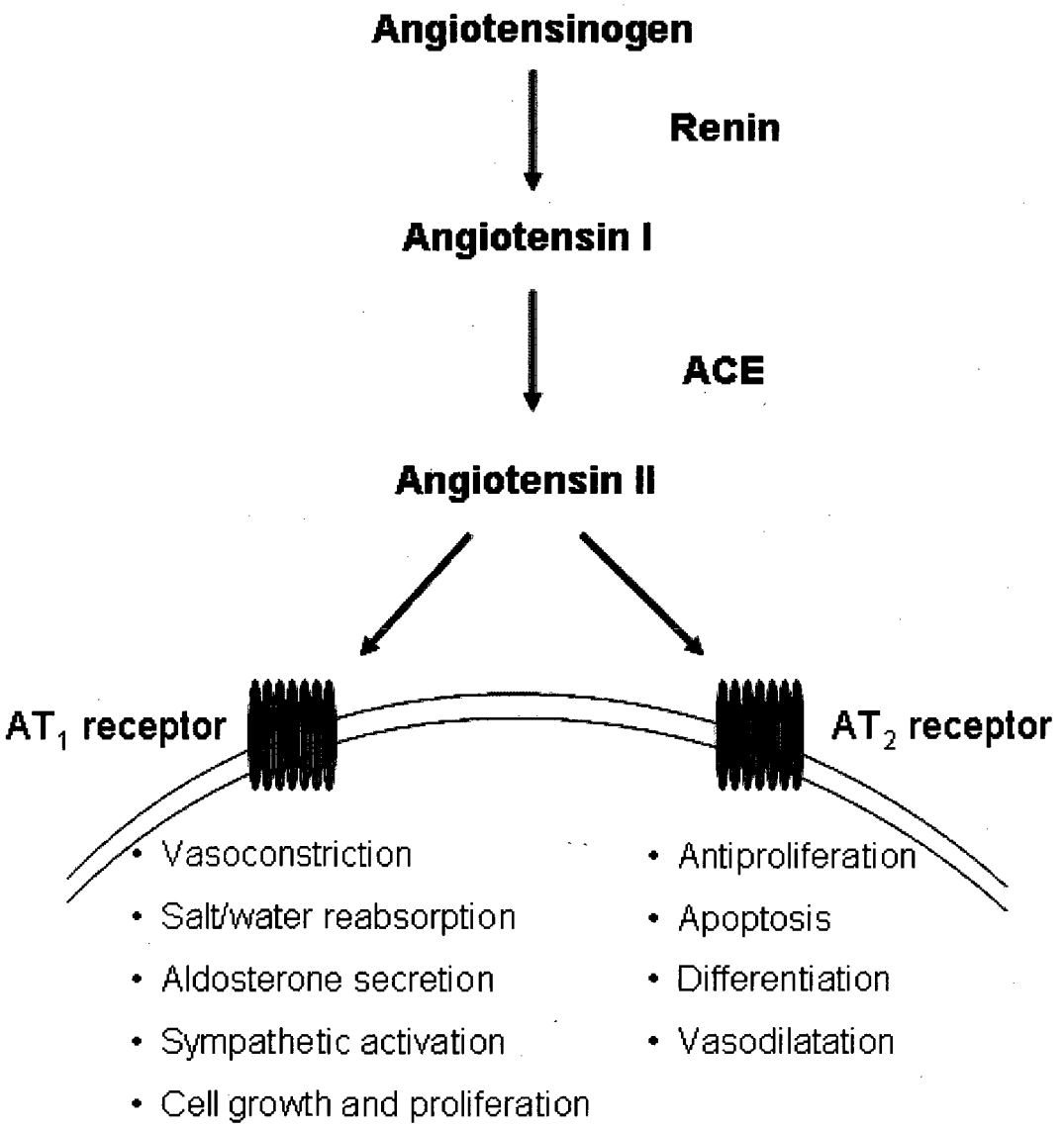

Figure 1.1. Overview of the enzymatic cascade and biological effects of the RAS. Adapted from Dinh et al., 2001.

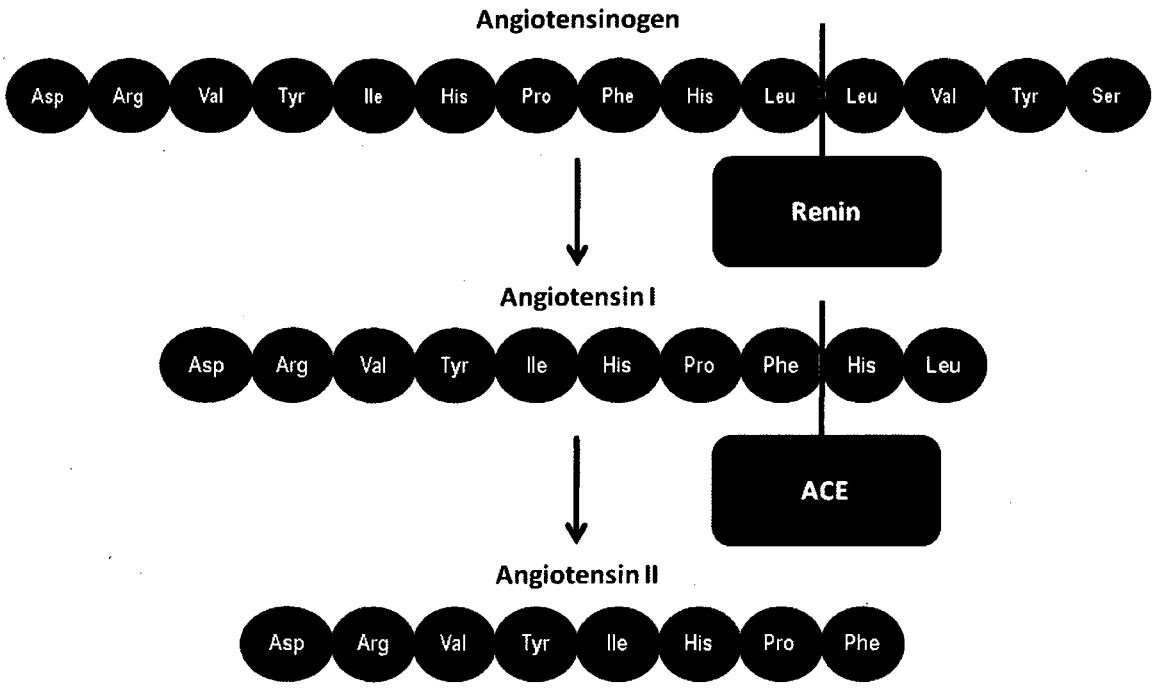

Figure 1.2. Amino acid sequences and location of hydrolysis (black bars) of angiotensinogen, Ang I and Ang II. Adapted from de Gasparo et al., 2000.

1.1.2. Ang II Type 1 Receptors

AT_1 receptors are expressed in several tissues (Table 1.1): lungs (Burson et al., 1994), brain (Burson et al., 1994; Chang et al., 1991), heart (Burson et al., 1994; Chang et al., 1991), adrenals (Burson et al., 1994; Chang et al., 1991), vasculature (Chang et al., 1991), and kidney (Burson et al., 1994; Chang et al., 1991). The AT_1 receptor (Figure 1.3) is expressed as a 359 amino acid protein in both humans and rodents (de Gasparo et al., 2000). In rodents, two subtypes of AT_1 receptors are expressed, AT_{1A} and AT_{1B}, and they share 95% sequence identity at the amino acid level (Chiu et al., 1993). The rat AT_{1A} gene is located on chromosome 17q12 whereas AT_{1B} is localized on chromosome 2q24 (de Gasparo et al., 2000). The two subtypes, AT_{1A} and AT_{1B}, are considered identical both pharmacologically and functionally (Chiu et al., 1993; Gasc et al., 1994). Unlike rodents, humans express only a single form of AT_1 receptor gene located on chromosome 3 q (de Gasparo et al., 2000). The human AT_1 receptor shares 94 and 97% sequence identity at the amino acid level with the rodent AT_{1A} and AT_{1B} receptor subtypes respectively (Chiu et al., 1993). AT_{1A} mRNA expression in rodents has been demonstrated in kidney, adrenals, liver, ovary, brain, testes, adipose tissue, lung, and heart (Burson et al., 1994). AT_{1B} mRNA expression was detected in kidney, brain and testes at very low levels, while adrenal gland AT_{1B} gene expression is readily detectable (Burson et al., 1994).

1.1.3. Structural Interactions

Structural interaction of key residues in the receptor and agonist has been reported in the literature. The three aromatic residues of Ang II, Tyr^4, His^6, and Phe^8, associate

Table 1.1. Relative tissue expression of the AT_1 receptor in rabbit, monkey and rat. Adapted from Chang and Lotti (1991).

Species	Tissue	Relative Expression (to Heart)
Monkey	Adrenal Cortex	316
	Aorta	12
	Brain	5
	Heart	1
	Kidney cortex	37
Rabbit	Adrenal Cortex	1454
	Aorta	4
	Brain	4
	Heart	1
	Kidney cortex	47
Rat	Adrenal Cortex	1460
	Aorta	8
	Brain	20
	Heart	1
	Kidney cortex	391

Ratios were obtained by ^{125}I-Ang II binding assays of membrane preparations.

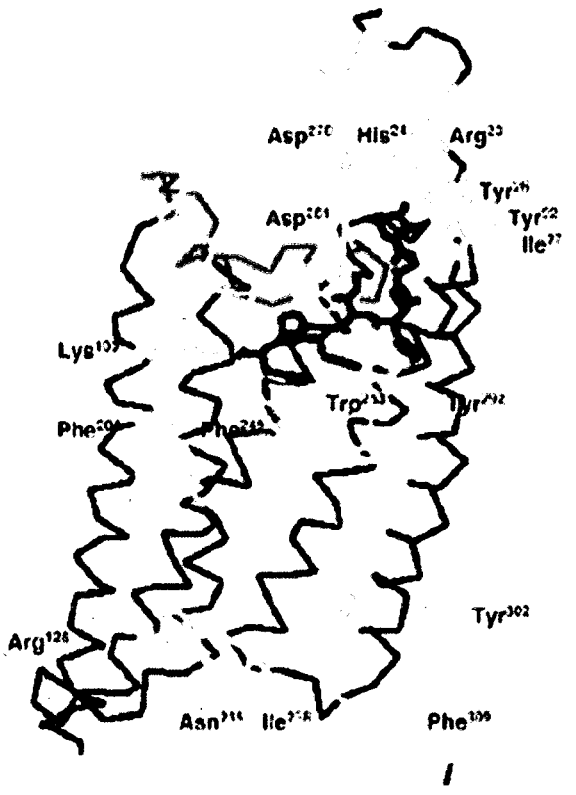

Figure 1.3. A computer generated model of the activated state conformation of Ang II (purple) bound to the AT_1 receptor. Used with permission from Oliveira et al., 2007.

together and are important for the biological activity and conformation (Matsoukas et al., 1994; Nikiforovich et al., 1994; Nikiforovich et al., 1993). The N- and C-terminal ends of Ang II also interact to help form the biologically active conformation of the peptide, as a twisted hairpin (Pierson et al., 1992). Ang II associates with both the extracellular region (Hjorth et al., 1994) and the transmembrane helices of the receptor (Noda et al., 1995; Yamano et al., 1995). Specific residues have been identified as being involved in this interaction. Lys^{199} in transmembrane domain 5 and Trp^{253} in transmembrane domain 6 play a role in the interaction with Phe^{8} of the Ang II peptide (Noda et al., 1995; Yamano et al., 1995). Two other residues in transmembrane domain 6, Phe^{259} and Asp^{263}, interact with His^{6} of Ang II (Yamano et al., 1995). Asp^{281} and His^{123} in the extracellular loops interact with Arg^{2} (Feng et al., 1995) and Asp^{1} (Yamano et al., 1995) of the ligand respectively. The Tyr^{4} and Phe^{8} residues are also important in receptor activation through association with Asn^{111} of the third transmembrane domain (Noda et al., 1996) and His^{256} of the sixth transmembrane domain (Noda et al., 1995). These associations with Asn^{111} and His^{256} reportedly aid in the conformational changes associated with receptor activation (Noda et al., 1996; Noda et al., 1995)

1.1.4. AT_1 Receptor Signalling

1.1.4.1. G Protein-Coupled Receptor Signalling

Agonist binding to the AT_1 receptor results in activation of several signalling cascades (Figure 1.4), through coupling to $G\alpha_{q/11}$, $G\alpha_{12}$, $G\alpha_{13}$, and $G\alpha_i$ proteins (Ushio-Fukai et al., 1998). Coupling to $G\alpha_{q/11}$ or $G\alpha_{12}$ activates phospholipase C (PLC), which can associate with the YIPP motif of the cytoplasmic region of the AT_1 receptor (Venema et al., 1998). PLC produces diacylglycerol (DAG) and inositol 1,4,5-triphosphate (IP_3)

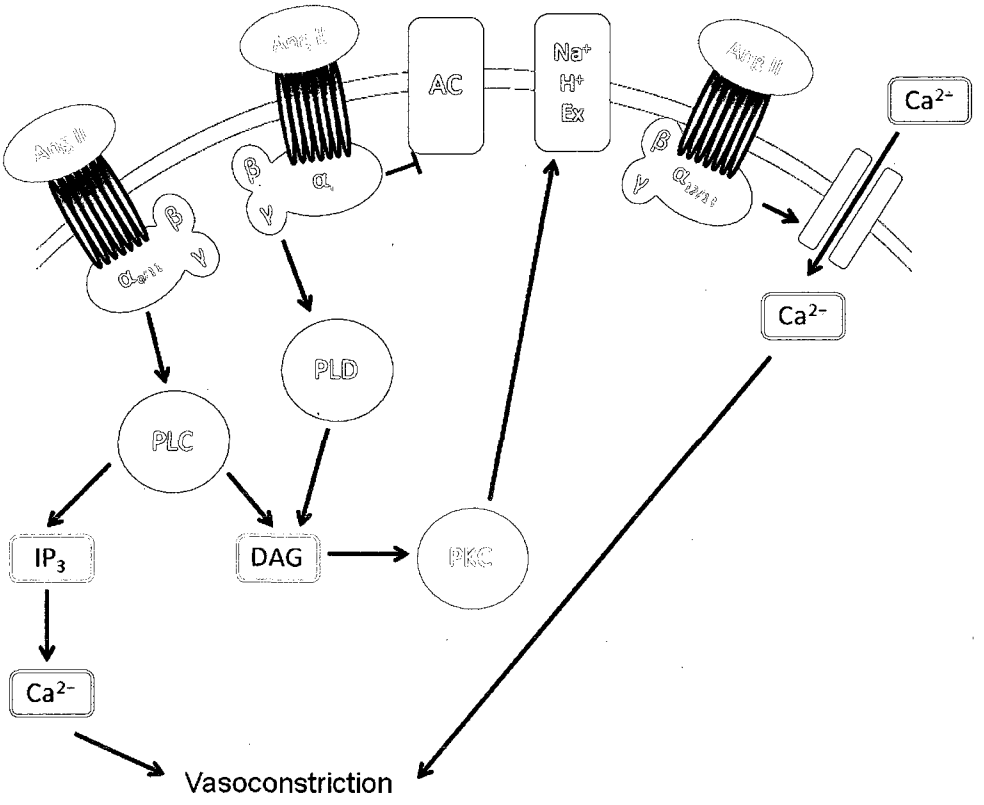

Figure 1.4. Signalling of Ang II through the AT_1 receptor coupled to G proteins. The following abbreviations are used: angiotensin II (Ang II); adenylate cyclase (AC); sodium hydrogen exchanger (Na^+/H^+ EX); phospholipase C (PLC); phospholipase D (PLD); inositol 1,4,5-triphosphate (IP_3); diacylglycerol (DAG); and protein kinase C (PKC)..

by hydrolysis of membrane phospholipids (Ushio-Fukai et al., 1998). DAG activates protein kinase C (PKC), which regulates the Na^+/H^+ exchanger and thus intracellular pH (Vallega et al., 1988). In smooth muscle cells IP_3 mobilizes calcium stores from the sarcoplasmic reticulum to increase intracellular calcium concentration (Berridge, 1987). Intracellular calcium promotes smooth muscle contraction and thus vasoconstriction (Ushio-Fukai et al., 1998). Elevated calcium levels in the adrenals promote aldosterone biosynthesis and secretion (Griendling et al., 1997). Signalling by coupling to $G\alpha_{12/13}$ also increases intracellular calcium concentration by opening plasma membrane calcium channels (Macrez et al., 1997; Suzuki et al., 2005).

Agonist binding to AT_1 coupled to $G\alpha_i$ inhibits adenylate cyclase to reduce cyclic adenosine monophosphate (cAMP) production (Ushio-Fukai et al., 1998). The remaining subunits of the G protein ($\beta\gamma$) act to stimulate PLC and PLD (Ushio-Fukai et al., 1999; Ushio-Fukai et al., 1998). Activation of PLC through this pathway results in similar downstream effects to those in $G\alpha_{q/11}$ signalling (Ushio-Fukai et al., 1999; Ushio-Fukai et al., 1998). PLD produces choline and phosphatidic acid from membrane phosphotidylcholine (Ushio-Fukai et al., 1999). Phosphatidic acid is further hydrolysed to DAG, which stimulates downstream effects as described above.

1.1.4.2. Tyrosine Kinase Signalling

Tyrosine kinase phosphorylation stimulated by Ang II results from effector protein association with the receptor (Figure 1.5). A YIPP motif in the cytoplasmic region is a location of interaction with PLC and the adaptor protein Src homology phosphatase-2 (SHP-2; Venema et al., 1998). SHP-2 allows association and activation of Janus kinase 2 (JAK 2; Ali et al., 1997; Bhat et al., 1994), which subsequently

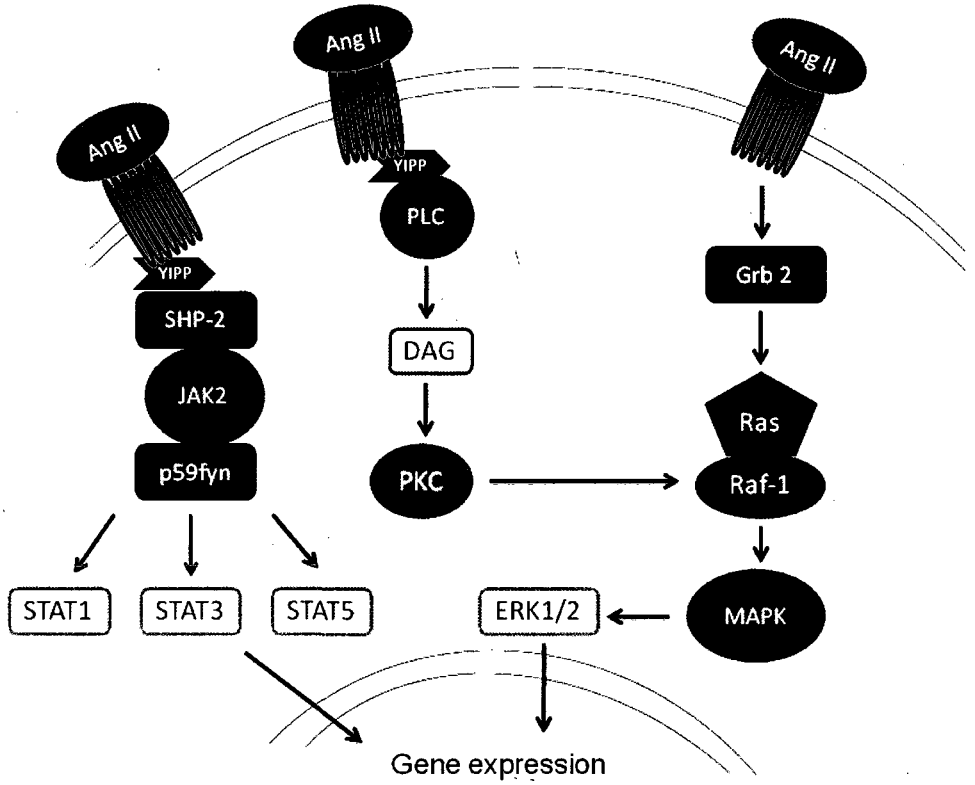

Figure 1.5. Signalling of Ang II by the AT_1 receptor through tyrosine kinase pathways. The following abbreviations are used: angiotensin II (Ang II); Src homology phosphatase-2 (SHP-2); Janus kinase 2 (JAK2); signal transducer and activator of transcription (STAT); phospholipase C (PLC); diacylglycerol (DAG); protein kinase C (PKC); mitogen-activated protein kinase (MAPK); and extracellular signal-related kinase (ERK).

activates signal transducers and activators of transcription (STATs) 1, 3, and 5 (Bhat et al., 1994; Bhat et al., 1995; Darnell et al., 1994; McWhinney et al., 1998; Schindler et al., 1995) through p59fyn (Venema et al., 1998). STATs then translocate to the nucleus to promote expression of early growth response genes such as c-fos, c-jun and c-myc (Clark et al., 1992).

Activation of the mitogen-activated protein kinase (MAPK) pathways is propagated through cascades of adaptor and kinase proteins. Ang II activation of Grb2 and Shc adaptor proteins results in enhancement of Ras, Rac, Rho and Pyk2 activities (Sadoshima et al., 1995). Ras, Rac and Rho, small guanosine triphosphate (GTP) binding proteins, recruit other factors, Sos, Raf-1, or Mor, which activate MAPK kinases and ultimately extracellular signal-related kinases (ERKs) 1 and 2 (de Gasparo et al., 2000). ERKs translocate to the nucleus to activate transcription factors and promote gene expression (de Gasparo et al., 2000). Pyk2 has been implicated in transactivation of other receptor signal cascades (Murasawa et al., 1993). Similar end effects are observed through activation of other tyrosine kinase pathways. Focal adhesion kinases associate with Src and Grb2 and small G proteins such as Ras to activate ERKs (Schlaepfer et al., 1998). This cascade results in ERK activation of DNA and protein synthesis (de Gasparo et al., 2000).

The AT_1 receptor has been reported to transactivate other receptors and their subsequent cascades. Endothelial growth factor (EGF) receptors (Figure 1.6) have been demonstrated to be activated in this fashion (Eguchi et al., 1996; Eguchi et al., 1998). Transactivation of the EGF receptor is propagated by the calcium-dependent kinase Pyk2

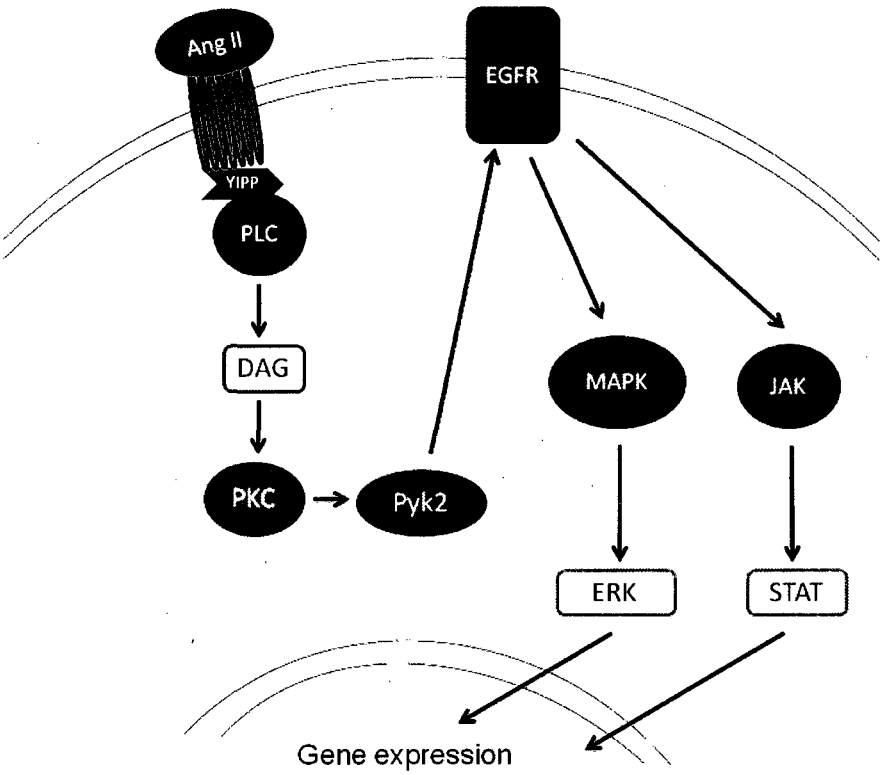

Figure 1.6. Signalling of Ang II by the AT_1 receptor through transactivation of EGF receptors. The following abbreviations are used: angiotensin II (Ang II); phospholipase C (PLC); diacylglycerol (DAG); protein kinase C (PKC); endothelial growth factor receptor (EGFR); mitogen-activated protein kinase (MAPK); extracellular signal-related kinase (ERK); Janus kinase (JAK); and signal transducer and activator of transcription (STAT).

(Murasawa et al., 1993). Downstream effectors of EGF receptors include the Ras/MAPK and the JAK/STAT pathways, which stimulate gene expression and protein synthesis (Eguchi et al., 1996; Eguchi et al., 1998; Frank et al., 2002; Sayeski et al., 1998).

1.1.5. AT_1 Receptor Regulation

1.1.5.1. AT_1 Desensitization and Internalization

AT_1 receptor expression and signalling is regulated by similar mechanisms to other GPCRs. Ang II binding (Figure 1.7) promotes phosphorylation of the AT_1 receptor (Balmforth et al., 1997; Oppermann et al., 1996; van Kats et al., 1997) through PKC and GPCR kinases (GRKs) 2 and 5, resulting in desensitization (Oppermann et al., 1996). Serine and threonine residues in a region from Thr^{332} to Ser^{338} in the intracellular portion of the receptor have been reported to be the sites of this phosphorylation (de Gasparo et al., 2000; Hunyady et al., 1994; Thomas et al., 1998). β-arrestin proteins (1 or 2) bind the phosphorylated AT_1 receptors, disrupting coupling to G proteins and attenuating further signalling through these pathways (Hunyady et al., 1994; Ouali et al., 1997; Thomas et al., 1995; Turu et al., 2006), although activation of MAPK pathways can still occur (Wei et al., 2003). β-arrestin association with the phosphorylated receptor results in rapid internalization of the agonist-receptor complex (Ouali et al., 1997; Turu et al., 2006) via clathrin mediated endocytosis (Thomas, 1999). Internalization occurs primarily into endosomes for degradation, but a proportion, approximately 25%, of the internalized receptors is recycled back to the cell surface (Griendling et al., 1987; Ullian et al., 1989).

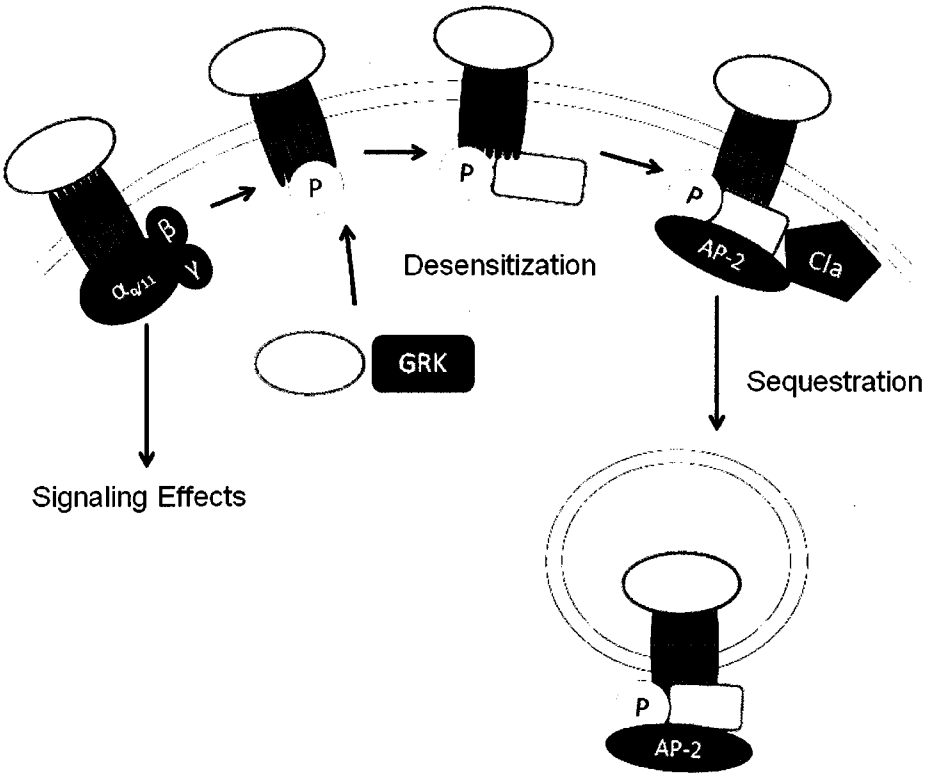

Figure 1.7. Regulation of the cell response by desensitization and internalization of cell surface receptors. The following abbreviations are used: angiotensin II (Ang II); protein kinase C (PKC); g protein-coupled receptor kinase (GRK); β-arrestin (β-Arr); adaptor protein-2 (AP-2); and clathrin (Cla).

1.1.5.2. Regulation of AT_1 Receptor Expression

Short term regulation of receptor response is accomplished through desensitization and internalization as described, but longer term regulation of AT_1 receptor expression occurs largely through transcriptional and post-transcriptional mechanisms (Guo et al., 1994; Nickenig et al., 1994; Sandberg, 1994). Investigations of receptor expression in rodent vascular and renal cells focus predominantly on AT_{1A} receptors, as these are the predominant isoform in these cells (Burson et al., 1994). The rat AT_{1A} gene contains regulatory elements in the 5' flanking sequence that both positively and negatively regulate expression (Murasawa et al., 1993). Through these elements, AT_{1A} receptor expression is modified at the transcriptional level. A more predominant mechanism is post-transcriptional, as modulation of AT_1 mRNA stability (Nickenig et al., 2001). Stability of the transcript is influenced by proteins that interact with the 3' untranslated region (Nickenig et al., 1994) to modulate degradation (Nickenig et al., 2002). One of these RNA binding proteins, calreticulin, negatively impacts AT_1 mRNA stability, reportedly through direct recruitment of RNAses or induction of RNA conformational changes to promote RNAse association (Nickenig et al., 2002). An increase in stability has been proposed to result from binding of factors that compete with RNAses or induce conformational changes to inhibit RNAse association (Nickenig et al., 2001).

In vascular smooth muscle cells, chronic stimulation of the AT_1 receptors by its agonist, Ang II, decreases the receptor mRNA and protein expression (Gunther et al., 1980; Lassegue et al., 1995; Nickenig et al., 1996). The mechanism for this

downregulation has been established to be decreased transcription (Lassegue et al., 1995; Nickenig et al., 1996) and decreased transcript stability (Nickenig et al., 2002; Nickenig et al., 2001). This downregulation of AT_1 receptor expression observed with Ang II stimulation is particularly important in disease states characterized by an activated RAS. Heart failure and diabetes are two examples (as described in sections 1.8 and 1.9) of states in which the RAS is activated.

In addition to Ang II, estrogen (Nickenig et al., 2000a) and EGF (Guo et al., 1994; Nickenig et al., 1994) have been shown to downregulate AT_1 receptors through a destabilization of the mRNA transcript. EGF has also been demonstrated to impact AT_1 expression through a decreased rate of transcription (Nickenig et al., 1994) and post-translationally through decreased localization to the cell surface (Ullian et al., 2004).

Upregulation of AT_1 receptors by factors such as low-density lipoproteins (LDL; Nickenig et al., 1997) and insulin (Takayanagi et al., 1992) has also been illustrated. LDL treatment of rat VSMCs increased AT_1 transcript and protein levels (Nickenig et al., 2000b) by increasing transcript stability (Nickenig et al., 1997). The upregulation of AT_1 gene expression by insulin, like that of LDL, is accomplished by influencing the half-life of the mRNA transcript (Nickenig et al., 1998). The stabilization of the mRNA by insulin is proposed to involve MAPK proteins (Nickenig et al., 1998). Although post-transcriptional modulation of expression is the predominant mechanism in these cases, changes in protein expression are ultimately affected. As elaborated in subsequent sections, changes in AT_1 receptor protein expression can be investigated non-invasively in vivo using imaging modalities.

1.1.6. Tissue Renin Angiotensin Systems

1.1.6.1. Cardiac RAS

In addition to the 'classical' systemic RAS, tissue systems have also been identified in the heart, brain, and kidney. Cardiac tissue expresses components of the RAS and this tissue RAS, and specifically AT_1 receptor activation, is particularly important in cardiac remodelling and heart failure (HF; Opie et al., 2001). Angiotensinogen, renin and ACE expression have been exhibited in cardiac tissue (Danser et al., 1994). Danser et al (1994) were also able to illustrate renin and ACE activity in the myocardium. Myocardium also expresses AT_1 receptors (Chang et al., 1991). Ang II in cardiac tissue has been detected at a much greater level than that of the plasma (Danser et al., 1994) suggesting that this tissue system is regulated separately from the circulating one. This separation in regulation from the circulating RAS has particular impact on peripheral measures of RAS activity. Plasma measurements of RAS components, particularly Ang II, could therefore be much different from those of the myocardium. A non-invasive imaging modality could provide the opportunity to expand the current knowledge of the RAS as a whole and within tissues with a minimal impact on the subjects.

1.1.6.2. Brain RAS

The blood-brain barrier (BBB) prevents circulating Ang II from reaching the brain. Despite this, AT_1 receptors are present in brain areas that regulate cardiovascular function (Allen et al., 2000; Bunnemann et al., 1992). Specific regions of the brain, the circumventricular organs, are not within the BBB and enable circulating Ang II to

interact with the RAS in these regions to modulate blood pressure, water and salt intake and vasopressin release (von Bohlen und Halbach et al., 2006). Furthermore, peptides and the relevant enzymes are detected in the brain at the gene or protein level: angiotensinogen (Stornetta et al., 1988), Ang I (Okamura et al., 1981), Ang II (Okamura et al., 1981), renin (Dzau et al., 1988; Dzau et al., 1986; Okamura et al., 1981), and ACE (Okamura et al., 1981; Whiting et al., 1991). A technique to study the brain RAS non-invasively in vivo would be beneficial to broaden the understanding of this system within this tissue.

1.1.6.3. Renal RAS

In the kidney, components of the RAS have been found: angiotensinogen (Mento et al., 1998), renin (Mento et al., 1998), ACE (Campbell et al., 1986), Ang II (van Kats et al., 1997) and Ang II receptors (Allen et al., 2000; Ardaillou, 1999). More importantly, like the heart, this system has been shown to be regulated separately from that of the circulating system (Mercure et al., 1998; van Kats et al., 1997). Peripheral markers of the RAS, such as plasma Ang II levels, therefore may provide a false indication as to the state of the system within the tissue. Furthermore, tissue measurements of the RAS components, particularly AT_1 receptors, currently require tissue samples and are thus an invasive technique (Northern or Western blots, RT-PCR etc.). As in cardiac and brain tissue, molecular imaging technology could be used to non-invasively investigate the renal RAS in normal and disease states.

1.1.6.4. Vascular RAS

Tissue-based RAS have been demonstrated in the heart, brain and kidney. The vascular system was shown to express RAS components. Angiotensinogen mRNA (Campbell et al., 1986), renin mRNA (Phillips et al., 1993) and protein (Re, 1987), and ACE mRNA (Phillips et al., 1993) have been detected in vasculature, specifically in the aorta. Ang I is produced in vascular tissues (Unger et al., 1991). Ang II secretion was previously demonstrated in cultured vascular cells (Kifor et al., 1987). AT_1 receptors were reported to be expressed in vascular tissue (Chang et al., 1991). In fact, many studies examining the regulation of AT_1 receptors are conducted in vascular smooth muscle cells as described in 1.1.5.2.

1.1.7. Cross-Talk Between the Sympathetic Nervous System and the RAS

RAS activation can be influenced by the sympathetic nervous system (SNS) and vice versa. In the kidney, sympathetic nerve activity (SNA) stimulates the release of renin from the juxtaglomerular cells (DiBona, 2000). Conversely, suppression of renal SNA has been demonstrated to oppose the antinatriuretic effects of Ang II (Lohmeier, 2001). In a rat model with increased renal SNA enhanced plasma renin activity is also observed (Francis et al., 2001). Further to the stimulation of the RAS by the SNS, the reverse has also been investigated in the literature.

In vitro peripheral norepinephrine (NE) transmission in heart (Starke et al., 1970), vascular (Cline, 1985), and kidney tissue (Kaufman et al., 1985) is augmented by Ang II. Enhancement of the neurotransmission has been shown in rats to result from increased NE release (Shepherd et al., 1981). Ang II also inhibits NE uptake to increase neurotransmission (Panisset et al., 1968). Several studies have also observed prolonged

peripheral SNA with chronic exposure to Ang II (Brooks, 1995; Brooks et al., 1997; Osborn et al., 1997; Reid, 1992). In states where both of these systems are abnormally regulated, the interaction between these systems becomes important, such as in heart failure (HF; Francis et al., 2001) or diabetes (Perin et al., 2001).

1.1.8. Renin Angiotensin System and HF

1.1.8.1. Cardiac Remodelling, Hypertrophy and HF

Chronic hemodynamic overload of the heart leads to activation of compensatory remodelling and hypertrophy (Dostal, 2000). These compensatory mechanisms can then result in the progression to HF (Dostal, 2000). In addition to alterations in AT_1 expression in HF, the receptors also play a role in changes associated with the disease (Liu et al., 1998; Opie et al., 2001). ACE inhibitors and AT_1 receptor blockers (ARBs) have been shown to prevent the progression of cardiac hypertrophy in ischemic HF models (Richer et al., 1999a; Richer et al., 2001) and in patients with ischemic and non-ischemic forms of HF as well as improving outcomes (Pfeffer et al., 2003a; Pfeffer et al., 2003b; Solomon et al., 2005) suggesting a prominent role for the AT_1 receptor in the progression of cardiac remodelling to HF. A common animal model that closely follows the disease progression in humans is the rat myocardial infarction (MI) model by coronary artery ligation (Gupta et al., 2007).

1.1.8.2. RAS Expression in Animal Models and Patients

Alterations in RAS components have been demonstrated in both animal models and in patients with HF and tissue and circulating levels of these components can differ. Early post-MI, within 6 hours, plasma renin activity and Ang II are increased (Leenen et

al., 1999). The plasma Ang II levels remain elevated up to 8 weeks post-MI (Leenen et al., 1999). Within cardiac tissue, the RAS is also activated early post-MI. At 3 days post-MI, cardiac Ang I and Ang II levels are elevated (Leenen et al., 1999). Enhanced Ang I persists for up to 8 weeks and Ang II remains increased for up to 7 days (Leenen et al., 1999). At about 4 weeks post-MI, activation of the kidney, heart and brain RAS have been illustrated. Renal levels of renin mRNA are 2-fold greater in post-MI than in controls (Kelly et al., 1997) but renal ACE densities decrease (Tan et al., 2004). Tan et al (2004) report increased ACE densities in heart and brain tissue at this time point. Late post-MI, 8 weeks following surgery, elevations in plasma Ang II (Leenen et al., 1999), cardiac Ang I (Leenen et al., 1999), and ACE gene and protein expression in heart (Seeland et al., 2003; Tan et al., 2004) and brain (Tan et al., 2004) are observed. The components of this system are dynamic over the disease progression and are activated in a tissue-specific manner.

AT_1 receptors post-MI, also demonstrate alterations in expression in various tissues and over the progression of disease. In early post-MI (4 days) studies of cultured myofibroblasts from non-infarcted myocardium, AT_1 mRNA expression decreased, but the protein expression remained unchanged (Staufenberger et al., 2001). In the same studies, AT_1 mRNA expression in cultured myofibroblasts from the infarct region was unchanged while receptor density decreased (Staufenberger et al., 2001). At 30 days post-MI, Kelly et al (1997) reported no change in cardiac AT_1 mRNA expression, although Tan et al (2004) demonstrated a marked increase in cardiac AT_1 receptor density at a similar time point post-MI. In the kidney, Mento et al (1998) showed significantly increased AT_1 receptor expression (about 97%) in glomeruli at 4-6 weeks post-MI. In the

same studies at 4-6 weeks post-MI, Ang II receptor expression was decreased in renal vasculature, by about 67%, although the contribution of AT_1 versus AT_2 was not determined (Mento et al., 1998). In studies using a similar model at 4 and 8 weeks post-MI, Tan and colleagues (2004) demonstrated that AT_1 receptor densities in the renal cortex did not change, while densities in the renal medulla decreased at both time points. The lack of change in AT_1 receptor density observed in the renal cortex in the Tan et al (2004) studies compared to those by Mento et al (1998) may be due to differences in methodology between the studies (autoradiography at 4 and 8 weeks and binding assays at 4-6 weeks respectively). Furthermore, the Mento et al (1998) studies isolated the glomerular and vascular structures while the studies by Tan et al (2004) used whole kidney slices. The differences in preparation may also contribute to this discrepancy as whole kidney slices would contain both of the structures isolated by Mento and colleagues.

Regulation of AT_1 receptor expression has been shown in animal models to be dynamic over the process of cardiac remodelling and the progression of HF. In end-stage human HF, the myocardium exhibits a down-regulation of AT_1 receptors and AT_1 receptor mRNA (Asano et al., 1997; Haywood et al., 1997; Regitz-Zagrosek et al., 1997; Regitz-Zagrosek et al., 1998). The expression changes observed over the course of disease progression are limited to discrete time points, not well defined in the literature and in the case of renal expression, conflicting. A better understanding of the regulatory changes in the RAS during HF is necessary. *In vivo* serial imaging of these receptors may provide detailed information on the expression changes that occur and insight into

the mechanisms of the progression of the disease. Advances in our current knowledge could improve diagnostic capabilities and targets for treatment.

1.1.9. Renin Angiotensin System and Diabetes

1.1.9.1. RAS, Hyperglycaemia and Insulin Resistance

Studies have shown that elevated Ang II induces insulin resistance (Henriksen et al., 2001). Conversely, reduction of Ang II signalling through ACE inhibition by enalaprilat or AT_1 antagonism by losartan increases insulin sensitivity (Aksnes et al., 2006; Kudoh et al., 2000). The enhancement of insulin resistance by Ang II has been attributed to altered insulin signalling (Bernobich et al., 2002; Ogihara et al., 2002; Wei et al., 2006) and inactivation of the insulin receptor (Marrero et al., 2004). Exposure to high glucose leads to an induction of Ang II production in renal mesangial cells (Singh et al., 2003; Vidotti et al., 2004). Studies in podocytes determined that high glucose stimulated Ang II production through augmented angiotensinogen mRNA expression in these cells (Wolf et al., 2005). These observations therefore have significance for the RAS in a diabetic milieu, particularly where glucose levels are not controlled.

1.1.9.2. Renal RAS in a Diabetic Milieu

The renal RAS is abnormally activated in diabetes (Anderson et al., 1993; Dzau et al., 1989). Anderson et al (1993) observed increased renal angiotensinogen expression, and renin expression and activity in diabetic rats. Renal ACE activity in these rats decreased (Anderson et al., 1993) but renin conversion of angiotensinogen to Ang I is considered the rate limiting step in Ang II generation (Robertson et al., 1992). The increases observed by Anderson and colleagues (1993) therefore suggest activation of the

system in a diabetic model. Interestingly, in a similar rat diabetic model, Harrison-Bernard et al (2002) demonstrated a rise in plasma Ang II activity that was not observed in renal tissue. These discrepancies in plasma and tissue measures of RAS components indicate a separation in the regulation of the circulating versus tissue RAS.

AT_1 receptor expression in whole kidney and renal cortex tissue is increased in diabetic rats compared to controls using Western blot analysis (Harrison-Bernard et al., 2002). In isolated glomeruli, AT_1 receptor expression has also been shown to be increased in the diabetic state using rat models of this disease and similar methods (Wehbi et al., 2001). AT_1 activation by Ang II results in the phosphorylation of STAT1, STAT3 and STAT5, which subsequently activate early growth response genes (Bhat et al., 1994; Darnell et al., 1994; McWhinney et al., 1998; Schindler et al., 1995) as described in section 1.1.4.2. *In vitro* studies have shown that high glucose increases the cellular responses of glomerular mesangial cells to Ang II and the extent of STAT phosphorylation (Amiri et al., 1999a; Amiri et al., 2000; Amiri et al., 1999b), thus Ang II signalling in these cells. A diabetic milieu therefore could enhance the responsiveness of cells to Ang II thus stimulating the gene expression and protein synthesis by Ang II and lead to hypertrophy.

1.1.9.3. RAS and Diabetic Nephropathy

Nephropathy is a common chronic complication of diabetes, affecting approximately 30% of diabetic patients (Gruden et al., 2005). In studies using rat models of diabetes, kidney ultrastructure is altered. Glomerular basement membrane thickness, glomerular volume, and total mesangial volume are increased in diabetes but returned to control levels with RAS blockade (Allen et al., 1997). Blockade of AT_1 receptors has

been shown to reduce proteinuria, a key predictor and component of nephropathy (Mimran et al., 2003; Remuzzi et al., 1993). Ang II increases glomerular capillary pressure and can initiate glomerulosclerosis (Ichikawi et al., 1991). Glomerular permeability was improved in early diabetic nephropathy (DN) with ARB treatment (Anderson et al., 2000). Clinical trials of ACE inhibitors or ARBs have demonstrated clinical benefit in diabetic patients with both insulin-dependent and non-insulin dependent diabetes (Brenner et al., 2001; Lewis et al., 1993) with reductions in progression to nephropathy with either treatment.

In addition to rat models, changes in RAS components have also been observed in diabetic patients. Mezzano et al (2003) described increased renal Ang II immunostaining in non-insulin dependent diabetes. In this type of diabetes when nephropathy is present, AT_1 receptor density was shown to be reduced by immunohistochemistry (Mezzano et al., 2003; Wagner et al., 1999). In renal biopsies of patients with non-insulin dependent diabetes and nephropathy AT_1 gene expression is reduced in relation to healthy individuals (Mezzano et al., 2003; Wagner et al., 1999). Other groups have reported increased gene expression of this receptor in diabetic patients without nephropathy (Reuter et al., 2006) but this could be a reflection of different stages of the disease. *In vivo* imaging studies with an AT_1 radioligand could expand on current human data of AT_1 expression in diabetes and progression to DN.

1.1.10. Renin Angiotensin System and Hypertension

Control of blood pressure is one of the primary functions of the RAS. Hyperactivity of the RAS has been shown to lead to hypertension (Griendling et al., 1997). Reductions in blood pressure have been repeatedly demonstrated using

pharmacological intervention of the RAS by ACE inhibition or AT_1 antagonism (e.g. Brenner et al., 2001; Brooks, 1995; Cervenka et al., 1998; Collis et al., 1981; Gohlke et al., 2002b; Pfeffer et al., 2003a; Richer et al., 1999b). There are several animal models to investigate this condition. One such model is the spontaneously hypertensive rat (SHR), a model of genetic hypertension. In SHR plasma Ang I, Ang II and renin are shown to be decreased at 11 weeks (Jessup et al., 2008). Otsuka and colleagues (1998) demonstrated increased plasma ACE activity in these rats. AT_1 receptor expression in SHR are increased in several tissues, including the brain (Reja et al., 2006), adrenal medulla (Reja et al., 2006), renal outer medulla (Song et al., 1995), heart (Song et al., 1995), and aorta (Otsuka et al., 1998). Furthermore, the AT_1 receptor expression in the brain of SHR has been correlated to blood pressure (Reja et al., 2006).

Two further examples of rat models of hypertension are one in which both kidneys are intact but one kidney is clipped producing hypertension, and another model is developed following a pharmacological treatment. The two-kidney, one-clip (2K1C) model has been found to have increased activity of the RAS. Increases in the activity of plasma renin (Lee et al., 2002a; Okamura et al., 1986) and ACE (Okamura et al., 1986) were observed in 2K1C rats. Aortic tissue demonstrates increases in renin and ACE activity as well (Okamura et al., 1986). Tissue Ang II is also enhanced in the aorta in this model (Okamura et al., 1986).

Hypertension can be induced by N^G-nitro-L-arginine methyl ester (L-NAME) in rats. In these rats, renin and ACE mRNA were reported to be elevated in plasma (Lee et al., 2002a). Plasma renin activity did not change in these rats at 4 weeks post-treatment, although plasma ACE activity increased (Lee et al., 2002b). AT_1 gene expression in rats

with L-NAME-induced hypertension is enhanced from normotensive controls (Lee et al., 2002b). Stimulation of the RAS activity has been documented in several pathologies (as described in this and previous sections). Investigation of the function of AT_1 receptors are important to understand progression, treatment and hopeful regression of these pathologies: heart failure, diabetic nephropathy, and hypertension. A non-invasive method allowing examination of this system has the potential to provide substantial information in this regard.

1.2. Positron Emission Tomography

1.2.1. General

Investigation of AT_1 receptors can be achieved by various methods in animal models but very few of those methods are used in a clinical setting or efficiently investigate the progression of human disease. One non-invasive method applied *in vivo* in both animal models and humans to image receptor function and kinetics is positron emission tomography (PET). This imaging modality yields serial imaging of subjects in both animal (Zober et al., 2006) and human studies (Luigi Zinzani et al., 2009).

A PET tracer contains an isotope which decays through emission of positrons. Positrons collide with electrons, annihilate and emit two photons (Figure 1.8). These antiparallel or so-called 'coincidence' photons travel to the detectors of the PET camera, which are arranged in a ring. The lines of coincidence are calculated to determine the point of annihilation. These points are recorded over time during the acquisition of the PET scan. The data are then reconstructed into 3-D images. The tracers characterized

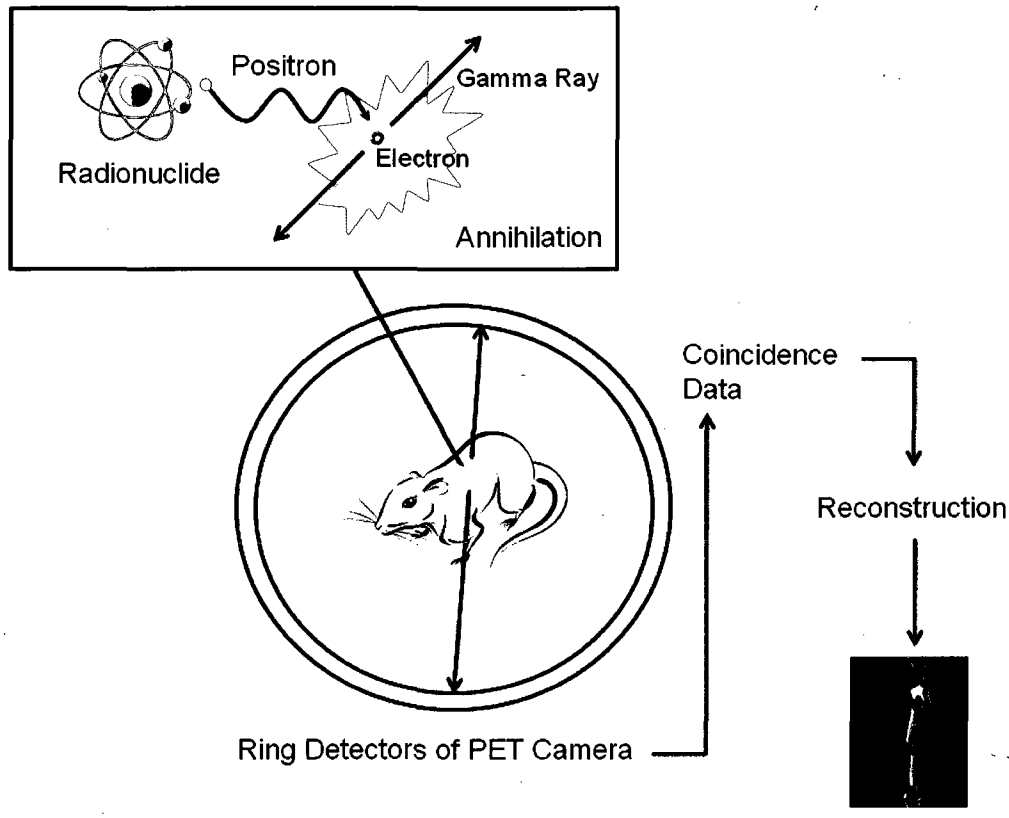

Figure 1.8. A general overview of PET camera function. Adapted from Cherry et al., 2001.

here, [^{11}C]methyl-candesartan (methyl-2-ethoxy-1-[[2'-(1H-tetrazol-5-yl)biphenyl-4-yl]methyl]-1H-benzimidazole-7-carboxylate) and [^{11}C]TH4 (methyl-1-[[2'-(1H-tetrazol-5-yl)biphenyl-4-yl]methyl]-2,3-dihydro-2-oxo-1H-benzoimidazole-7-carboxylate), contain a carbon-11 isotope, which has a half-life of 20.38 minutes.

1.2.2. Receptor Imaging Using PET

Imaging receptors can be impacted by unlabeled compound in the tracer formulation (Hume et al., 1998). Specific activity, the measure of labeled to unlabeled component in the total mass of an injected tracer, therefore has influence on detectable receptor signals. Hume et al (1998) suggest that to satisfy tracer kinetic modelling in PET imaging, receptor occupancy by the tracer should be 1-5%. In cases where low specific activity is combined with a low receptor density, this is not feasible because the receptors can easily become saturated by unlabeled ligand (Hume et al., 1998). Furthermore the signal (activity associated with the receptor) may be too low to detect and produce an image. In the RAS, normal cardiac AT_1 receptor density is low (Tan et al., 2004) relative to that of other tissues and to that of other cardiac receptors. Normal cardiac tissue AT_1 expression is 2-5% that of β-adrenergic receptors (Dostal, 2000) and less than 1% that of renal AT_1 receptors (Chang et al., 1991). Cardiac AT_1 receptors could be considered saturable based on the low density of receptors. Production of high specific activity tracers is necessary to perform PET imaging studies for evaluation of AT_1 receptors in tissues with low receptor density. In addition to limitations of specific activity, radioligands applied in receptor imaging must exhibit both specific and selective binding that is, the radioligand must bind the receptor target and only the receptor target. Characterization of radioligands in the literature use similar techniques to demonstrate

binding specificity and selectivity to their target (Kenk et al., 2007; Lourenco et al., 2001; Zober et al., 2006).

1.2.3. Johns Hopkins AT_1 Radioligands

There are several carbon-11 labeled tracers that have been developed from non-peptide ARBs: MK-996, L-159,884 (a methoxy analogue of MK-996), and KR31173 (Figure 1.9). [^{11}C]MK-996 and [^{11}C]L-159,884 were reported to have difficult syntheses (Hamill et al., 1996). [^{11}C]L-159,884 was found to be readily metabolized in humans reducing the feasibility of its application in a clinical setting (Hamill et al., 1996). [^{11}C]KR31173 has emerged as the most promising of these three tracers, with very high kidney activity but low uptake in the heart and minimal uptake in the brain (Zober et al., 2006). [^{11}C]KR31173 in a normal state is thus not feasible for cardiac or brain AT_1 receptor imaging, two important sites involved in the progression of HF. Recently however, Fukushima et al, presented preliminary data demonstrating cardiac uptake of [^{11}C]KR31173 in infarcted myocardium in a rat model of myocardial infarction (Fukushima et al., 2009). In this study, cardiac [^{11}C]KR31173 uptake was markedly increased in the infarct versus non-infarct region, suggesting that cardiac AT_1 imaging is possible in states where the RAS is upregulated states such as post-MI. Neither the parent compound nor this novel compound are currently approved by regulatory bodies (e.g. Health Canada or the Food and Drug Administration) for human study which could make obtaining approval for human use more difficult. The radiotracers currently available are thus at present, not easily translated to a clinical setting to examine AT_1 receptors *in vivo*

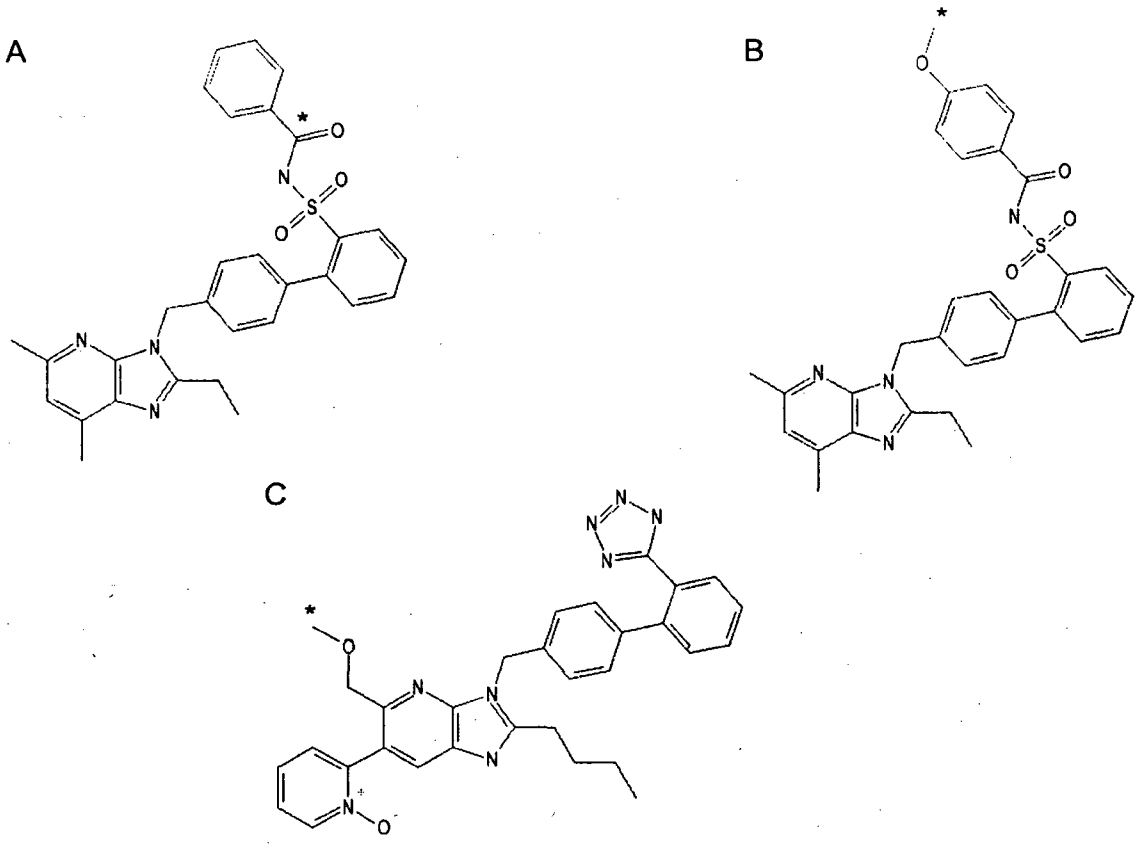

Figure 1.9. AT_1 radioligands previously published in the literature (A) [^{11}C]MK996, (B) [^{11}C]L-159,884 and (C) [^{11}C]KR31173. The asterisk indicates the location of the carbon-11 label.

1.2.4. University of Ottawa Heart Institute Novel AT_1 Radioligands

To attempt to improve upon current AT_1 radioligands, our laboratory developed two novel AT_1 tracers (Hadizad et al., in press). A selective and potent, clinically used ARB, candesartan (2-ethoxy-1-[(2'-(1*H*-tetrazol-5-yl)biphenyl-4-yl)methyl]-1*H*-benzimidazoline-7-carboxylic acid, CV-11974) (Vanderheyden et al., 1999) served as the parent molecule for the developed *O*-methyl and desethyl derivatives. Candesartan was selected for 3 primary reasons: 1) published synthesis mechanisms; 2) known properties of candesartan; and 3) safety data for transition to human studies. Kubo and colleagues (1993a,b) have published synthesis mechanisms for ester derivatives of candesartan. These mechanisms were used as the basis for the radiosynthesis for [^{11}C]methyl-candesartan and [^{11}C]TH4. Candesartan binds reversibly with high affinity (IC_{50} of 0.66 x 10^{-7} M) and also crosses to a certain extent the BBB based on central effect blockade of Ang II by peripheral application (Gohlke et al., 2002a; Gohlke et al., 2001), indicating a promising potential radiotracer. Candesartan and its metabolites are approved for use in humans and are widely used clinically, potentially facilitating transition of the radioligands

1.2.4.1. [^{11}C]Methyl-candesartan

The *O*-methylated derivative of candesartan, first developed by Kubo et al (1993), may be attractive as a potential radioligand. Methyl-candesartan also binds reversibly with similar affinity (IC_{50} of 1.1 x 10^{-7} M) to AT_1 receptors (Kubo et al., 1993a; Kubo et al., 1993b). Since candesartan is more hydrophilic than methyl-candesartan and was shown to produce central effect (Gohlke et al., 2002a; Gohlke et al., 2001), BBB

penetration by methyl-candesartan might also be expected. Studies have shown that antagonist binding does not result in internalization of the receptor-antagonist complex (Fierens et al., 1999; Fierens et al., 2000; Fierens et al., 2002). [^{11}C]Methyl-candesartan (Figure 1.10) could therefore be considered to provide a measure of cell surface AT_1 receptors. Furthermore, the parent compound methyl-candesartan is based on a clinically approved AT_1 receptor blocker which may facilitate approval for use in clinical investigation.

1.2.4.2. [^{11}C]TH4

TH4 is synthesized similarly to methyl-candesartan (Hadizad et al., in press), except for the conversion of the ethoxy group to an amide derivative (Figure 1.10). Characterization work on this compound, a carboxylic acid ester analogue, is not found in the literature but the structure is similar to that of the inactive metabolite of candesartan, CV-15959, the carboxylic acid derivative (Schmidt et al., 2003). It is possible that this compound binds AT_1 and also provides a measure of cell surface receptors. As with methyl-candesartan, the parent compound is clinically approved and this may facilitate approval for human use therefore expediting translation to clinical investigations.

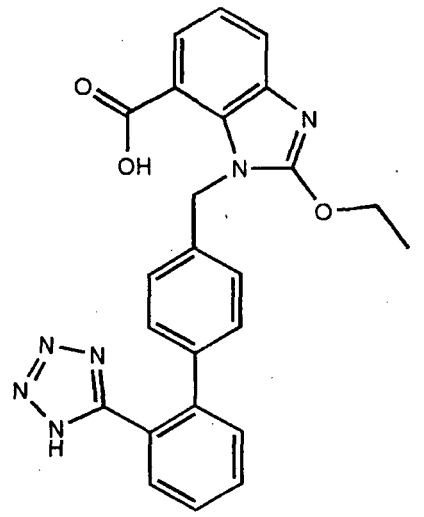

Candesartan

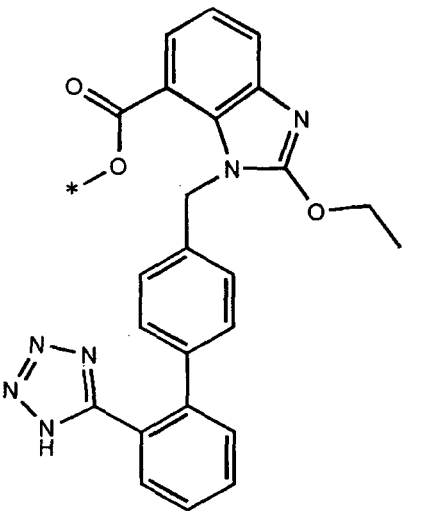

[^{11}C]Methyl-Candesartan

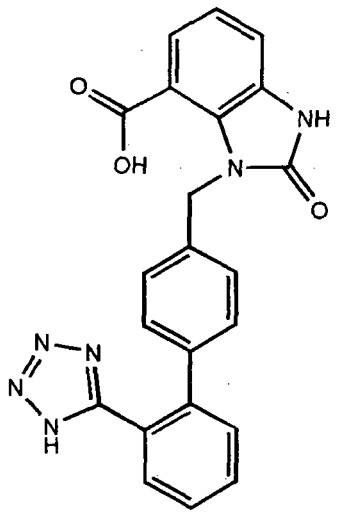

CV-15959

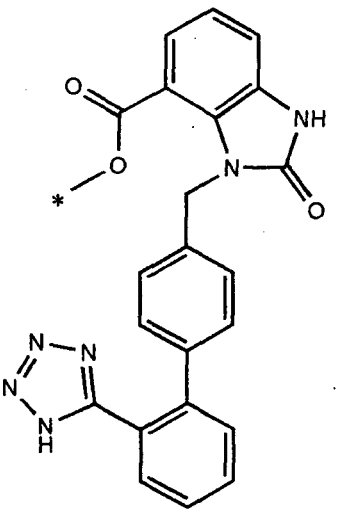

[^{11}C]TH4

Figure 1.10. The parent compound candesartan, its primary metabolite CV-15959 and two novel AT_1 radioligands produced at the University of Ottawa Heart Institute [^{11}C]methyl-candesartan and [^{11}C]TH4. The asterisk indicates the location of the carbon-11 label.

1.3. Research Objectives and Hypotheses

1.3.1. General Objective

The overall aim of this project was to characterize two novel radioligands, [^{11}C]methyl-candesartan and [^{11}C]TH4, for non-invasive, *in vivo* PET imaging of the AT_1 receptor with the ultimate long-term goal of application in clinical investigation and clinical use.

1.3.2. Hypotheses

i. [^{11}C]Methyl-candesartan and/or [^{11}C]TH4 exhibits *in vivo* properties favourable for use in rat studies, including binding characteristics, kinetics, and metabolism;

ii. A non-invasive approach using kinetic imaging of [^{11}C]methyl-candesartan with PET can be used to measure AT_1 receptors *in vivo*;

iii. [^{11}C]Methyl-candesartan exhibits favourable dosimetry for potential future use in human studies.

1.3.3. Specific Objectives

i. Characterize the *in vivo* time course of [^{11}C]methyl-candesartan and [^{11}C]TH4 in rats using *ex vivo* methods;

ii. Characterize the *in vivo* binding specificity and selectivity of [^{11}C]methyl-candesartan and [^{11}C]TH4 for AT_1 over AT_2, Mas (Ang(1-7)), β-adrenergic or α_2-adrenergic receptors in rats using *ex vivo* methods at 15 minutes post-injection;

iii. Characterize the *in vivo* binding kinetics of [^{11}C]methyl-candesartan in rats by small animal PET;

iv. Characterize the *in vivo* binding specificity and selectivity of [^{11}C]methyl-candesartan in rats for AT_1 over AT_2 receptors using small animal PET;

v. Determine the metabolism profile of [^{11}C]methyl-candesartan in rat plasma, and kidney;

vi. Determine the dosimetry profile of [^{11}C]methyl-candesartan using *ex vivo* biodistribution in rats.

2. MATERIALS AND METHODS

2.1. Radiochemical Synthesis of [^{11}C]Methyl-Candesartan and [^{11}C]TH4

The synthesis of both the [^{11}C]-labeled and unlabeled methyl-candesartan and TH4 is outlined in Figure 2.1. In brief, the process occurred in three overall steps: protection of the tetrazole group using trityl chloride preventing formation of undesired by-products; methylation by methyl iodide; and de-protection of the tetrazole group through acid hydrolysis. The synthesis of [^{11}C]methyl-candesartan and [^{11}C]TH4 was a modification for radiolabeling of a previously published method (Kubo et al., 1993a; Kubo et al., 1993b) as described in Hadizad et al (in press). A reaction temperature of 65-75°C produced [^{11}C]methyl-candesartan whereas a higher temperature (90°C) resulted in the formation of [^{11}C]TH4, the des-ethyl derivative of candesartan, in which the ethoxy group is converted to a cyclic-urea derivative. A proposed mechanism for this conversion is displayed in Figure 2.2.

2.2. Animals

All experiments were conducted in male Sprague-Dawley rats (Charles River Canada, Montreal) in accordance with the Canadian Council on Animal Care guidelines and with approval from the Animal Care Committee at the University of Ottawa Heart Institute. Female Sprague-Dawley rats (Charles River Canada, Montreal) were also used for the dosimetry studies. Rats were housed in pairs on a 12-hour light:dark cycle. Standard rat chow and water were provided *ad libitum*. Radioligand injections were administered directly through the lateral tail vein or via a catheter inserted to the lateral

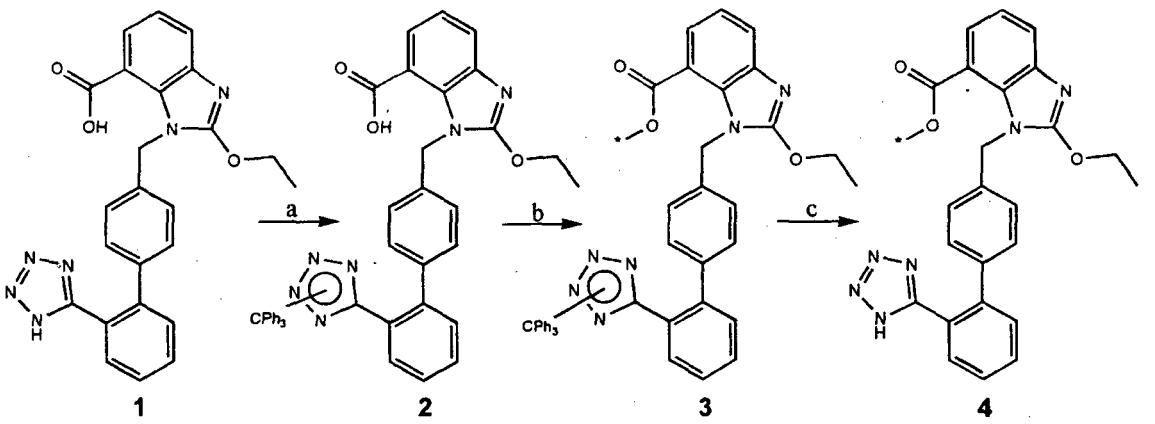

Figure 2.1. Proposed structures for the synthesis of methyl-candesartan. (a) TEA, Trityl chloride, CH_2Cl_2; (b) [^{11}C]MeI, K_2CO_3, Kryptofix, DMF, 65-70°C, 3 min; (c) HCl (1N), DMF, 65-70 °C, 2 min. The candesartan (1) precursor undergoes tetrazole protection (2) followed by methylation (3) and deprotection to produce methyl-candesartan (4). The asterisk indicates the location of the carbon-11 label. Adapted from Hadizad et al Bioorganic Medicinal Chemistry (in press).

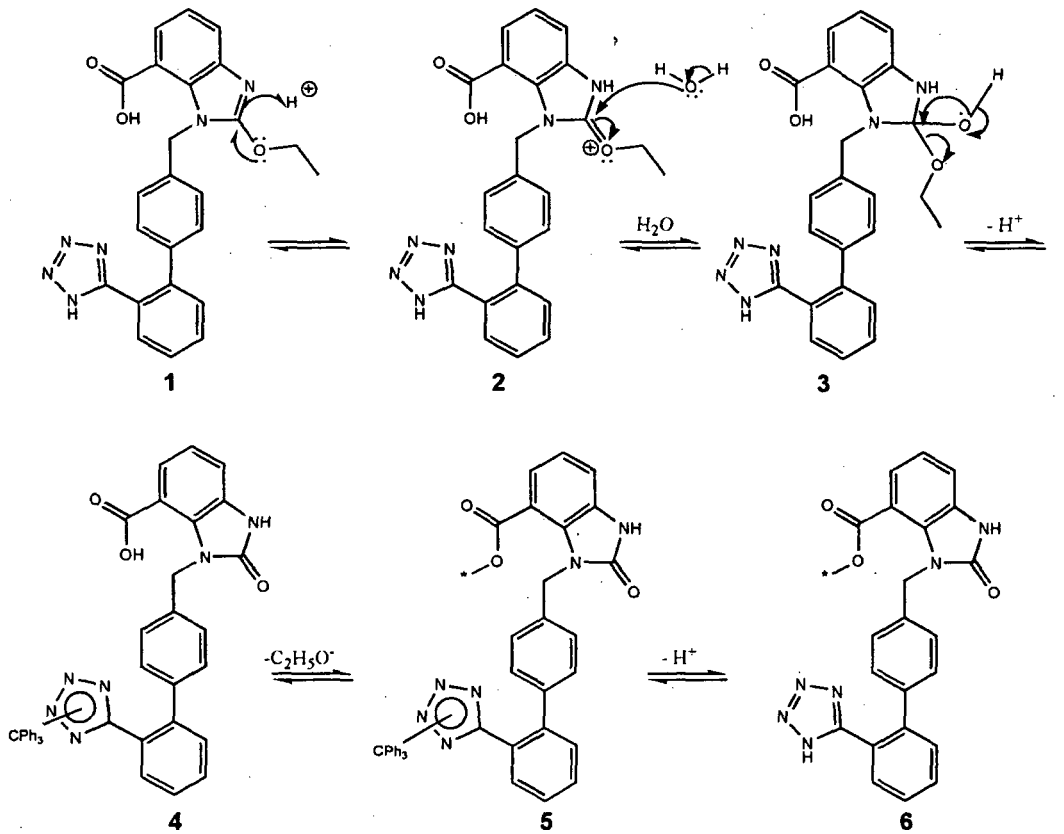

Figure 2.2. Proposed structures for the synthesis of TH4. The candesartan precursor (1) undergoes a substitution reaction (1-3), tetrazole protection (4) followed by methylation (5) and deprotection to produce TH4 (6). The substitution reaction can also occur following the tetrazole protection. The asterisk indicates the location of the carbon-11 label. Adapted from Hadizad et al Bioorganic Medicinal Chemistry (in press).

tail vein. Catheters, when used, were flushed with 100-200 µl of heparinized saline to reduce residual activity in the catheter.

2.3. Ex Vivo Time Course

Rats (200-250 g) were restrained and injected intravenously (iv) with 1.5-1.7 mCi (at the time of first injection) of [^{11}C]methyl-candesartan or [^{11}C]TH4 (specific activity 300-1000 mCi/µmol; corresponding to injected masses of 0.77-2.19 µg methyl-candesartan and 0.80-1.83 µg TH4). Animals were sacrificed by decapitation without anaesthesia at 5, 15, 30, 45 or 60 minutes post-injection of [^{11}C]methyl-candesartan and at 5, 15, 30, or 60 minutes post-injection of [^{11}C]TH4 (n=3 at each time point). Trunk blood was collected in heparinized tubes, from which 1 mL was removed and transferred into pre-weighed gamma tubes. Tissue samples were rapidly dissected out and collected into pre-weighed gamma tubes: left atrium (LA), right atrium (RA), left ventricle (LV), right ventricle (RV), septum, aorta, renal cortex, renal outer medulla, renal inner medulla, adrenals, hypothalamus, cerebellum, brain stem, the remainder of the brain, lung, liver and skeletal muscle (quadriceps). Tissue and blood samples, along with injected standard solutions, were counted for retained radioactivity using a gamma counter (Packard) and weighed to provide the net weight for each sample. Data were expressed as a percent of the absolute injected dose per gram of tissue or sample (%ID/g).

2.4. Ex Vivo Competition

[^{11}C]Methyl-candesartan and [^{11}C]TH4 were evaluated for *in vivo* binding selectivity for the AT_1 receptor over AT_2, Mas (Ang(1-7)), β-adrenergic and α_2-adrenergic receptors using previously published procedures (Kenk et al., 2007; Lourenco

et al., 2001) and established saturating doses of receptor antagonists. Candesartan (Toronto Research Chemicals) and losartan (generously provided by Dr. F.H.H. Leenen's laboratory) block AT_1 receptors. PD123,319 (Sigma Aldrich) and A-779 (Bachem Bioscience) antagonize AT_2 and Mas receptors respectively. β-adrenergic and α_2-adrenergic receptors were blocked by propranolol (Sigma Aldrich) and yohimbine (Sigma Aldrich) respectively. Candesartan, losartan, PD123,319 and A-779 were injected iv whereas propranolol and yohimbine were administered intraperitoneally (ip). Candesartan was co-injected with the radioligands at 3, 5 or 10 mg/kg (Nossaman et al., 2007). Losartan was injected 5 minutes prior to the tracers at 20 mg/kg or co-injected with the tracers at 30 mg/kg (Sun et al., 2007). PD123,319 was administered 5 minutes prior to the radioligands. [^{11}C]Methyl-candesartan was tested using a 2 mg/kg dose (Zober et al., 2006) or a 5 mg/kg dose (Naruse et al., 2002). [^{11}C]TH4 was tested using only the 5 mg/kg dose of PD123,319. A-779 at 100 μg/kg (Bayorh et al., 2002) was administered 5 minutes prior to the radioligands. Propranolol at 20 mg/kg (Friedman et al., 2001) and yohimbine at 10 mg/kg (Munzar et al., 1999) were administered 15 minutes prior to the tracers.

Similar procedures to the time course studies (section 2.3) were employed to assess binding selectivity of the two radioligands. Briefly, rats (200-275g) were restrained and injected with 1.5-1.7 mCi tracer iv (at time of first injection) and sacrificed by decapitation without anaesthesia 15 minutes after radioligand injection. Trunk blood and tissue samples were collected and counted as in the time course studies. Data were expressed as %ID/g and tissue data was normalized to that of the blood (tissue-to-blood

ratio) to correct for any differences in tracer delivery between treatment groups. The percent change from controls was calculated from the following equation:

$$\frac{(Mean\ Tissue:Blood)_{treatment} - (Mean\ Tissue:Blood)_{control}}{(Mean\ Tissue:Blood)_{control}} \times 100\%$$

Based on competition results, [^{11}C]methyl-candesartan was tested in further studies and [^{11}C]TH4 was not.

2.5. Plasma Protein Binding

Plasma protein binding was assessed using published procedures (Lourenco et al., 2001) and a commercially available kit (Micon Bioseparations). Duplicate whole trunk blood samples were collected into heparinized tubes from a male Sprague-Dawley rat sacrificed by decapitation without anaesthesia. Whole blood samples were centrifuged for 5 minutes at 4000 rpm (Jouan). Plasma was transferred into glass culture tubes to which 100 µl of authentic [^{11}C]methyl-candesartan was added. The assay was then completed in duplicate. A 1.0 ml aliquot of plasma with tracer was separated into a free tracer plasma fraction and a plasma protein fraction in an MPS Micropartition Device (MPS No. 4010) following the manufacturer's specifications. Briefly, the 1.0 ml aliquot was added to the upper chamber of the two chamber separation device. The sample was centrifuged for 30 minutes at 2000 xg. Free tracer in plasma passes into the bottom chamber through the membrane separating the two chambers. The filtrate (in the bottom chamber) and the plasma protein bound tracer (in the upper chamber) were then transferred to pre-weighed gamma tubes and counted in a gamma counter (Packard) along side a 100 µl aliquot of the unfiltered plasma and tracer in a pre- weighed gamma

tube to act as a measure of the total plasma activity. The proportion of free tracer in plasma was calculated by the following equation:

$$\frac{\left(Activity/Mass\right)_{filtrate}}{\left(Total\ activity/Mass\right)_{plasma}} \times 100\%$$

The remaining proportion was then made up of the plasma protein-bound radioligand. An average of the duplicate assays was used to calculate the final proportion of plasma protein binding.

2.6. Dosimetry

[^{11}C]Methyl-candesartan was further assessed as described (Lourenco et al., 2001) for the collection of rodent data for estimations of human radiation dose equivalents and residence times. Briefly, restrained male and female rats (n=3 for each sex at all time points) were injected iv with 1.5 mCi of [^{11}C]methyl-candesartan (at time of first injection) and were sacrificed by decapitation without anaesthesia at 5, 15, 30 or 60 minutes after [^{11}C]methyl-candesartan injection. Brain, thymus, thyroid, heart, lungs, pancreas, spleen, marrow, bone, adrenals, kidneys, liver, urine, lower large intestine (LLI) contents, upper large intestine (ULI) contents, small intestine (SI) contents, and stomach contents were dissected from every animal. Testes were removed from male rats, and breasts, ovaries and uteri were removed from female rats. Trunk blood and tissue samples were collected and counted as described in the previous *ex vivo* studies. Activity in the carcass was also recorded for use in the calculations. All activity data was back corrected to the time of first injection.

The activity at time zero was assumed to be zero. Mean activity data for each organ were plotted versus time and integrated to calculate the residence times. OLINDA/EXM software calculated the effective dose (ED) and effective dose equivalent (EDE) by the MIRD method and established ICRP 60/80 protocols (ICRP, 1987; ICRP, 1998). Conversion from rat data to human data used the following equation (Feller et al., 1975):

$$\left(\frac{Total\ Body\ Mass}{Mass\ of\ Organ}\right)_{rat} \times \left(\frac{Total\ Body\ Mass}{Mass\ of\ Organ}\right)_{human}$$

Gastrointestinal contents, blood, and bone masses were as reported in the Cristy and Eckerman phantom series (Stabin et al., 1999) while the remaining tissue masses were as described in ICRP Publication 23. The total marrow and bone values were divided into red and yellow marrow and cortical and trabecular bone respectively in equal ratios as per guidelines (ICRP, 1975). Estimations of the human injected dose were based on the correction factor described by Jagoda and colleagues (2004). Safety limits were applied as published in FDA regulations Code of Federal Regulations Title 21, Volume 5, Section 361.1.

2.7. Metabolism

To detect any radiolabeled metabolites present in the plasma and tissues following administration of ^{11}C-labeled compounds, a modification of the column-switch high performance liquid chromatography (HPLC) method was employed (Hilton et al., 2000; Kenk et al., 2008). High amounts (6-20 mCi at the time of injection) of [^{11}C]methyl-candesartan were administered to restrained rats iv. Rats were sacrificed at 3, 15 or 20

minutes post-injection, trunk blood was collected and the kidneys quickly dissected out. Trunk blood was centrifuged (Jouan) at 4000 rpm for 5 minutes. Urea (Sigma Aldrich) was added to plasma samples to a final concentration of 1.0 g/ml to disrupt plasma protein binding (Hilton et al., 2000). Plasma samples (approximately 0.5 ml) were injected onto the HPLC system. For separation of radiolabeled components, two HPLC columns were used (Figure 2.3); a capture column (Oasis HLB VAC RC Extraction solid phase in a refillable cartridge) and an analytical HPLC column (Luna C18 10 µm 100 A 250 x 4.60 mm, Phenomenex). The various components were assessed by two detectors in series: a Waters UV detector, and a Biorad coincidence detection radiation detector. Briefly, the column-switch procedure involved injection of the sample onto the capture column in solvent 1 (1/99 acetonitrile/water) and passing the detectors. This initial phase detects any lost radioactivity and the eluted macromolecules such as plasma proteins and cellular debris. Once the UV signal had returned to baseline, flow was switched such that Solvent 2 (35/65 acetonitrile/0.1 M ammonium formate) back-flushed the retained compounds off the capture column and over the analytical column passing by the detectors. Any compounds captured were then eluted based on polarity. Chromatogram data (retention time and area under the curve; AUC) were analysed using PeakSimple 3.77 and corrected for noise and radioactive decay. Radioactive decay was corrected using the following equation:

$$AUC_{peakA} \times \frac{1}{e^{\left(\left(-0.6931472 / t_{1/2}\right) \times \left(t_A - t_{unchanged}\right)\right)}} = Corrected\ AUC$$

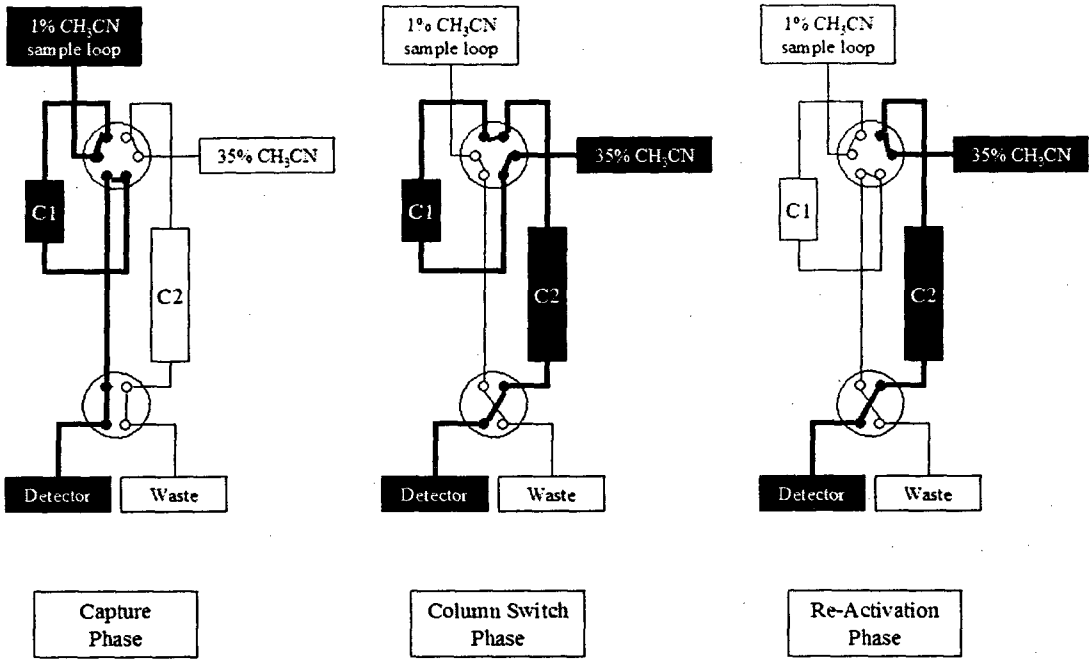

Figure 2.3. Flow diagram of the HPLC column-switch method for analysis of [^{11}C]metabolites in plasma and kidney homogenate. C1 represents the 'capture' column – a refillable cartridge containing Oasis HLB sorbent. C2 represents the analytical column – a Luna C18. Diagram adapted from Hilton et al 2000.

Retention times were calculated from the point of back-flush onto the analytical column (the time of switch) and activity data were expressed as the percent of the total radioactivity signal, as in the following equation:

$$\frac{(Corrected\ AUC)_{peak}}{(Corrected\ AUC)_{total}} \times 100\%$$

Control samples of plasma and kidney were processed as described above, spiked with authentic [^{11}C]methyl-candesartan prior to processing. A plasma and kidney sample from a rat sacrificed 15 min post-injection was also spiked with authentic [^{11}C]TH4 prior to processing and processed as described. A group of rats received a 5 mg/kg co-injection of candesartan and [^{11}C]methyl-candesartan and sacrificed at 15 minutes post-injection to assess for possible interactions of metabolites and the AT_1 receptor. Candesartan was administered at 5 mg/kg for this and subsequent studies based on previous work from (Nossaman et al., 2007). All samples from these rats were processed and analyzed as described above. Sample sizes for the groups were as follows: control plasma n=10; control kidney n=6; 3 minutes post-injection plasma n=4; 3 minutes post-injection kidney n=3; 15 minutes post-injection plasma and kidney n=4; 20 minutes post-injection plasma n=3; 20 minutes post-injection kidney n=4; candesartan co-injection plasma n=6; and candesartan co-injection kidney n=6.

2.8. Small Animal PET Studies

2.8.1. General Scan Protocol

Rats were injected with [^{11}C]methyl-candesartan and underwent 60-minute list-mode PET scans using the on-site small animal PET camera (Inveon, Siemens) under 1-

2% isoflurane anaesthesia. A 10-minute transmission scan was performed immediately prior to each PET scan without moving the animal to allow application of scatter and attenuation corrections during image reconstruction (Figure 2.4). Corrections for spillover (discussed in section 4.5.3) were not applied to PET data. However, spillover effect was minimized as much as possible in generation of the ROIs. Where possible, 2 animals were scanned sequentially using the same tracer formulation. When this occurred, the PET and transmission scans were completed in reverse order to minimize tracer decay. Animals were scanned in a supine position on a heated scanner bed and physiological parameters were monitored for the duration of the scans.

2.8.2. Data analysis

Activity count data were reconstructed into 26 frames: twelve 10-second frames, three 1-minute frames, and eleven 5-minute frames. All images were analyzed with Inveon Research Workplace software (Siemens). Regions of interest (ROI) were created on reconstructed images based on known AT_1 receptor expression and/or visual presence of uptake or activity: LV cavity blood pool, LA region blood pool, liver, kidneys, and lungs. LV cavity ROIs were created by selecting the threshold of highest intensity pixels from a 3-D elliptical shape encompassing the LV such that shapes of similar sizes were manually generated to avoid myocardium tissue as much as possible. LA region ROIs were created similarly by selecting the threshold of highest intensity pixels from a sphere above the LV ROI. Lung and liver ROIs were 2 spheres of 10-20 pixels placed carefully to avoid overlap with other tissues, within each side of the lungs and in different regions of the liver. The left and right kidney ROIs were created from 3-D elliptical shapes by removing portions of the ellipse in close proximity to the liver to minimize spillover from

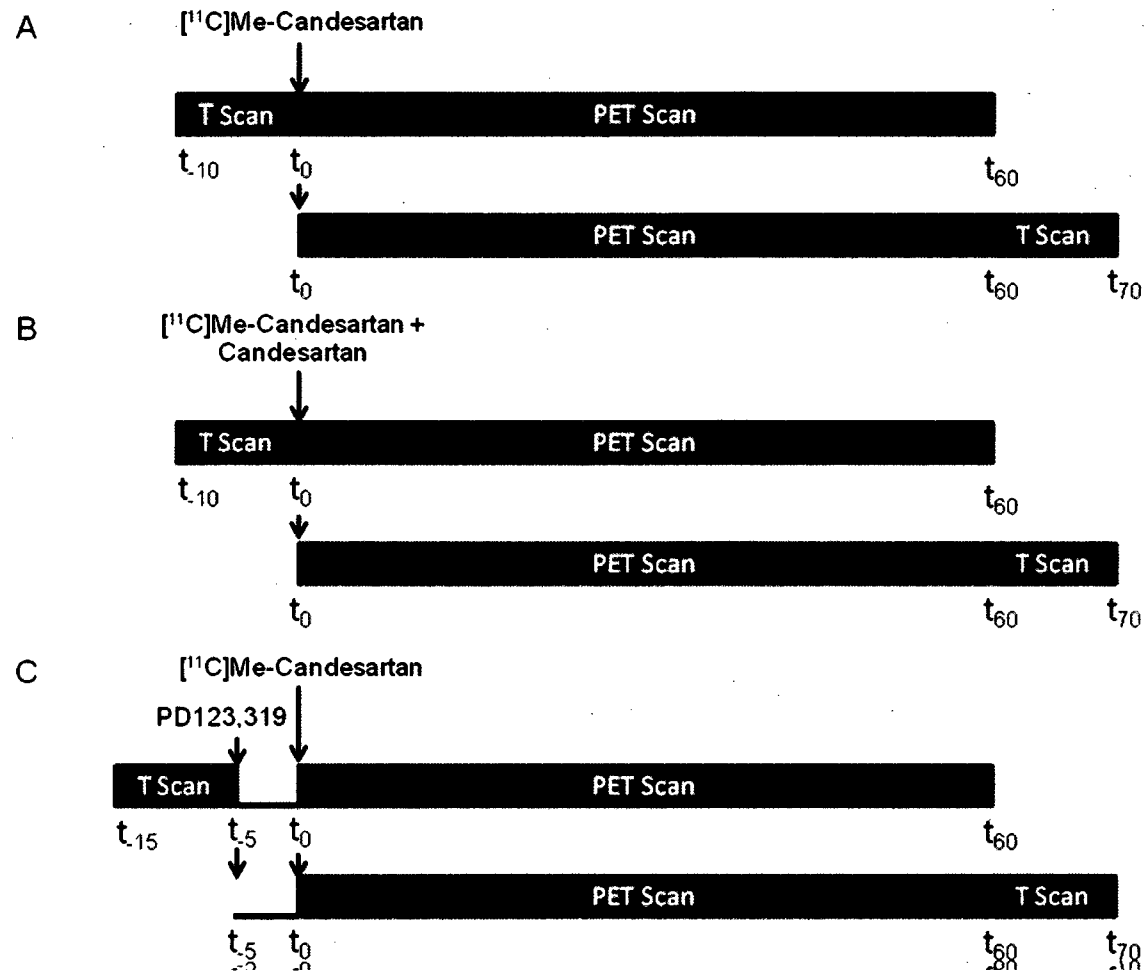

Figure 2.4. Timeline schematics of the PET scan protocols. [^{11}C]Methyl-candesartan ([^{11}C]Me-candesartan) was administered iv at t_0 in all scans. Transmission scans (T scans; blue) were completed either prior to or immediately following the PET scans (red). (A) Control scans received only tracer at t_0. (B) Candesartan (5 mg/kg) was administered as a co-injection with the tracer at t_0. (C) PD123,319 was administered iv 5 minutes prior to the initiation of the PET scan and [^{11}C]methyl-candesartan injection.

the liver. Threshold contours of the highest intensity pixels were then generated in the remaining shape. The thresholds were manually created such that a ribbon of consistent size was applied to each kidney.

For all ROIs in each scan, time course data were collected and distribution volumes (DVs) were generated by Logan graphical analysis in the Inveon Research Workplace software. Briefly, the DV is calculated as the slope of plots produced from the ROIs such that the y- and x-axes are as follows:

$$y-axis=\int_0^t \frac{C_t(\tau)dt}{C_t} \qquad x-axis=\int_0^t \frac{C_p(\tau)dt}{C_t}$$

2.8.3. Initial Scan Optimization

Fourteen rats were injected with 0.4-2.4 mCi [^{11}C]methyl-candesartan, scanned as described in section 2.8.1, and the images were analysed as preliminary test data for protocol optimization. The effects of injected mass, activity, specific activity, and dose on DV data were investigated. In a subset of 3 rats, images were reconstructed with and without corrections for scatter and attenuation to select appropriate reconstruction protocols. Using identical protocols, a subset of 6 rats underwent a second scan to assess reproducibility and any effects of rat mass on DV data. The data from the 14 control rats and the 6 rats that received multiple scans determined the sample size for the subsequent treatment groups. From these initial scans the standard protocol was applied for the subsequent candesartan and PD123,319 treatment groups.

2.8.4. Plasma Activity Correction

To correct the whole blood curves for the activity in the plasma fraction over time, the contribution of the plasma activity to that of the total blood was determined. Four rats received arterial cannulation surgery under 1-2% isoflurane anaesthesia for arterial blood sampling. Immediately prior to sampling, 2 mCi of [^{11}C]methyl-candesartan was administered iv. 200 µl blood samples were collected at 0.5, 1, 5, 10, 20, 30, 45, and 60 minutes post-injection into EDTA-coated Microvettes. Whole blood was transferred to pre-weighed gamma tubes, counted in a gamma-counter (Packard) and weighed to express the count data as counts per minute per mg sample (CPM/mg). Blood samples were then centrifuged (Jouan) at 4000 rpm for 5 minutes. Plasma was removed and transferred to clean, pre-weighed gamma tubes and counted for radioactivity decay correcting the data to the same time as that of the whole blood. The plasma samples were also weighed to express data as CPM/mg. The ratio of plasma CPM/mg to blood CPM/mg was calculated for each time point. The mean ratio for all time points was applied as a correction factor to the blood data in the Inveon Research Workplace software in the generation of DV values from images (section 2.8.5).

2.8.5. Time Course and Competition

The initial protocol optimization scans from the 14 rats (section 2.8.3) functioned as the control group to generate time course data (Figure 2.4). A full kinetic study (0-60 minutes) was also completed in four rats treated with 5 mg/kg candesartan (Nossaman et al., 2007) or six rats treated with 5 mg/kg PD123,319 (Naruse et al., 2002). In AT_1-antagonized rats, candesartan and 1.0-2.0 mCi of [^{11}C]methyl-candesartan were co-injected through the tail vein at the same time as a 60-minute list-mode PET scan was

started. PD123,319-treated (AT_2-antagonized) rats were iv injected 5 minutes prior to [^{11}C]methyl-candesartan (0.6-2.9 mCi at time of injection). All reconstructions included corrections for both scatter and attenuation. Activity data were collected from each ROI as described above (section 2.8.2; LA region, lungs, liver, and kidneys) for the 26-frame images. 'Whole blood' activity was considered to be the LA region for all scans based on the optimization results. The activity data for the lungs, liver and kidneys were normalized to the peak 'blood' activity to remove any effect of differences in injected activity across scans. From the activity data, DV values were generated as described (section 2.8.2), applying the established correction factor for plasma to whole blood activity (section 2.8.4 and 3.6.2). The percent change from controls was calculated from the following equation:

$$\frac{(Mean\ DV\ value)_{treatment} - (Mean\ DV\ value)_{control}}{(Mean\ DV\ value)_{control}} \times 100\%$$

2.9. Statistical Analysis

Ex vivo competition data were evaluated by analysis of variance (ANOVA) with Bonferroni post-hoc analysis. Mean tissue-to-blood ratios of antagonist treated groups were compared to that of the control group. Small animal PET mean DV values of candesartan and PD123,319 treatment groups were compared to the control group using a Student's t-test. SPSS 16.0 software was employed for all comparisons with a p-value less than 0.05 considered significant. Sample size requirements were calculated to detect a 20% difference between groups with SigmaStat 3.0 software.

3. RESULTS

3.1. Ex Vivo Time Course

3.1.1. [^{11}C]Methyl-candesartan

[^{11}C]Methyl-candesartan tissue uptake trends across tissues were generally similar for all time points (Figure 3.1). Within tissues, over time there was more washout than expected, reducing signal and approaching background levels by 45 minutes. Throughout the study radioligand retention in the liver was observed at a level more than 2-fold higher than the remaining tissues and accumulated over time (Figure 3.1). The renal cortex and outer medulla retention was also high relative to other tissues but to a much lesser degree than the liver (Figure 3.2). The tissue uptake of the remaining tissues was moderate to low with very minimal uptake observed in the brain.

Tracer uptake within heart regions and within brain regions was similar. Data were therefore expressed on a whole tissue basis for heart and brain. Liver uptake was much more than the remaining tissues and increased over time, but as a potential site of metabolism and excretion this is not unexpected. Additionally, the liver is not an organ of interest in the context of future research (HF and DN). For this reason, the liver was excluded from further figures. Contrast between the tissue and blood radioactivity was optimal at 15 minutes following radioligand injection and was selected for the subsequent competition studies (contrast ratio of renal cortex to blood: 12, 12, 12, 5, and 7 at 5, 15, 30, 45 and 60 minutes; contrast ratio of outer medulla: 4.4, 4.7, 4.5, 3.1 and 3.8 at 5, 15, 30, 45 and 60 minutes).

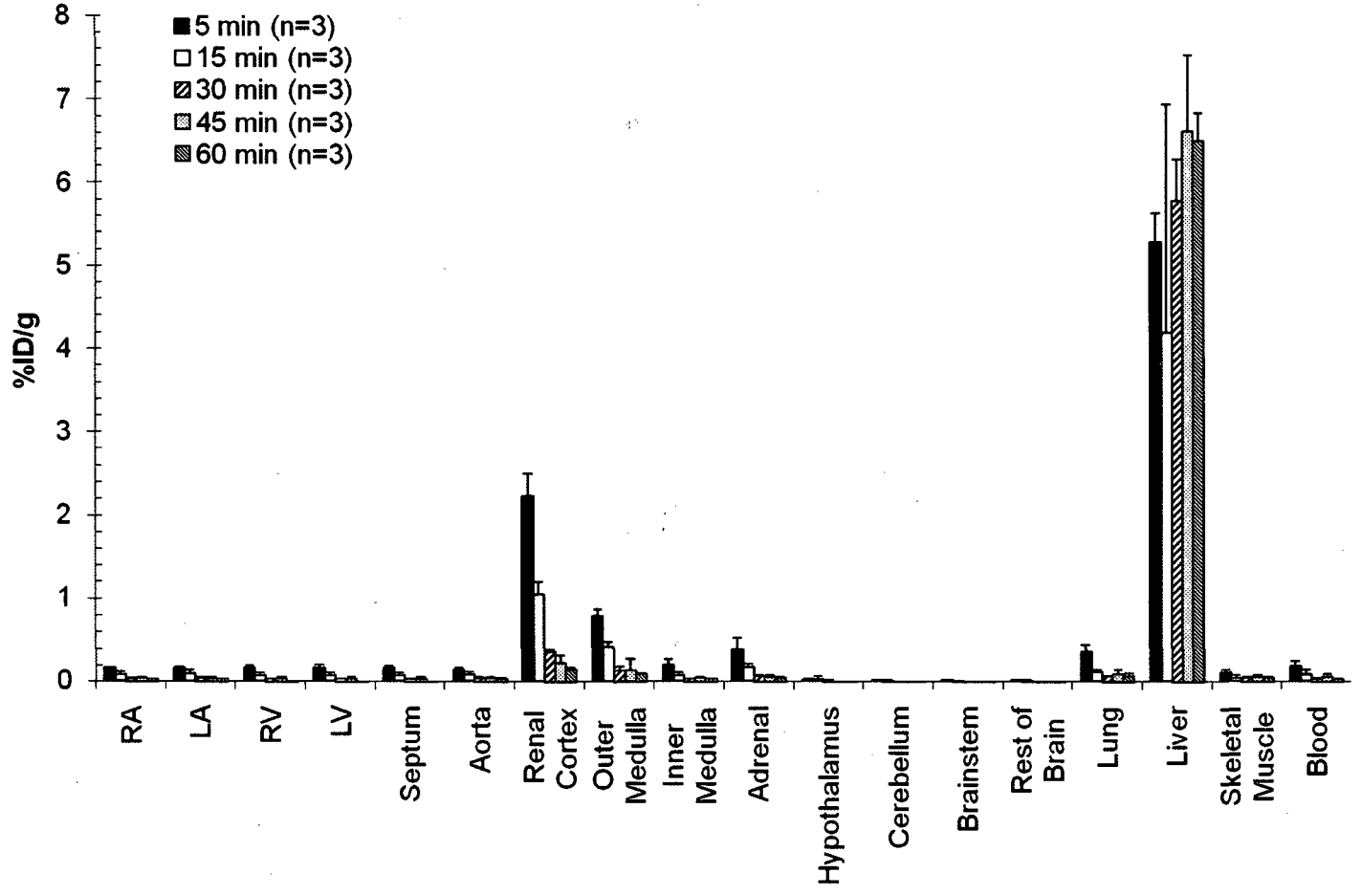

Figure 3.1. Time course of [^{11}C]methyl-candesartan in male Sprague-Dawley rats. Data were expressed as mean % ID/g ± standard deviation. Right atrium (RA), left atrium (LA), right ventricle (RV), left ventricle (LV), septum, aorta, renal cortex, outer medulla, inner medulla, adrenals, hypothalamus, cerebellum, brainstem, the rest of the brain, lung, liver, and skeletal muscle were dissected quickly after sacrifice and counted in a gamma counter.

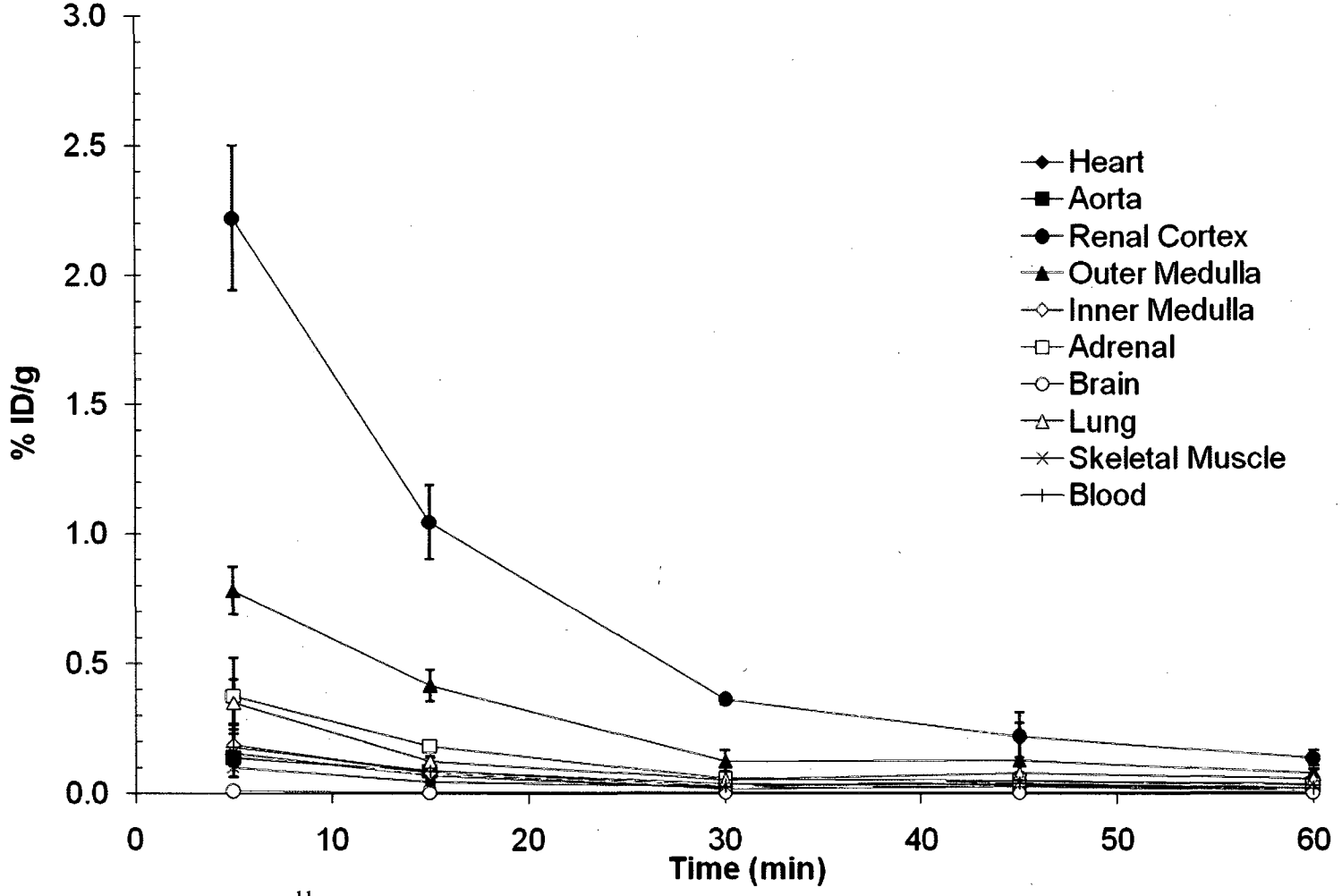

Figure 3.2. Time course of [^{11}C]methyl-candesartan in male Sprague-Dawley rats. Data were expressed as mean % ID/g ± standard deviation. Trunk blood was collected and heart, aorta, renal cortex, outer medulla, inner medulla, adrenals, brain, lung, and skeletal muscle were dissected quickly after sacrifice and counted in a gamma counter. Data presented here exclude the liver to highlight tissue activity of the kidney and other tissues.

3.1.2. [^{11}C]TH4

[^{11}C]TH4 retention compared to that of [^{11}C]methyl-candesartan but was generally lower for all tissues with exception of the renal cortex (Figure 3.3). [^{11}C]TH4 retention in the liver was higher (about 37%) than the remaining tissues at 5 minutes and accumulates to much higher levels at later time points. Similar to [^{11}C]methyl-candesartan, the renal cortex and outer medulla retention was high and tissue uptake of the remaining tissues was moderate to low (Figure 3.4). Uptake in the brain was minimal. Tracer retention was expressed on a whole tissue basis for heart and brain, as regional differences were not observed within these tissues. Liver uptake of this radioligand was also much more than the remaining tissues and similarly to [^{11}C]methyl-candesartan the liver was excluded from further figures. Optimal tissue to blood contrast was also observed at 15 minutes following radioligand injection and therefore this time point was selected for [^{11}C]TH4 competition studies as well (contrast ratio of renal cortex to blood: 19, 14, 8, and 5 at 5, 15, 30, and 60 minutes; contrast ratio of outer medulla: 2.9, 5.3, 4.0, and 2.5 at 5, 15, 30, and 60 minutes).

3.2. Ex Vivo Competition

3.2.1. [^{11}C]Methyl-candesartan

Fluctuations were observed in blood % ID/g values between groups for [^{11}C]methyl-candesartan (Figure 3.5) hence, competition data was normalized for differences in delivery. Data were expressed as a ratio of the % ID/g of the tissue to that of the blood from the same animal. This tissue-to-blood ratio was used for all subsequent

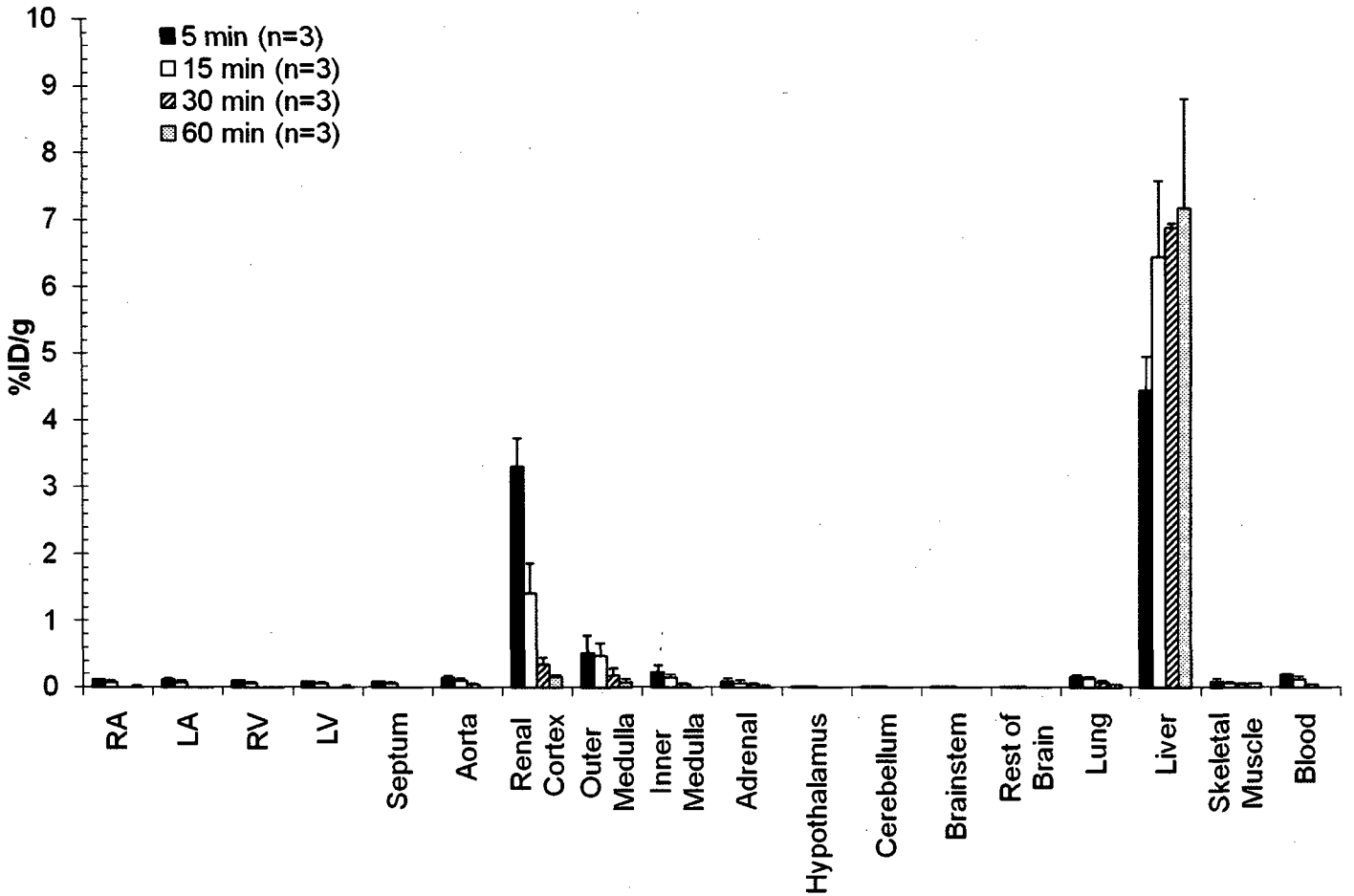

Figure 3.3. Time course of [^{11}C]TH4 in male Sprague-Dawley rats. Data were expressed as mean % ID/g ± standard deviation. Right atrium (RA), left atrium (LA), right ventricle (RV), left ventricle (LV), septum, aorta, renal cortex, outer medulla, inner medulla, adrenals, hypothalamus, cerebellum, brainstem, the rest of the brain, lung, liver, and skeletal muscle were dissected quickly after sacrifice and counted in a gamma counter.

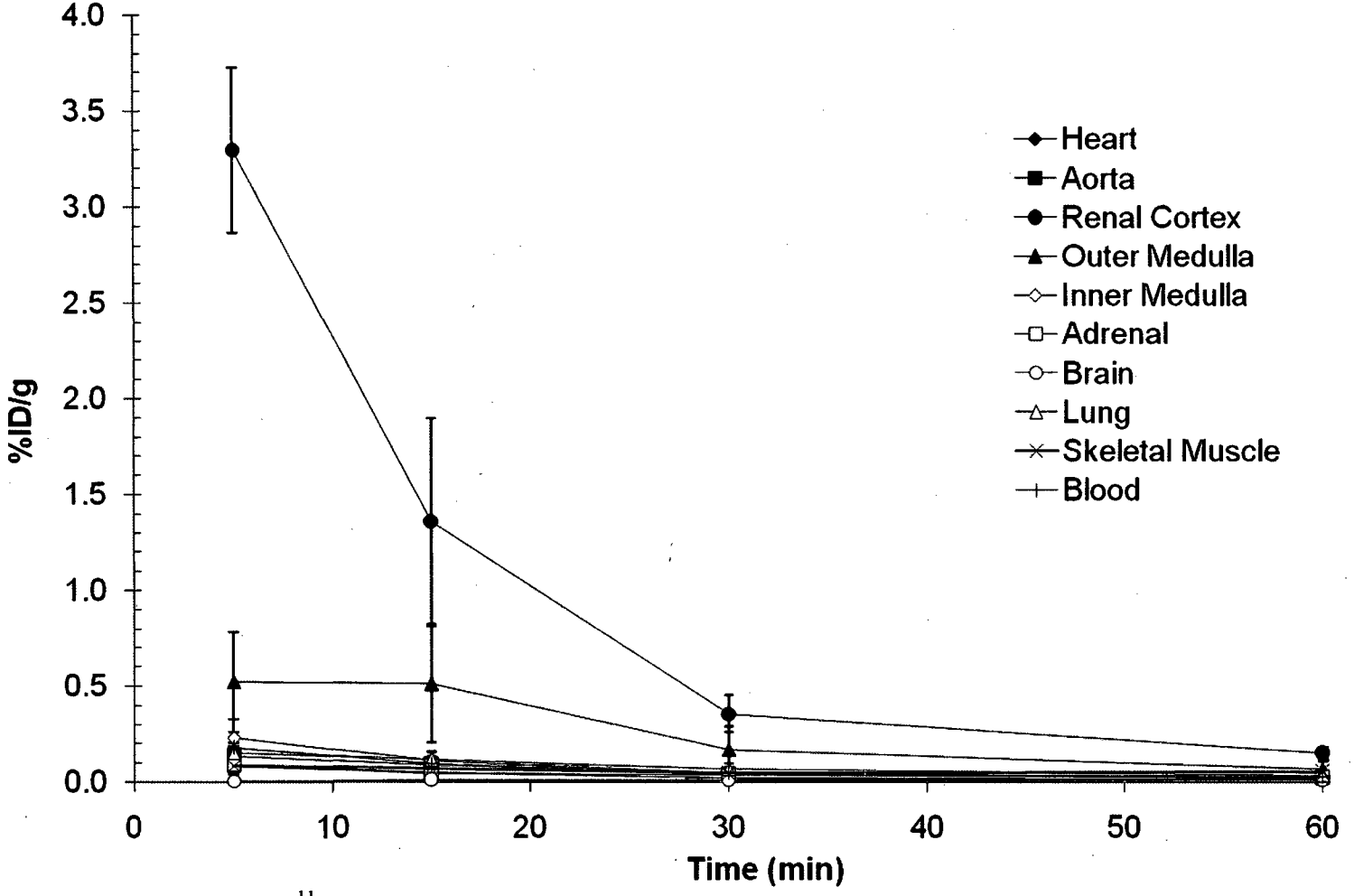

Figure 3.4. Time course of [^{11}C]TH4 in male Sprague-Dawley rats. Data were expressed as mean % ID/g ± standard deviation. Heart, aorta, renal cortex, outer medulla, inner medulla, adrenals, brain, lung, and skeletal muscle were dissected quickly after sacrifice and counted in a gamma counter. Data presented here exclude the liver to highlight tissue activity of the kidney and other tissues.

comparisons. Similar regional uptake in the heart and brain (as described in section 3.1.1) was also observed in these studies.

Overall, high specific binding was observed in the kidney regions for [^{11}C]methyl-candesartan (Figure 3.6). The specific binding component of [^{11}C]methyl-candesartan was expressed as the percent change of the AT_1 antagonist treatment groups relative to controls (Table 3.1). In the renal cortex, candesartan or losartan produced 57-81% and 89-90% reductions in uptake respectively. The specific binding component of [^{11}C]methyl-candesartan in the renal outer medulla with candesartan or losartan was 74-81% and 87-90% respectively.

Competition of [^{11}C]methyl-candesartan binding using other receptor antagonists had minimal effects. PD123,319 (Figure 3.7) at the higher dose (5 mg/kg) significantly decreased tissue retention in the renal cortex and outer medulla (38% and 59% respectively; Table 3.2) but these reductions were not observed in 2 mg/kg PD123,319 treated rats. This lower dose of 2 mg/kg has previously characterized PET AT_1 radioligand selectivity to AT_1 over AT_2 (Zober et al., 2006). Pretreatment with A-779, propranolol or yohimbine did not produce significant reductions in tissue retention of [^{11}C]methyl-candesartan.

3.2.2. [^{11}C]TH4

Fluctuations in blood % ID/g values were also observed using [^{11}C]TH4 (Figure 3.8) and data were therefore normalized as in the [^{11}C]methyl-candesartan studies. Similar regional uptake in the heart and brain (as described in section 3.1.2) was also observed in these studies such that those data could be expressed on a whole tissue basis.

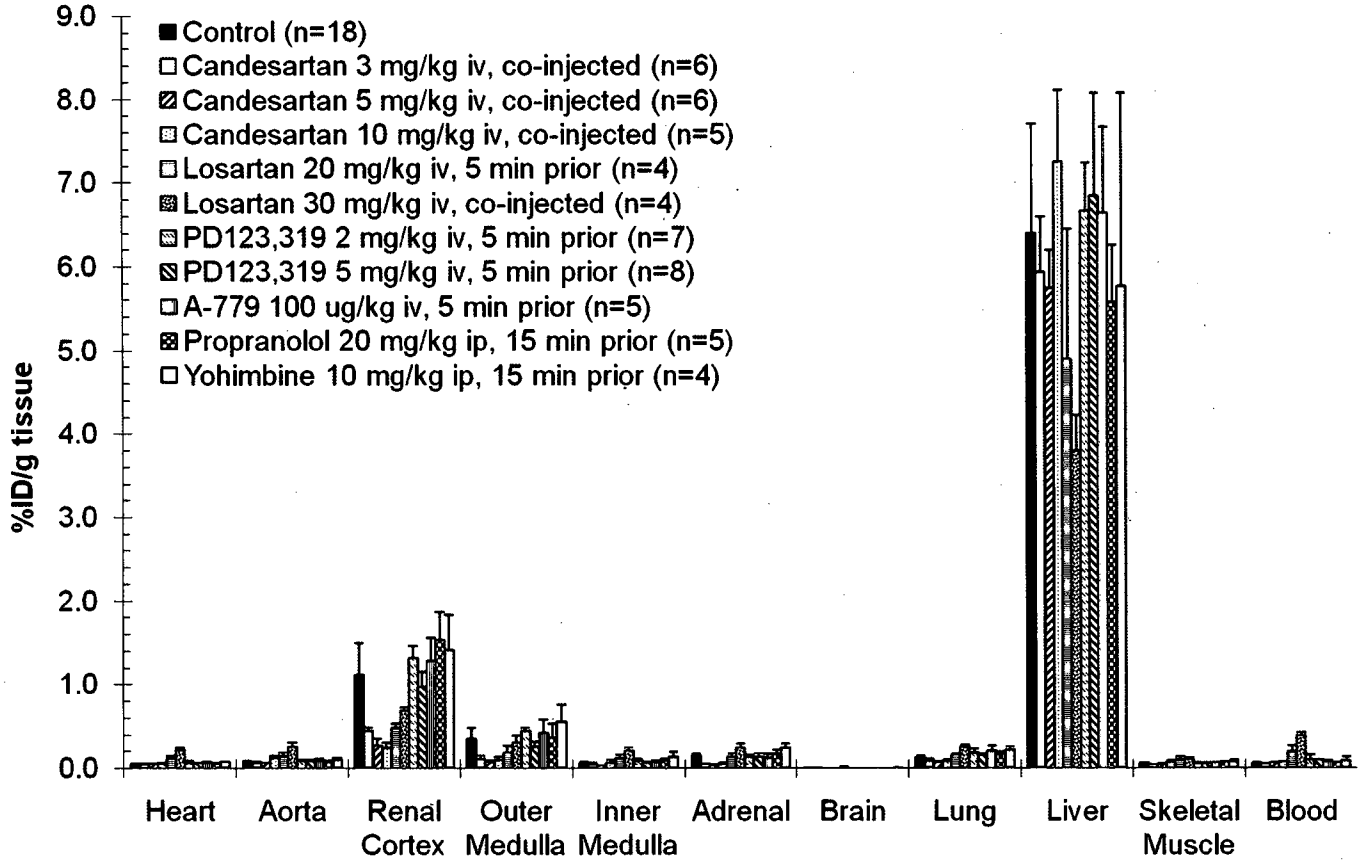

Figure 3.5. Effect of AT_1, AT_2, Mas, β-adrenergic and α_2-adrenergic receptor antagonists on [^{11}C]methyl-candesartan binding 15 minutes post-injection. Data were expressed as mean % ID/g ± standard deviation. Controls received the radiotracer injection iv without pretreatment. Competing drugs were administered as described in the legend. Heart, aorta, renal cortex, outer medulla, inner medulla, adrenals, brain, lung, liver, and skeletal muscle were dissected quickly after decapitation and counted in a gamma counter. Figure 3.6 and 3.7 provide a more detailed view of the renal specificity and selectivity as well as associated statistics.

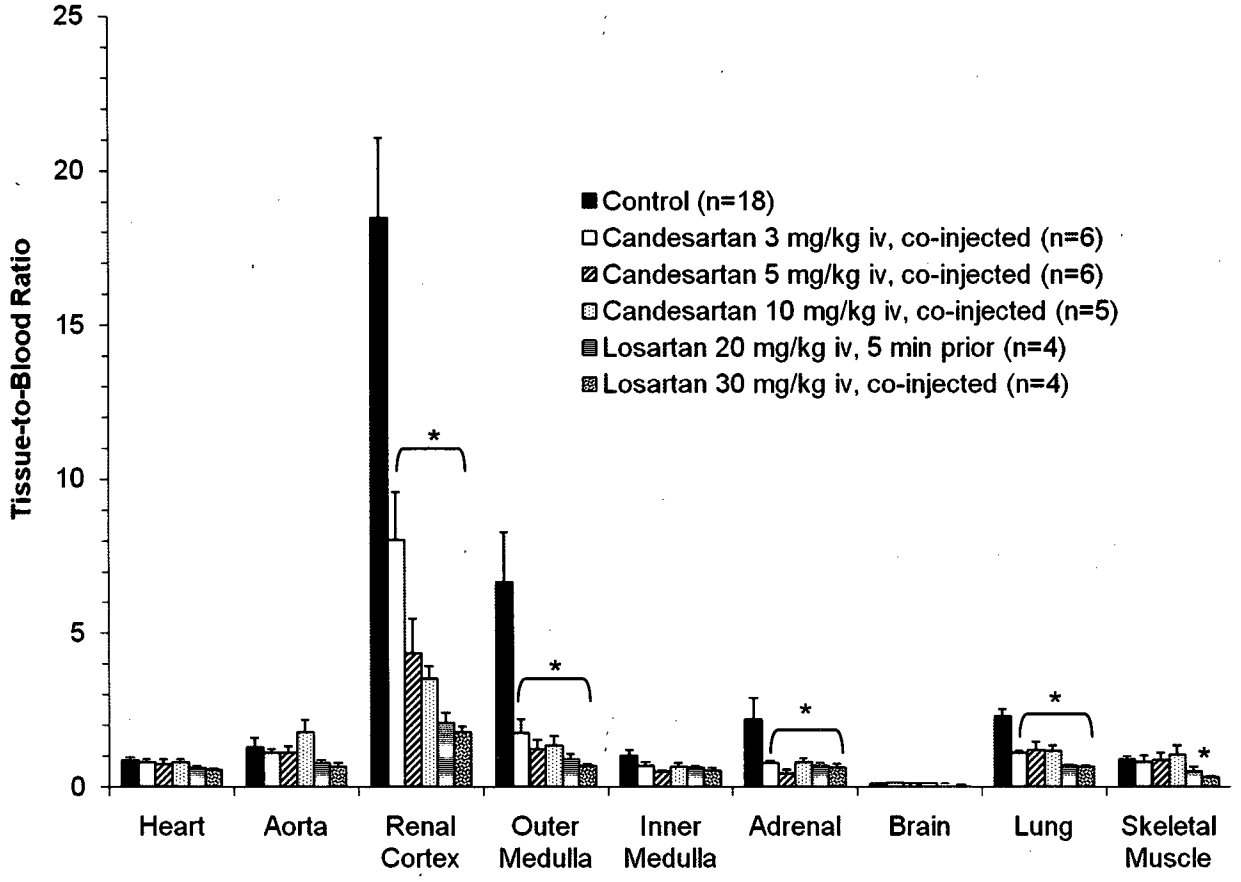

Figure 3.6. Effect of AT_1 receptor antagonists on [^{11}C]methyl-candesartan binding 15 minutes. Data were expressed as mean tissue-to-blood ratio ± standard deviation. Controls received the radiotracer injection iv without pretreatment. Competing drugs were administered as described in the legend. Heart, aorta, renal cortex, outer medulla, inner medulla, adrenals, brain, lung, and skeletal muscle were dissected quickly after decapitation and counted in a gamma counter.

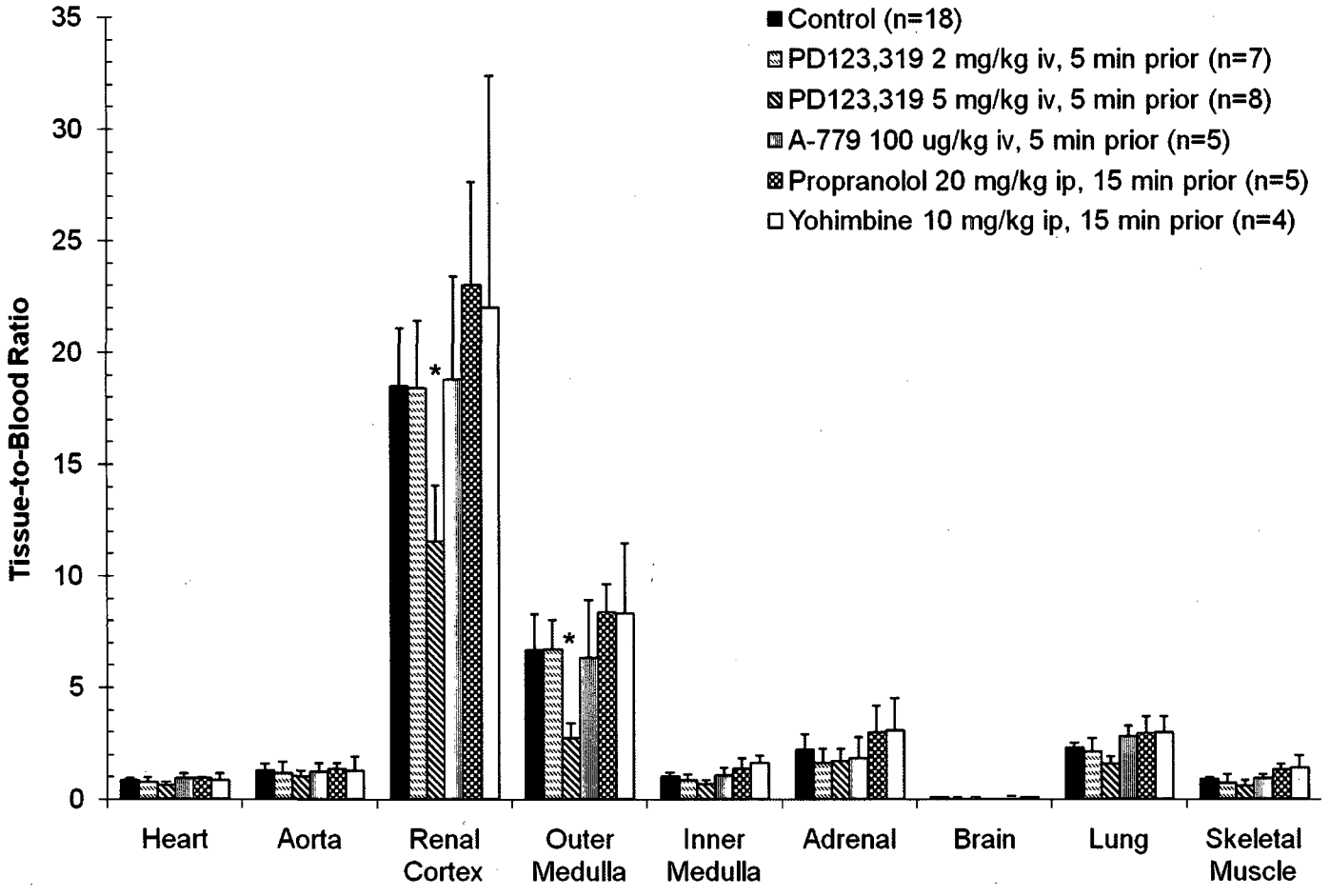

Figure 3.7. Effect of AT_2, Mas, β-adrenergic and α_2-adrenergic receptor antagonists on [^{11}C]methyl-candesartan binding 15 minutes post-injection. Data were expressed as mean tissue-to-blood ratio ± standard deviation. Controls received the radiotracer injection iv without pretreatment. Competing drugs were administered as described in the legend. Heart, aorta, renal cortex, outer medulla, inner medulla, adrenals, brain, lung, and skeletal muscle were dissected quickly after decapitation and counted in a gamma counter.

Table 3.1. Percent change in [^{11}C]methyl-candesartan tissue-to-blood ratio in AT_1 receptor antagonist treated animals as compared to controls at 15 minutes post-injection. *corresponds to a significant difference ($p<0.05$) in mean tissue-to-blood ratio compared to controls.

Tissue	Control	Candesartan			Losartan	
	(mean±st dev)	3 mg/kg	5 mg/kg	10 mg/kg	20 mg/kg	30 mg/kg
Heart	0.86±0.09	-8	-13	-8	-28	-34
Aorta	1.27±0.34	-14	-12	40*	-40	-48
Renal Cortex	18.48±2.58	-57*	-76*	-81*	-89*	-90*
Outer Medulla	6.64±1.62	-74*	-81*	-80*	-87*	-90*
Inner Medulla	1.00±0.19	-34	-49*	-35	-38	-48
Adrenals	2.18±0.70	-65*	-80*	-64*	-69*	-71*
Brain	0.09±0.02	16	-3	-4	-18	-44
Lung	2.29±0.25	-53*	-47*	-50*	-71*	-72*
Liver	108.01±14.16	-2	-12	-3	-84*	-91*
Skeletal Muscle	0.88±0.09	-11	-2	19	-44	-66*

Table 3.2. Percent change in [^{11}C]methyl-candesartan tissue-to-blood ratio in AT_2, Mas, β-adrenergic and α_2-adrenergic receptor antagonist treated animals as compared to controls at 15 minutes post-injection. *corresponds to a significant difference ($p<0.05$) in mean tissue-to-blood ratio compared to controls.

Tissue	Control	PD123,319		A-779	Propranolol	Yohimbine
	(mean±st dev)	2 mg/kg	5 mg/kg	100 µg/kg	20 mg/kg	10 mg/kg
Heart	0.86±0.09	-9	-15	10	8	0
Aorta	1.27±0.34	-9	-21	-1	7	-1
Renal Cortex	18.48±2.58	0	-38*	2	24	19
Outer Medulla	6.64±1.62	1	-59*	-5	26	25
Inner Medulla	1.00±0.19	-13	-32	6	37	60
Adrenals	2.18±0.70	-26	-22	-17	36	40
Brain	0.09±0.02	-16	-29	8	10	-28
Lung	2.29±0.25	-8	-32	22	28	30
Liver	108.01±14.16	-24	-32	-10	-13	4
Skeletal Muscle	0.88±0.09	-18	-31	5	51	58

High AT_1 specific binding of [^{11}C]TH4 was observed in the kidney regions (Figure 3.9). The overall percent change of the AT_1 antagonist treatment groups relative to controls (Table 3.3; 45-70% and 72-78% for the renal cortex and 56-73% and 73-81% for the renal outer medulla) was less than that of [^{11}C]methyl-candesartan.

Pretreatment of rats receiving [^{11}C]TH4 with PD123,319, propranolol or yohimbine did not alter [^{11}C]TH4 uptake (Figure 3.10). A-779 pretreatment, at a dose of 100 μg/kg, resulted in a significant reduction in [^{11}C]TH4 retention in the outer medulla (53%; Table 3.4). Although selectivity for AT_1 over AT_2 and β-adrenergic and α_2-adrenergic receptors was demonstrated, selectivity over Mas receptors was not. Studies involving [^{11}C]TH4 were discontinued for this reason and the lower specific binding proportion and further characterization was not undertaken.

3.3. Plasma Protein Binding

Plasma protein binding was assessed in a male Sprague-Dawley rat in duplicate. The mean proportion of activity bound to plasma proteins for the duplicate measurements was 99.83%.

3.4. Dosimetry

[^{11}C]Methyl-candesartan tissue uptake at 5, 15, 30, and 60 minutes post-injection correlate with the time course data for those tissues in common between the two studies. Uptake data are displayed in Tables 3.5 and 3.6. Similar trends were observed for both males and females. At 5 minutes post-injection, several organs and tissues show uptake: liver, kidneys, lungs, adrenals, small intestine contents, heart, pancreas, spleen, ovaries, urine and blood. From 15 to 60 minutes post-injection uptake levels in several of these

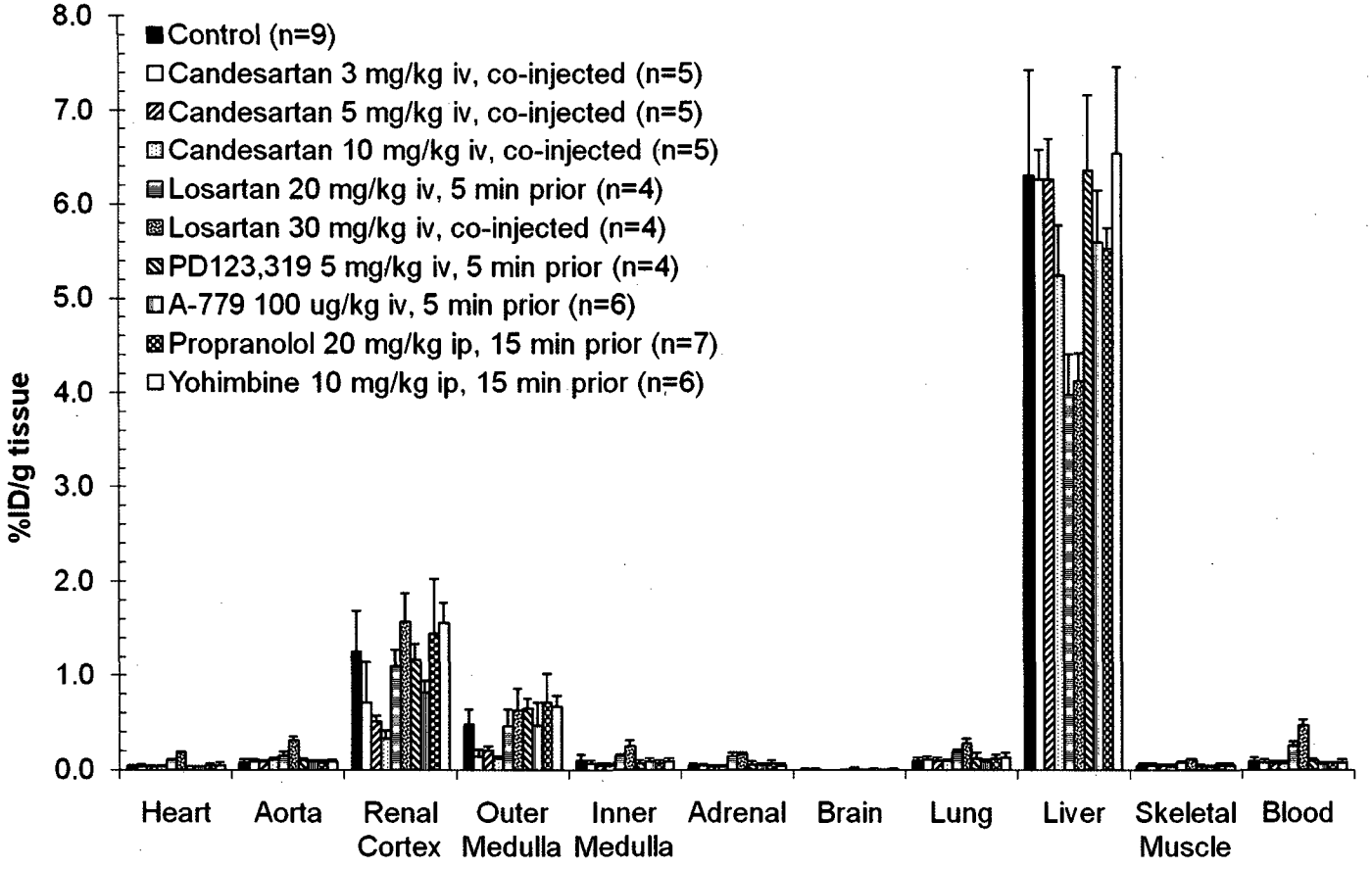

Figure 3.8. Effect of AT_1, AT_2, Mas, β-adrenergic and α_2-adrenergic receptor antagonists on [^{11}C]TH4 binding 15 minutes post-injection. Data were expressed as mean % ID/g ± standard deviation. Controls received the radiotracer injection iv without pretreatment. Competing drugs were administered as described in the legend. Heart, aorta, renal cortex, outer medulla, inner medulla, adrenals, brain, lung, liver, and skeletal muscle were dissected quickly after decapitation and counted in a gamma counter. Figure 3.9 and 3.10 provide a more detailed view of the renal specificity and selectivity as well as associated statistics.

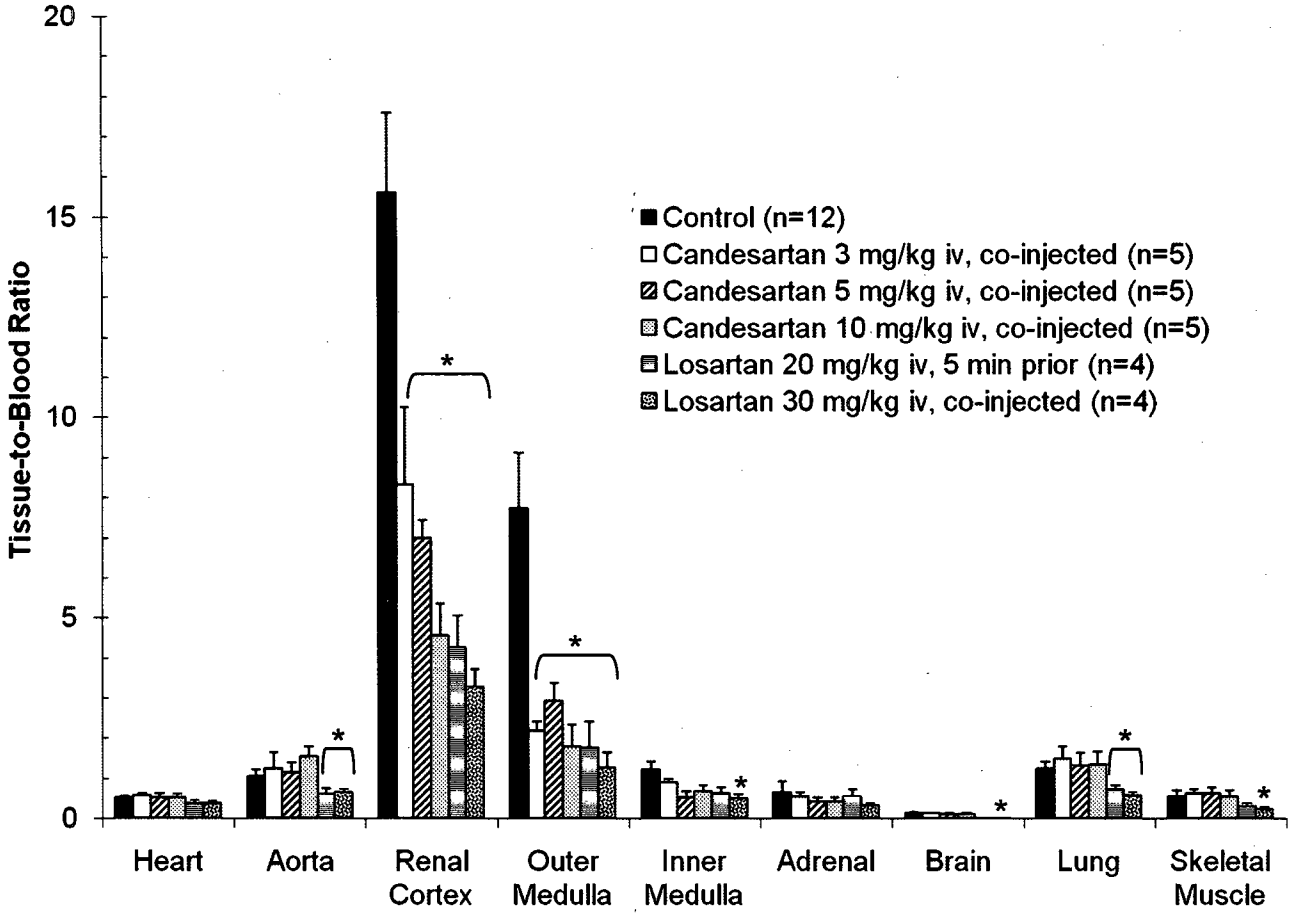

Figure 3.9. Effect of AT_1 receptor antagonists on [^{11}C]TH4 binding 15 minutes post-injection. Data were expressed as mean tissue-to-blood ratio ± standard deviation. Controls received the radiotracer injection iv without pretreatment. Competing drugs were administered as described in the legend. Heart, aorta, renal cortex, outer medulla, inner medulla, adrenals, brain, lung, and skeletal muscle were dissected quickly after decapitation and counted in a gamma counter.

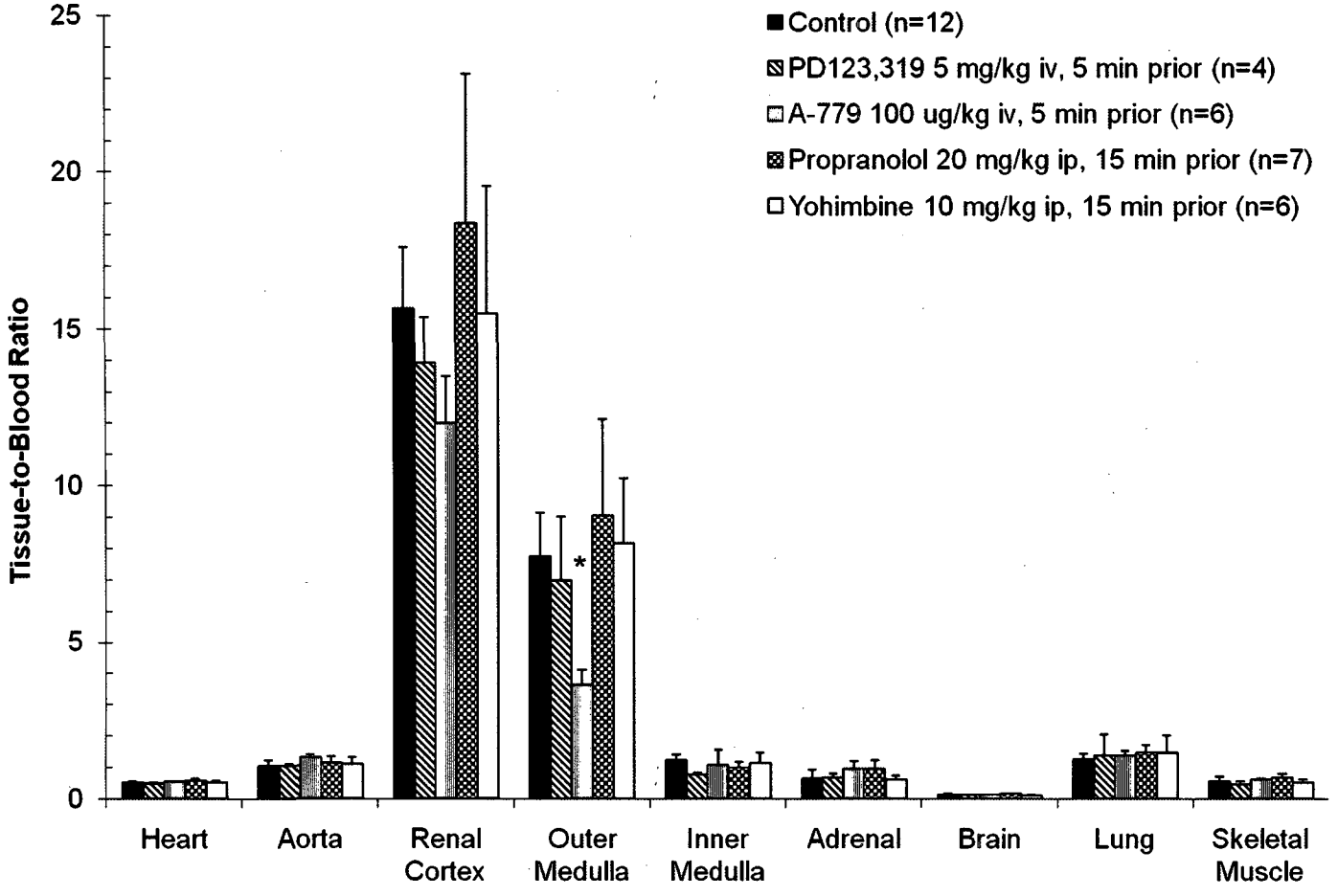

Figure 3.10. Effect of AT_2, Mas, β-adrenergic and α_2-adrenergic receptor antagonists on [^{11}C]TH4 binding 15 minutes post-injection. Data were expressed as mean tissue-to-blood ratio ± standard deviation. Controls received the radiotracer injection iv without pretreatment. Competing drugs were administered as described in the legend. Heart, aorta, renal cortex, outer medulla, inner medulla, adrenals, brain, lung, and skeletal muscle were dissected quickly after decapitation and counted in a gamma counter.

Table 3.3. Percent change in [^{11}C]TH4 tissue-to-blood ratio in AT_1 receptor antagonist treated animals as compared to controls at 15 minutes post-injection. *corresponds to a significant difference ($p<0.05$) in mean tissue-to-blood ratio compared to controls.

Tissue	Control	Candesartan			Losartan	
	(mean±st dev)	3 mg/kg	5 mg/kg	10 mg/kg	20 mg/kg	30 mg/kg
Heart	0.52±0.02	9	4	4	-23*	-25*
Aorta	1.09±0.17	18	12	49	-42	-37
Renal Cortex	15.19±2.31	-47*	-55*	-71*	-73*	-79*
Outer Medulla	6.74±1.86	-72*	-62*	-77*	-77*	-83*
Inner Medulla	1.26±0.24	-26	-55	-43	-47	-58*
Adrenals	0.71±0.29	-17	-32	-32	-14	-47
Brain	0.13±0.02	-4	-6	-7	-39	-65*
Lung	1.22±0.20	19	7	9	-40	-52
Liver	84.66±5.12	-4	-6	-16	-82*	-90*
Skeletal Muscle	0.57±0.15	10	14	0	-45	-58*

Table 3.4. Percent change in [^{11}C]TH4 tissue-to-blood ratio in AT_2, Mas, β-adrenergic and α_2-adrenergic receptor antagonist treated animals as compared to controls at 15 minutes post-injection. *corresponds to a significant difference ($p<0.05$) in mean tissue-to-blood ratio compared to controls.

Tissue	Control	PD123,319	A-779	Propranolol	Yohimbine
	(mean±st dev)	5 mg/kg	100 µg/kg	20 mg/kg	10 mg/kg
Heart	0.52±0.02	-6	2	11	-1
Aorta	1.09±0.17	0	26	8	6
Renal Cortex	15.19±2.31	-11	-23	17	-1
Outer Medulla	6.74±1.86	-10	-53*	17	6
Inner Medulla	1.26±0.24	-38	-12	-20	-8
Adrenals	0.71±0.29	2	43	45	-8
Brain	0.13±0.02	0	8	16	-18
Lung	1.22±0.20	9	11	18	19
Liver	84.66±5.12	-16	-5	-25	-15
Skeletal Muscle	0.57±0.15	-20	6	18	-7

tissues return much closer to baseline: ovaries, heart, pancreas, and spleen. Tissues such as the lungs and adrenals maintain uptake above background until 30 minutes post-injection while kidneys maintain uptake until 60 minutes post-injection. Metabolism related tissues (liver, small intestine contents, and upper and lower intestine contents) generally increased over time. Residence times were generally similar between the sexes (Tables 3.7 and 3.8). The liver, in both sexes, account for more than 40% of the effective dose (ED) and the effective dose equivalent (EDE). Liver is the limiting tissue for both the ED and EDE (Table 3.9). After the liver, the gonads also contributed to the overall ED (12% in males and 7% in females) and EDE (12% in males and 7% in females). Based on the ratio proposed by Jagoda and colleagues (2004), and assuming a 10-fold difference in scanner efficiency between small animal and human scanners, the human injected activity would be 33.3 times greater than that used rat, . All tissue and whole body dose values are below the 3-5 rem safety limits recommended by the Food and Drug Administration, even when the estimated human dose is applied.

3.5. Metabolism

Oasis HLB VAC RC Extraction solid phase (HLB sorbent) was shown to retain 100% of the radioactivity signal in authentic [^{11}C]methyl-candesartan standards (Figure 3.11). When tracer was applied to unaltered control plasma or kidney tissue homogenate (Figure 3.12) HLB sorbent was unable to completely capture authentic [^{11}C]methyl-candesartan. In plasma, up to 55% of the total radioactivity signal was not captured in the initial phase of the study. In kidney, this value was lower but still substantial (17%). Addition of urea has been shown to disrupt plasma protein binding (Hilton et al., 2000)

Table 3.5. Tissue uptake (%ID/g) of [^{11}C]methyl-candesartan for all time points and tissues of female Sprague-Dawley rats (n=3 at all time points) receiving 1.5 mCi (at time of first injection). Gastrointestinal contents were collected from the lower large intestine (LLI), upper large intestine (ULI), and small intestine (SI).

Tissue	5 minutes %ID/g	15 minutes %ID/g	30 minutes %ID/g	60 minutes %ID/g
Brain	0.012±0.005	0.004±0.001	0.006±0.003	0.004±0.001
Thymus	0.052±0.005	0.028±0.003	0.031±0.010	0.017±0.003
Thyroid	0.090±0.020	0.037±0.007	0.114±0.136	0.036±0.022
Breasts	0.077±0.018	0.033±0.011	0.049±0.023	0.026±0.002
Ovaries	0.187±0.049	0.048±0.006	0.050±0.033	0.025±0.006
Uterus	0.072±0.005	0.053±0.023	0.076±0.050	0.038±0.012
Heart	0.244±0.047	0.058±0.001	0.068±0.061	0.022±0.009
Lungs	0.515±0.113	0.127±0.006	0.143±0.136	0.043±0.016
Pancreas	0.206±0.035	0.031±0.006	0.044±0.037	0.024±0.007
Spleen	0.169±0.029	0.030±0.002	0.043±0.038	0.019±0.007
Marrow	0.004±0.003	0.001±0.000	0.001±0.000	0.001±0.000
Bone	0.023±0.008	0.019±0.001	0.011±0.006	0.008±0.001
Adrenals	0.324±0.075	0.111±0.055	0.365±0.497	0.064±0.016
Kidneys	2.569±0.275	1.021±0.182	0.922±0.591	0.279±0.062
Liver	9.102±1.137	7.831±0.583	10.567±1.480	9.644±1.325
Urine	0.145±0.271	0.106±0.054	0.100±0.090	0.544±0.488
LLI contents	0.046±0.015	0.023±0.018	0.041±0.025	0.079±0.058
ULI contents	0.035±0.003	0.035±0.005	0.061±0.014	0.094±0.007
SI contents	0.257±0.018	0.234±0.025	0.377±0.047	0.711±0.129
Stomach contents	0.060±0.072	0.011±0.008	0.132±0.084	0.032±0.032
Blood	0.378±0.110	0.059±0.007	0.143±0.170	0.042±0.020

Table 3.6. Tissue uptake (%ID/g) of [^{11}C]methyl-candesartan for all time points and tissues of male Sprague-Dawley rats (n=3 at all time points) receiving 1.5 mCi (at time of first injection). Gastrointestinal contents were collected from the lower large intestine (LLI), upper large intestine (ULI), and small intestine (SI).

Tissue	5 minutes %ID/g	15 minutes %ID/g	30 minutes %ID/g	60 minutes %ID/g
Brain	0.010±0.005	0.005±0.000	0.005±0.001	0.006±0.004
Thymus	0.035±0.004	0.026±0.001	0.020±0.002	0.027±0.018
Thyroid	0.133±0.057	0.037±0.006	0.024±0.009	0.025±0.013
Testes	0.029±0.020	0.016±0.003	0.015±0.001	0.020±0.010
Heart	0.192±0.052	0.052±0.010	0.031±0.016	0.031±0.022
Lungs	0.387±0.126	0.115±0.020	0.072±0.041	0.052±0.037
Pancreas	0.167±0.056	0.037±0.007	0.023±0.004	0.033±0.021
Spleen	0.151±0.046	0.032±0.006	0.023±0.011	0.026±0.013
Marrow	0.002±0.000	0.001±0.000	0.001±0.000	0.001±0.000
Bone	0.026±0.009	0.021±0.003	0.012±0.008	0.012±0.005
Adrenals	0.352±0.104	0.142±0.020	0.108±0.069	0.051±0.024
Kidneys	2.151±0.366	0.936±0.069	0.396±0.118	0.232±0.176
Liver	5.604±1.105	6.340±0.293	6.495±0.593	7.820±2.278
Urine	0.266±0.391	0.066±0.061	0.041±0.042	0.052±0.004
LLI contents	0.025±0.015	0.014±0.012	0.035±0.016	0.056±0.033
ULI contents	0.025±0.007	0.040±0.008	0.057±0.006	0.112±0.040
SI contents	0.177±0.045	0.162±0.097	0.200±0.011	0.544±0.256
Stomach contents	0.032±0.042	0.006±0.002	0.037±0.020	0.021±0.023
Blood	0.324±0.140	0.061±0.014	0.042±0.023	0.055±0.052

Table 3.7. Residence times (Bq-h/Bq) of [^{11}C]methyl-candesartan in rats. Gastrointestinal contents were collected from the lower large intestine (LLI), upper large intestine (ULI), and small intestine (SI).

Tissue	Males Bq-h/Bq	Females Bq-h/Bq
Brain	6.183×10^{-5}	6.871×10^{-5}
Thymus	6.135×10^{-5}	4.109×10^{-5}
Thyroid	6.245×10^{-5}	7.199×10^{-6}
Testes	1.101×10^{-4}	-
Breasts	-	1.903×10^{-5}
Ovaries	-	4.029×10^{-5}
Uterus	-	3.109×10^{-5}
Heart	3.536×10^{-4}	3.273×10^{-4}
Lungs	1.715×10^{-4}	9.970×10^{-5}
Pancreas	1.743×10^{-4}	9.248×10^{-5}
Spleen	2.259×10^{-4}	1.348×10^{-4}
Marrow	4.558×10^{-6}	6.547×10^{-6}
Bone	1.503×10^{-5}	1.342×10^{-5}
Adrenals	2.425×10^{-5}	5.068×10^{-5}
Kidneys	1.381×10^{-2}	1.116×10^{-2}
Liver	3.290×10^{-2}	5.771×10^{-2}
Urine	2.037×10^{-6}	1.543×10^{-6}
LLI contents	1.537×10^{-4}	2.521×10^{-4}
ULI contents	5.170×10^{-4}	7.586×10^{-4}
SI contents	1.990×10^{-3}	7.946×10^{-3}
Stomach contents	9.383×10^{-5}	6.393×10^{-5}
Blood	6.072×10^{-4}	7.800×10^{-4}
Remainder	3.201×10^{-1}	3.069×10^{-1}

Table 3.8. Residence times (Bq-h/Bq) of [^{11}C]methyl-candesartan in humans calculated from rat data. Gastrointestinal contents were collected from the lower large intestine (LLI), upper large intestine (ULI), and small intestine (SI). In the OLINDA/EXM software, heart is considered 'heart wall', urine is termed 'urinary bladder contents', and blood is termed 'heart contents'.

Tissue	Males Bq-h/Bq	Females Bq-h/Bq
Brain	1.610×10^{-4}	1.898×10^{-4}
Thymus	8.150×10^{-6}	9.933×10^{-6}
Thyroid	2.870×10^{-5}	8.279×10^{-6}
Testes	1.068×10^{-5}	-
Breasts	-	1.978×10^{-4}
Ovaries	-	1.281×10^{-5}
Uterus	-	5.450×10^{-5}
Heart Wall	4.864×10^{-4}	4.788×10^{-4}
Lungs	2.297×10^{-3}	2.281×10^{-3}
Pancreas	1.152×10^{-4}	9.674×10^{-5}
Spleen	1.950×10^{-4}	1.800×10^{-4}
Red Marrow	1.193×10^{-5}	1.798×10^{-5}
Cortical Bone	4.6432×10^{-4}	3.7808×10^{-4}
Trabecular Bone	1.1608×10^{-4}	9.4520×10^{-5}
Adrenals	2.305×10^{-5}	3.109×10^{-5}
Kidneys	7.872×10^{-3}	8.367×10^{-3}
Liver	1.939×10^{-1}	3.016×10^{-1}
Urinary Bladder Contents	3.696×10^{-5}	2.537×10^{-4}
LLI Contents	1.352×10^{-4}	2.846×10^{-4}
ULI Contents	2.729×10^{-4}	4.048×10^{-4}
SI Contents	1.443×10^{-3}	6.084×10^{-3}
Stomach contents	5.459×10^{-5}	7.219×10^{-5}
Heart contents	1.207×10^{-3}	1.553×10^{-3}
Remainder	2.782×10^{-1}	2.632×10^{-1}

Table 3.9. Effective dose equivalent (EDE) and effective dose (ED) for [^{11}C]methyl-candesartan in humans. EDE and ED were calculated from the MIRD method and ICRP protocols 60 and 80 using OLINDA/EXM software.

	Effective Dose Equivalent mSv/MBq	Effective Dose mSv/MBq
Male	4.8×10^{-3}	3.6×10^{-3}
Female	7.7×10^{-3}	5.9×10^{-3}
Average	6.2×10^{-3}	4.8×10^{-3}

and this reduced lost radioactivity to less than 2% in plasma and kidney samples (Table 3.10; Figure 3.13).

Four total peaks were observed in HPLC chromatograms (Table 3.11, 3.12; Figure 3.14). Any radioactivity not trapped by the capture column and hydrophilic metabolites eluting in the initial phase of the study were designated peak 1. The peaks eluting after the column switch were any metabolites retained by the capture column as well as unchanged [^{11}C]methyl-candesartan. Peaks 2 and 3 eluted at 3.73 and 6.96 minutes post-switch respectively and corresponded to hydrophilic metabolites. The final peak (peak 4) at 15.77 minutes post-switch was unchanged [^{11}C]methyl-candesartan. In samples with authentic [^{11}C]TH4 added, peak 3 co-eluted with the [^{11}C]TH4 peak (Figure 3.15).

In injected rat plasma samples, the proportion of radioactivity not captured (peak 1) did not change over any time point tested (Table 3.12). Peak 2 was observed as a very small proportion of the total radioactivity in injected rat plasma or control plasma samples and did not vary over time. The total proportion of radioactivity of peak 3, as with the previous 2 peaks, was generally similar over all time points (3, 15 and 20 minutes) only increasing slightly but not significantly over time (1.26% at 3 minutes to 4.17% at 20 minutes). Peak 4, unchanged [^{11}C]methyl-candesartan, decreases slightly from 3 to 20 minutes (95.23% and 90.98% respectively). Overall, the proportions of total radioactivity for the 4 peaks in rat plasma samples varied only slightly with time.

Rat kidney homogenate samples displayed more variation than observed in plasma samples (Table 3.12). Kidney samples had a smaller proportion of unretained radioactivity (0.96-1.95%) compared to plasma samples (3.37-4.80%). Peak 2 is

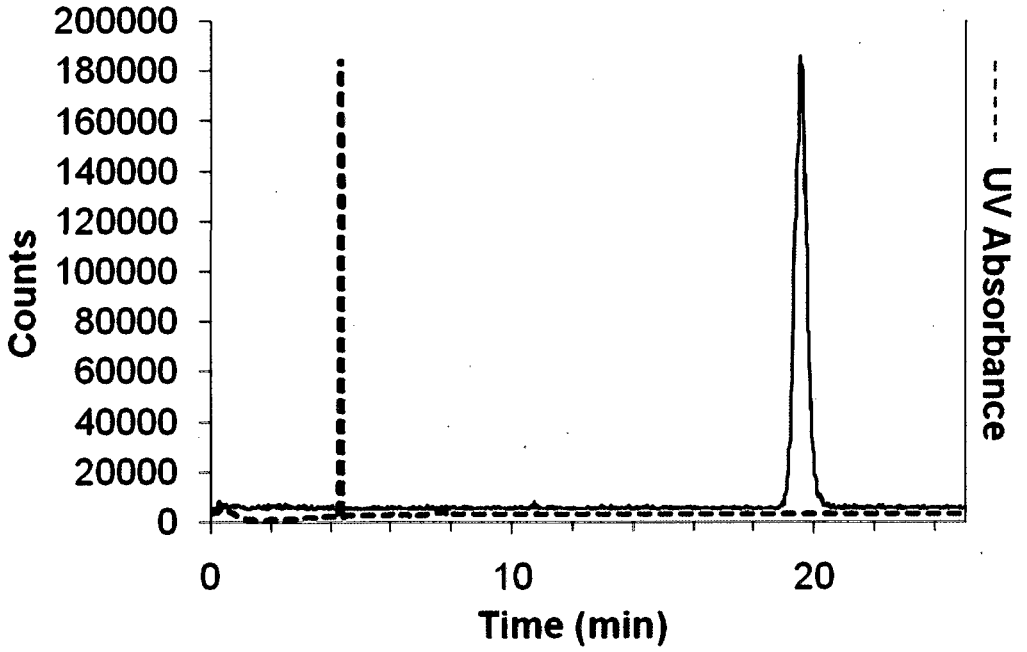

Figure 3.11. A sample chromatogram depicting the radioactive peaks with the injection of authentic [^{11}C]methyl-candesartan standard. Columns and solvents were switched at 4.0 minutes.

A

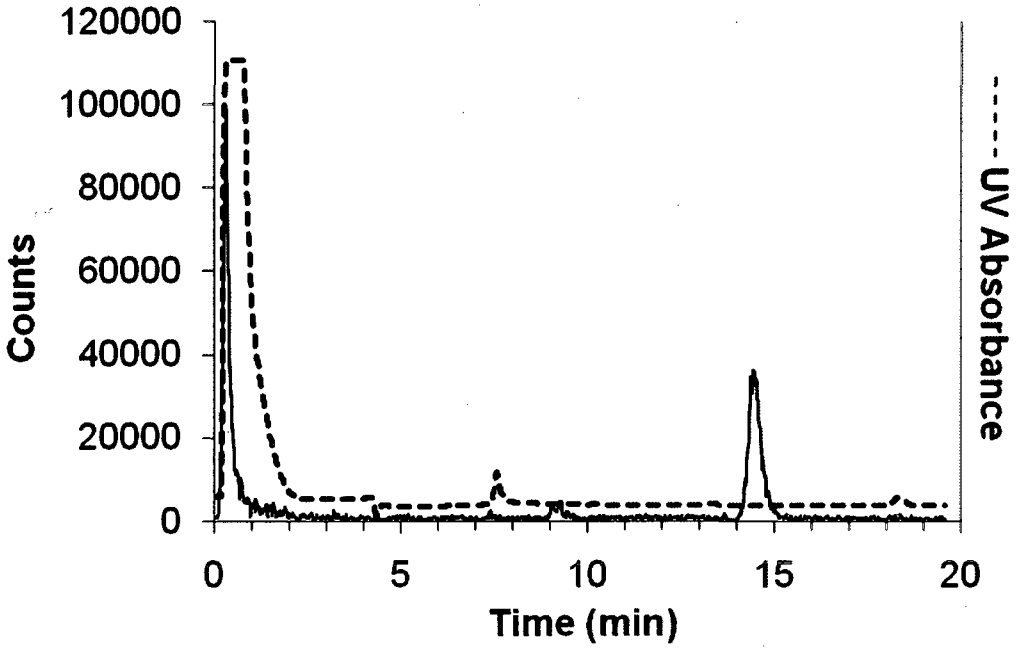

B

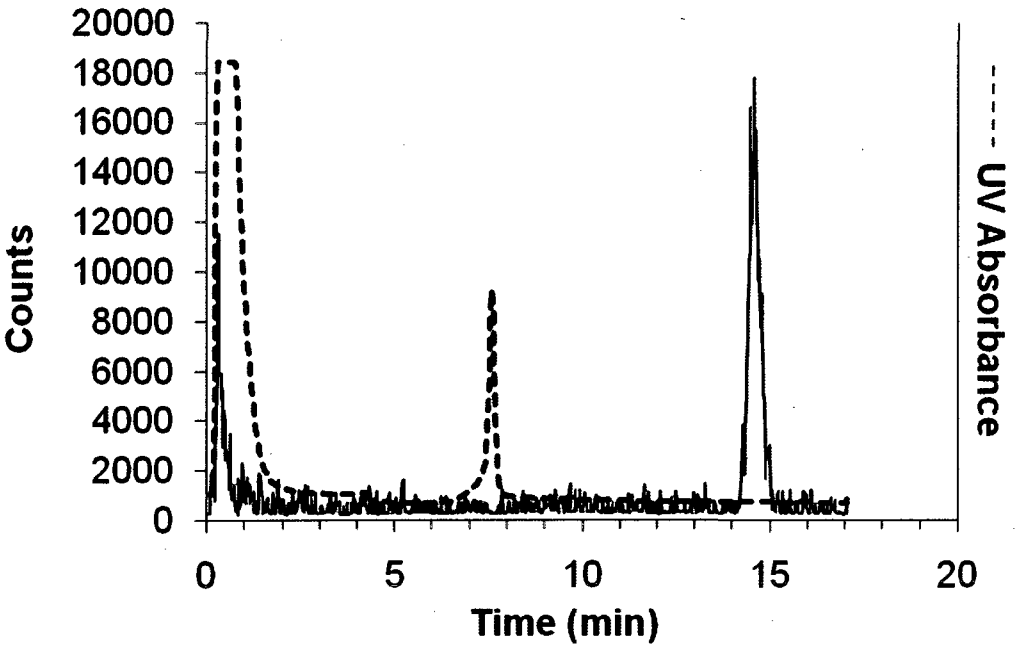

Figure 3.12. A sample chromatogram depicting the radioactive peaks with the injection of rat plasma (A) or kidney homogenate (B), spiked with authentic [^{11}C]methyl-candesartan prior to processing. Columns and solvents were switched at 4.01 and 4.04 minutes for plasma and kidney samples respectively.

A

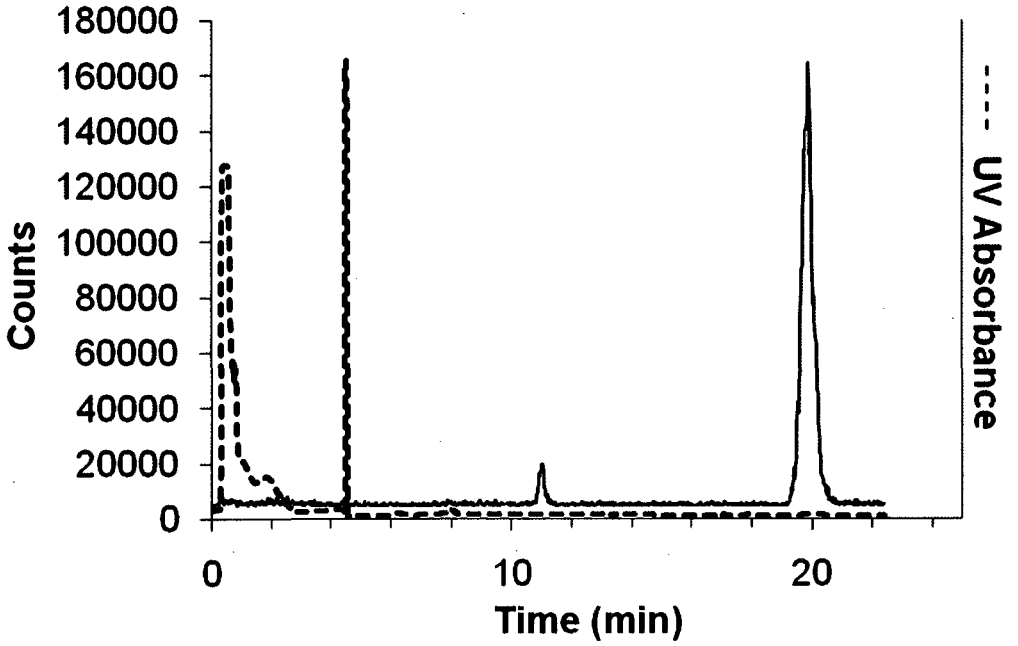

B

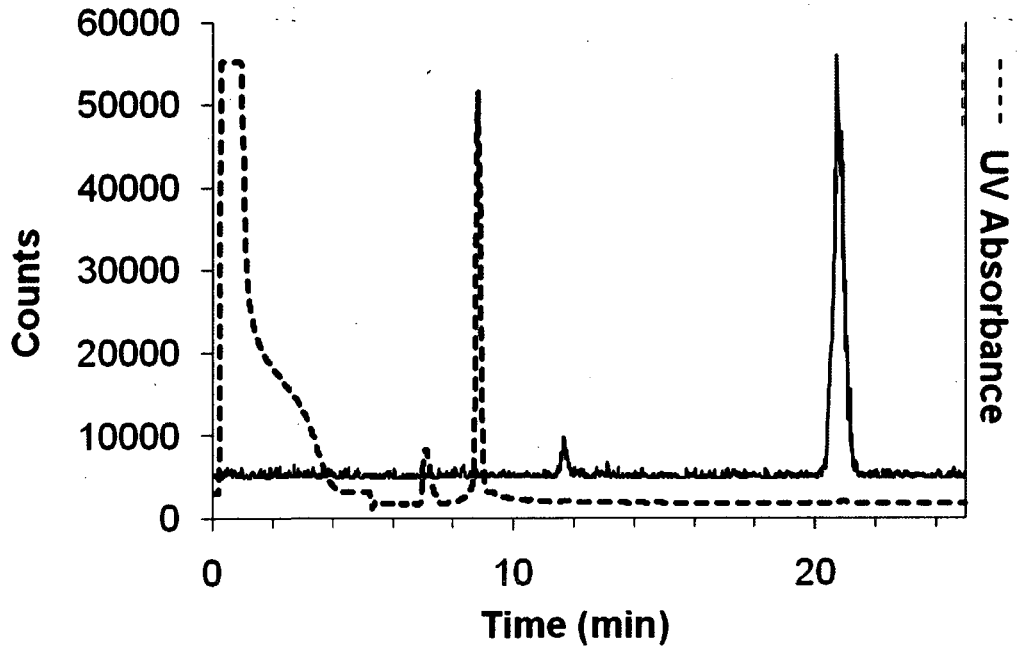

Figure 3.13. A sample chromatogram depicting the radioactive peaks with the injection of rat plasma (A) or kidney homogenate (B), spiked with authentic [^{11}C]methyl-candesartan prior to processing. Urea at 1.0 and 0.4 g/ml was added to plasma and kidney samples respectively to disrupt plasma protein binding. Columns and solvents were switched at 4.2 and 5.0 minutes for plasma and kidney samples respectively.

Table 3.10. Percent of total radioactivity signal for unretained radioactivity (Peak 1) in plasma and kidney samples from processing with and without urea.

Concentration Urea	Plasma	Kidney
0 g/mL	45.9%	18.3%
0.4 g/mL	16.6%	1.2%
1.0 g/mL	1.7%	n.d.

Table 3.11. Mean retention times (± standard deviation) of each radioactivity signal peak in [^{11}C]methyl-candesartan control and injected rat plasma and kidney homogenate samples. All times are after the flow switch. Peak 1 (unretained radioactivity) elution occurs prior to the flow-switch, thus retention time is not applicable (n.a.). Peak 2 and 3 are hydrophilic metabolites and peak 4 is unchanged [^{11}C]methyl-candesartan.

	Peak 1	Peak 2	Peak 3	Peak 4
Retention Time (min)	n.a.	3.73 ± 0.06	6.96 ± 0.20	15.77 ± 0.30

Table 3.12. Mean proportion of the radioactivity signal (± standard deviation) from chromatograms of [^{11}C]methyl-candesartan rat plasma and kidney homogenate samples. Noise and decay corrections were applied. Peak 1 is unretained radioactivity. Peak 2 and 3 are hydrophilic metabolites and peak 4 is unchanged [^{11}C]methyl-candesartan.

	Peak 1	Peak 2	Peak 3	Peak 4
Control Plasma	1.73±2.77	0.03±0.08	1.45±1.42	96.9±3.37
3 min Plasma	3.37±3.22	0.14±0.28	1.26±0.97	95.23±2.74
15 min Plasma	4.80±3.22	2.23±2.58	1.91±1.98	91.05±6.83
20 min Plasma	4.32±3.99	0.52±0.91	4.17±4.83	90.98±8.68
Control Kidney	1.17±1.89	0.0±0.0	2.63±1.86	96.20±3.54
3 min Kidney	1.95±0.63	0.41±0.17	6.79±1.20	90.86±1.00
15 min Kidney	0.78±0.92	6.16±3.90	22.35±7.93	70.71±10.12
20 min Kidney	0.96±1.11	4.99±4.41	26.22±15.21	65.83±18.63

A

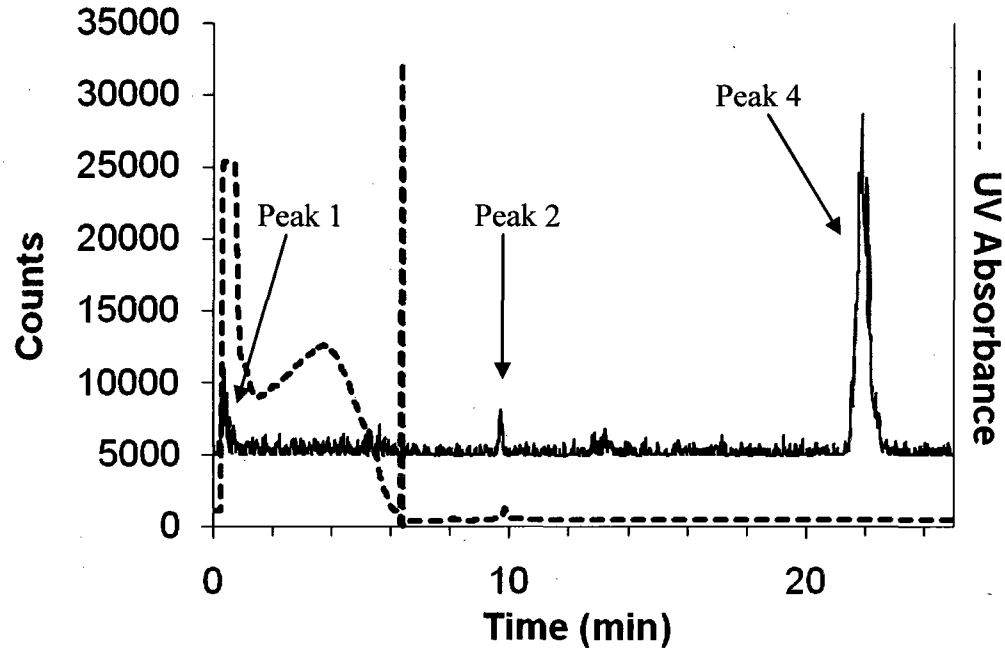

B

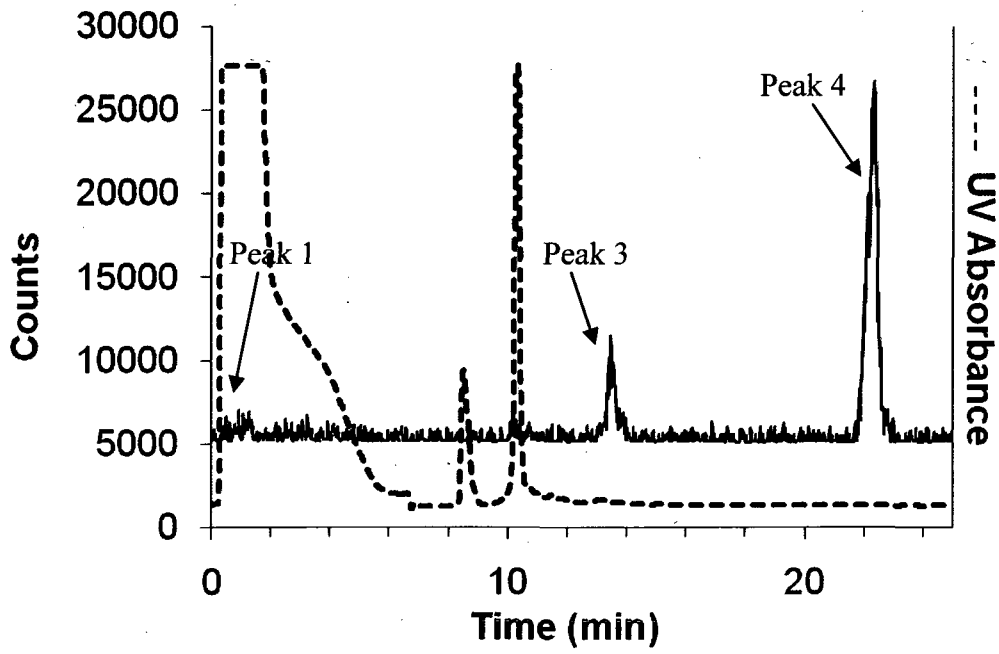

Figure 3.14. A sample chromatogram depicting the radioactive peaks with the injection of rat plasma (A) or kidney homogenate (B), 20 minutes following [^{11}C]methyl-candesartan injection. Columns and solvents were switched at 6.1 and 6.4 minutes for plasma and kidney samples respectively.

A

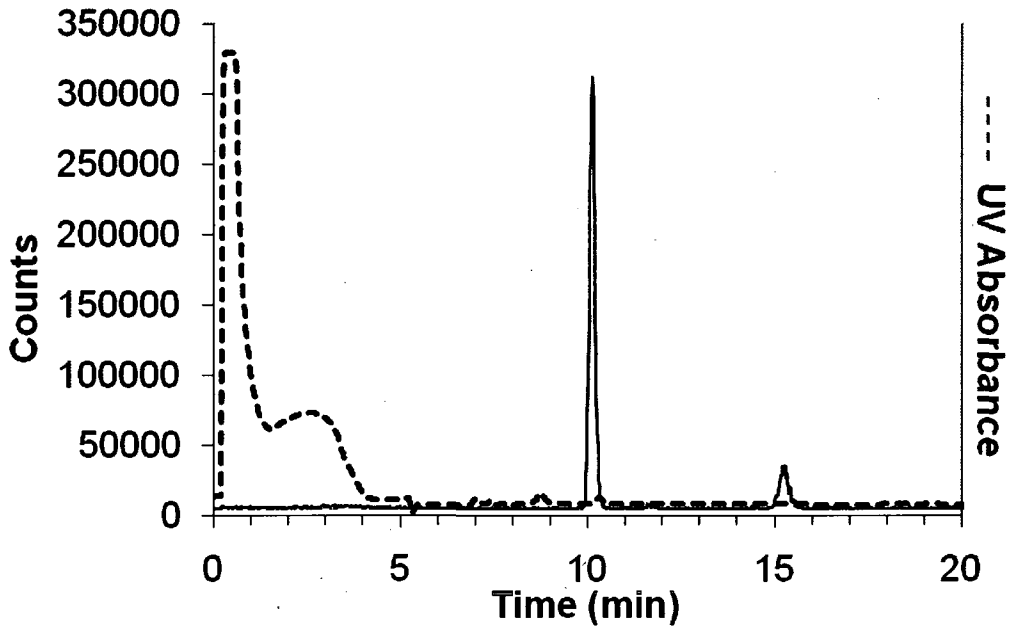

B

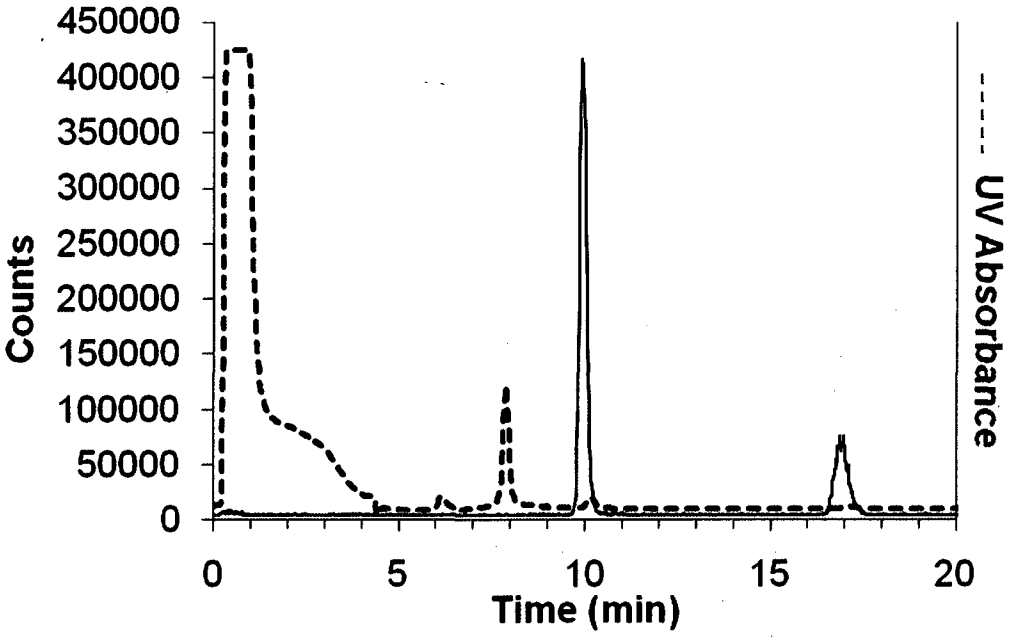

Figure 3.15. A sample chromatogram depicting the radioactive peaks with the injection of rat plasma (A) or kidney homogenate (B), 15 minutes following [^{11}C]methyl-candesartan injection and spiked with authentic [^{11}C]TH4 prior to processing. Columns and solvents were switched at 5.0 and 4.05 minutes for plasma and kidney samples respectively.

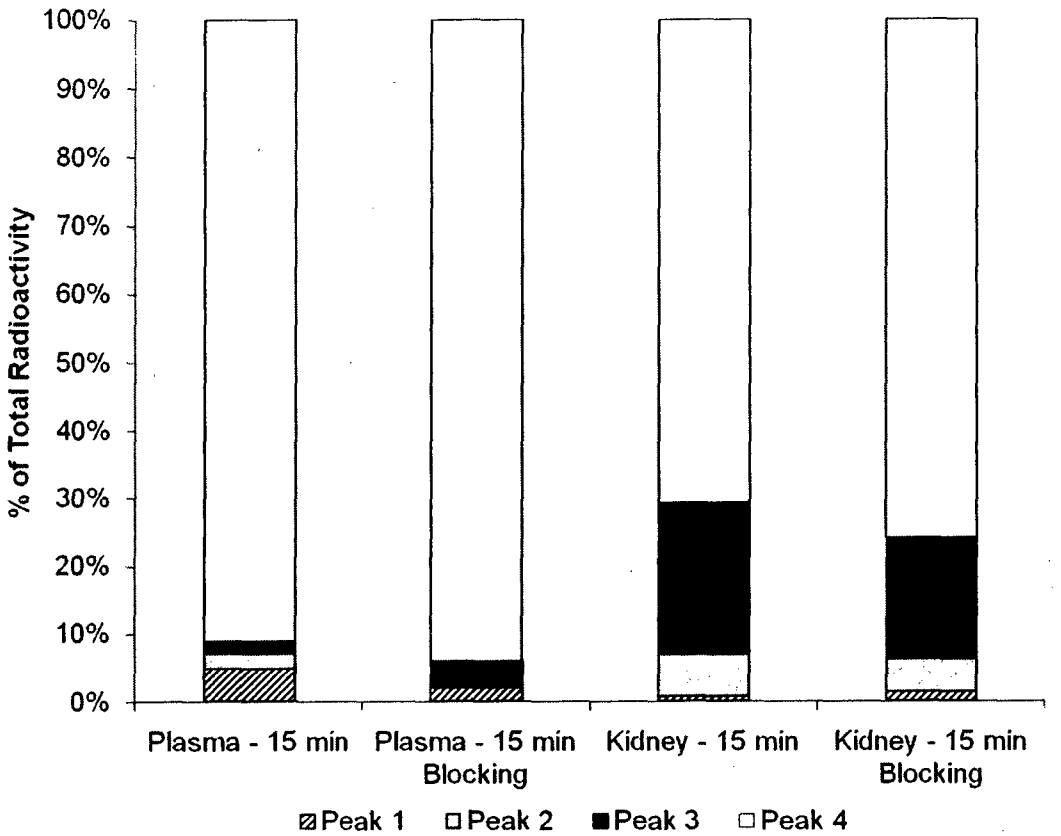

Figure 3.16. Proportion of total radioactivity for all metabolite peaks in plasma and kidney at 15 minutes post-injection in control and candesartan (5 mg/kg) blocked rats. Peak 1 is unretained radioactivity. Peak 2 and 3 are hydrophilic metabolites and peak 4 is unchanged [^{11}C]methyl-candesartan.

A

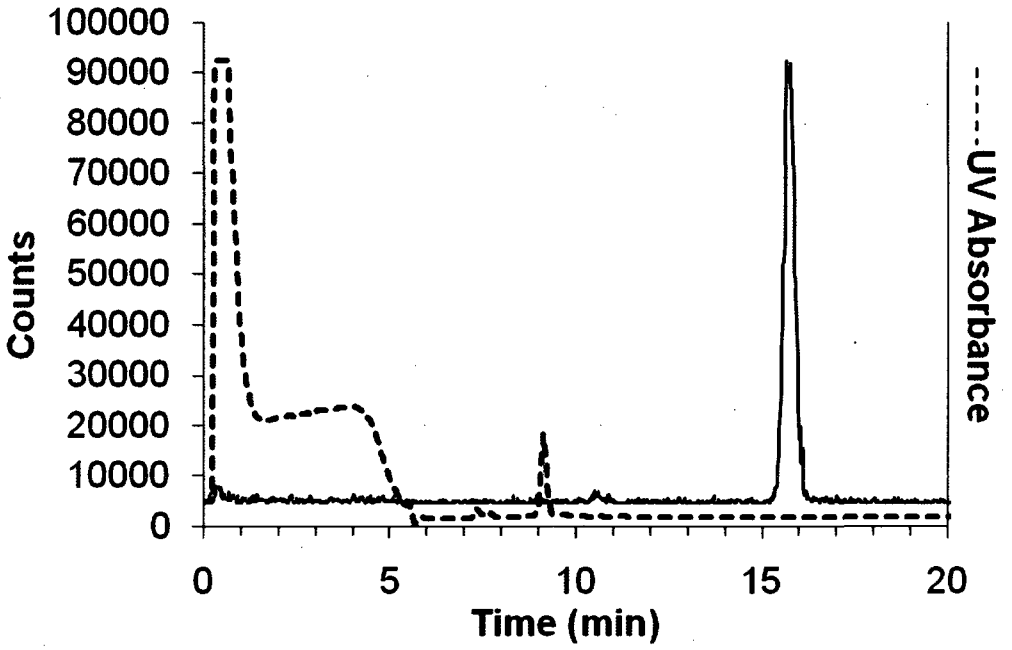

B

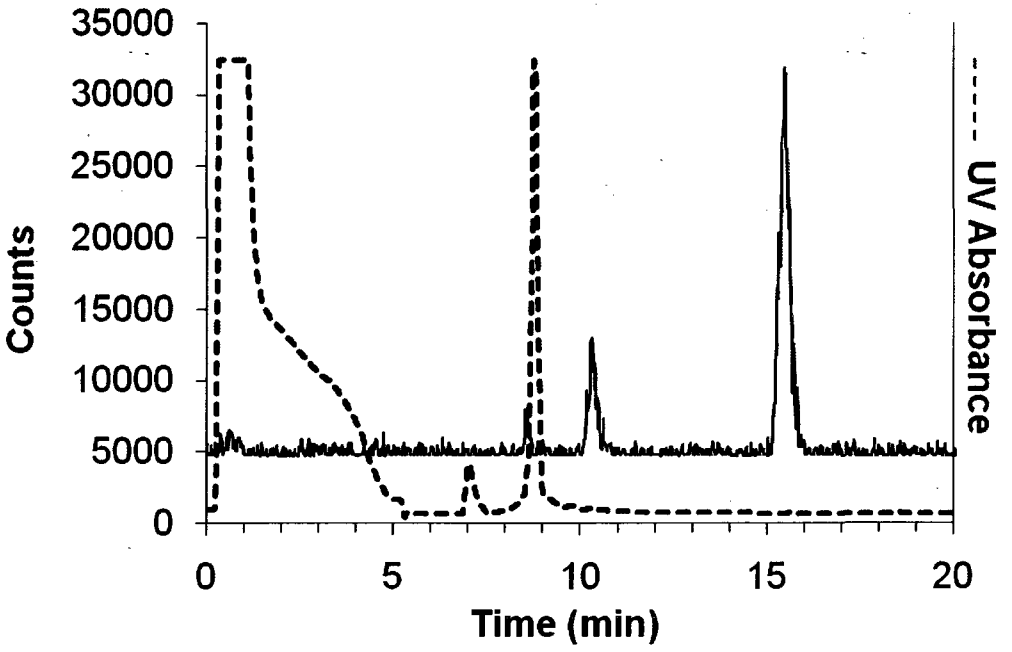

Figure 3.17. A sample chromatogram depicting the radioactive peaks with the injection of rat plasma (A) or kidney homogenate (B), 15 minutes following a co-injection of 5 mg/kg candesartan and [^{11}C]methyl-candesartan. Columns and solvents were switched at 5.3 and 5.0 minutes for plasma and kidney samples respectively.

observed as a small proportion of the total radioactivity, slightly higher than in injected plasma samples, increasing marginally over time. The proportions of radioactivity measured for peak 3 increased much more over time (6.79% at 3 minutes to 26.22% at 20 minutes) and appeared at levels higher than in plasma samples. Unchanged [^{11}C]methyl-candesartan proportions decreased from 90.86% at 3 minutes to 65.83% at 20 minutes. Rat plasma and kidney samples for rats injected with tracer alone at 15 minutes post-injection and rats co-injected with tracer and 5 mg/kg candesartan were compared. Chromatograms between these two groups were quite similar as well as the proportion of radioactivity for each of the observed peaks (Figure 3.16, 3.17).

3.6. Small Animal PET Studies

3.6.1. Initial Condition Optimization

Initial scans (Figures 3.18-3.19) at injected activities varying from 0.4-2.4 mCi produced images of sufficient quality to allow for creation of ROIs and produce time activity as well as DV data. It was found that approximately 2 mCi (or more up to 2.9 mCi tested) of injected activity, however, produced images that were of higher quality and more easily analyzed. An injected activity of 2 mCi was therefore employed as the ideal threshold of injected activity for all studies. Since they are the target organs, kidneys were used as the ROI to determine reproducibility. Serial scans in the same animal generated reproducible results in normal rats (Table 3.13) such that only a small number of rats were needed in treatment groups.

Assessment of scan parameters, using the kidneys as the ROI, determined that neither injected mass, specific activity, injected activity, nor injected dose impacted on the DV values over the ranges tested (Figures 3.20-3.24; Table 3.14). Generated DV

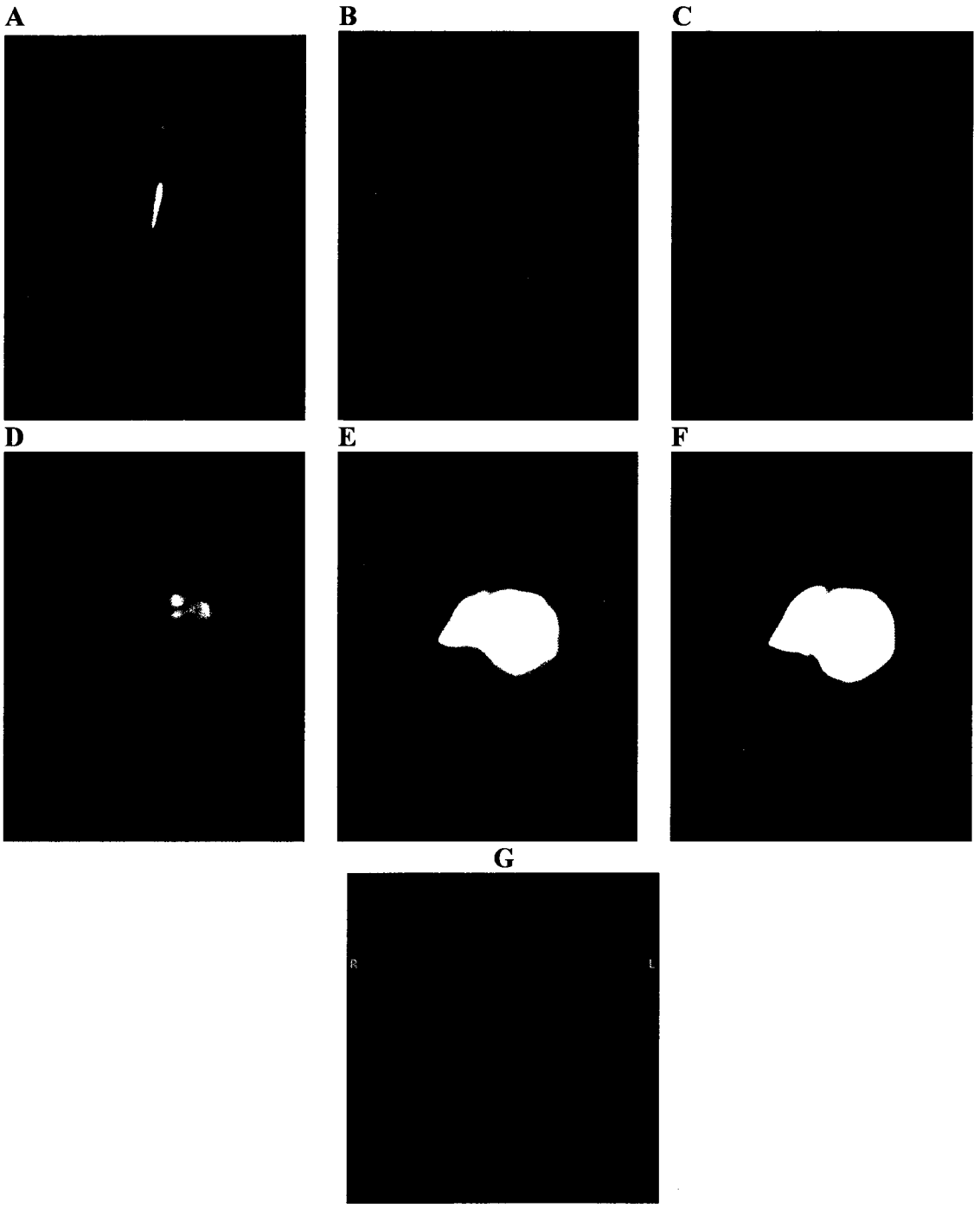

Figure 3.18. (A-F) Sample images from a control scan at (A) 20-30 seconds, (B) 50-60 seconds, (C) 80-90 seconds, (D) 2-3 minutes, (E) 5-10 minutes, and (F) 55-60 minutes post-injection. (G) A coronal slice of a control scan image at 2-3 minutes post-injection showing liver and kidney uptake.

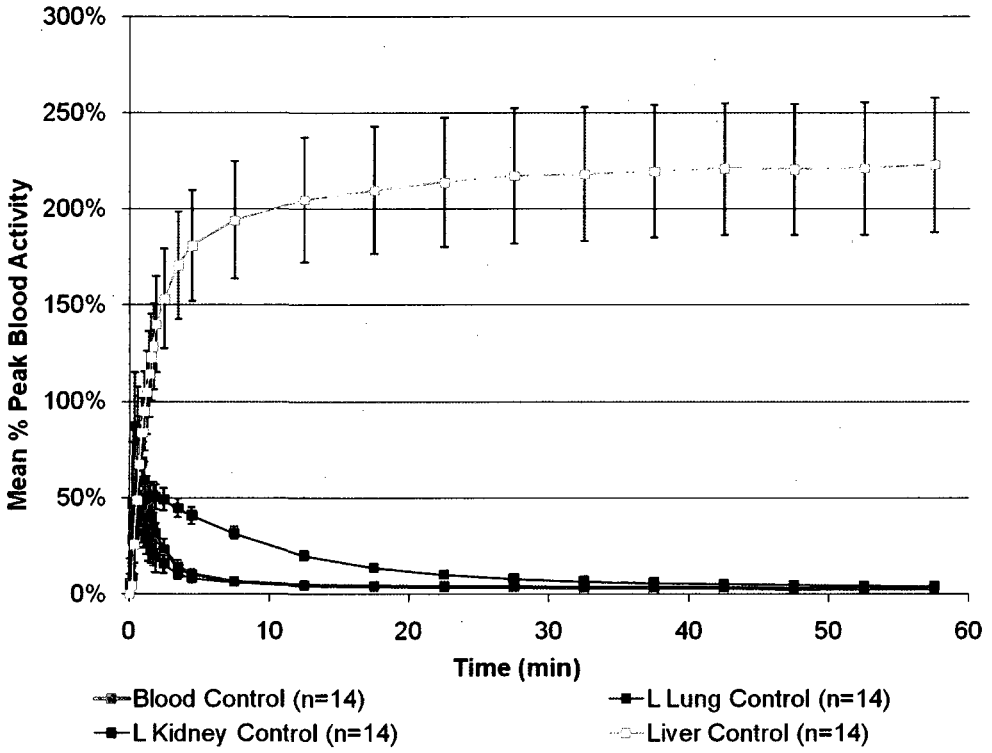

Figure 3.19. Mean percent of peak blood activity over time (± standard deviation) in control rats (n=14) in blood, left kidney, left lung, and liver.

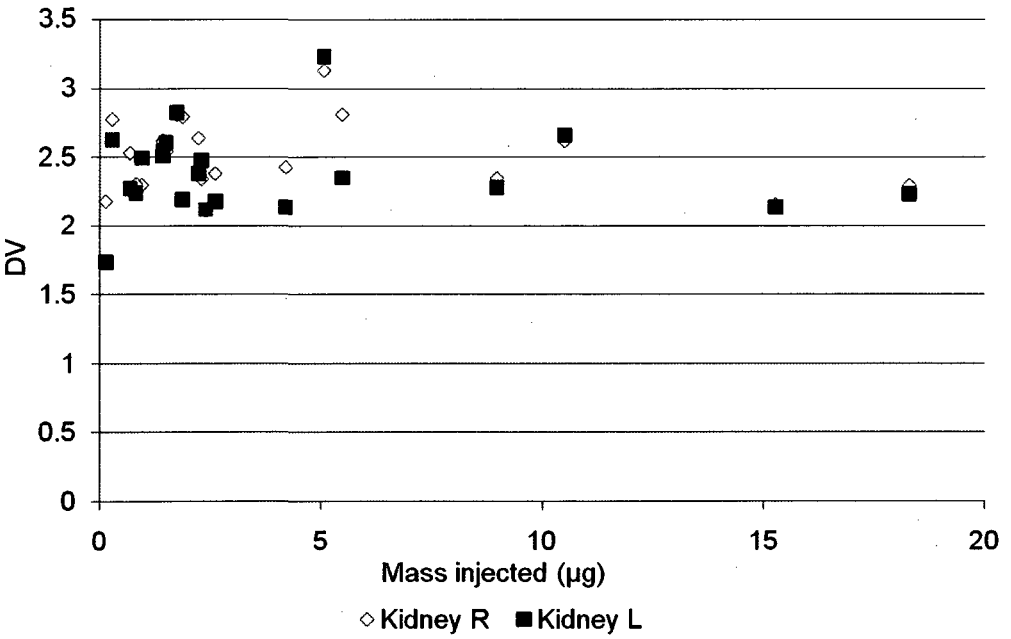

Figure 3.20. Calculated DV values in the right and left kidney over mass (µg) of methyl-candesartan injected. The LA region was considered the 'whole blood' input. No corrections for plasma to blood activity were applied for the initial analyses. No effect of injected mass on DV value was observed.

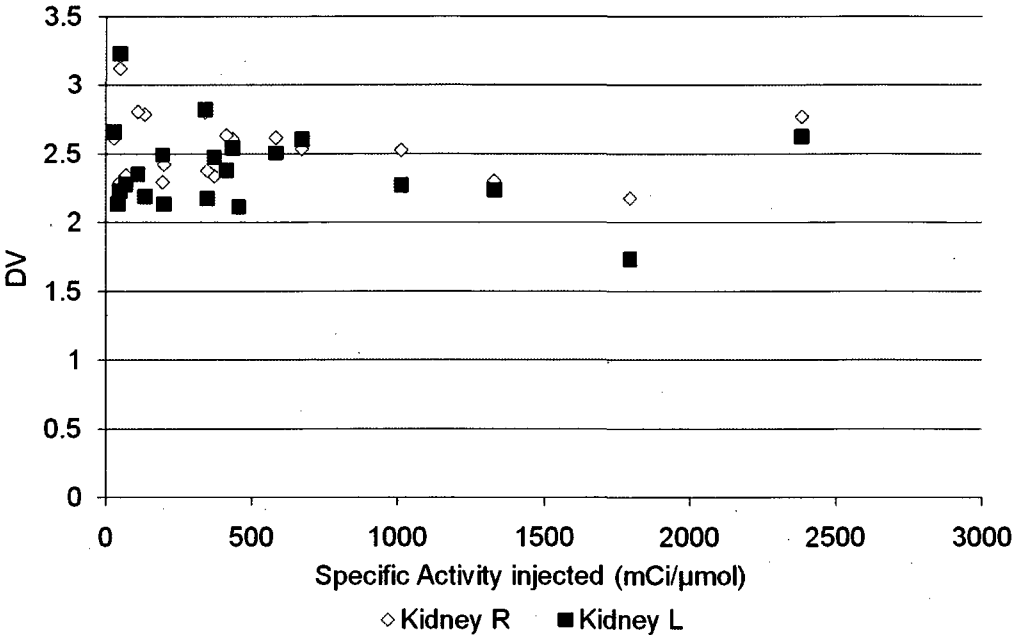

Figure 3.21. Calculated DV values in the right and left kidney over specific activity (mCi/µmol) injected. The LA region was considered the 'whole blood' input. No corrections for plasma to blood activity were applied for the initial analyses. No effect of specific activity on DV value was observed.

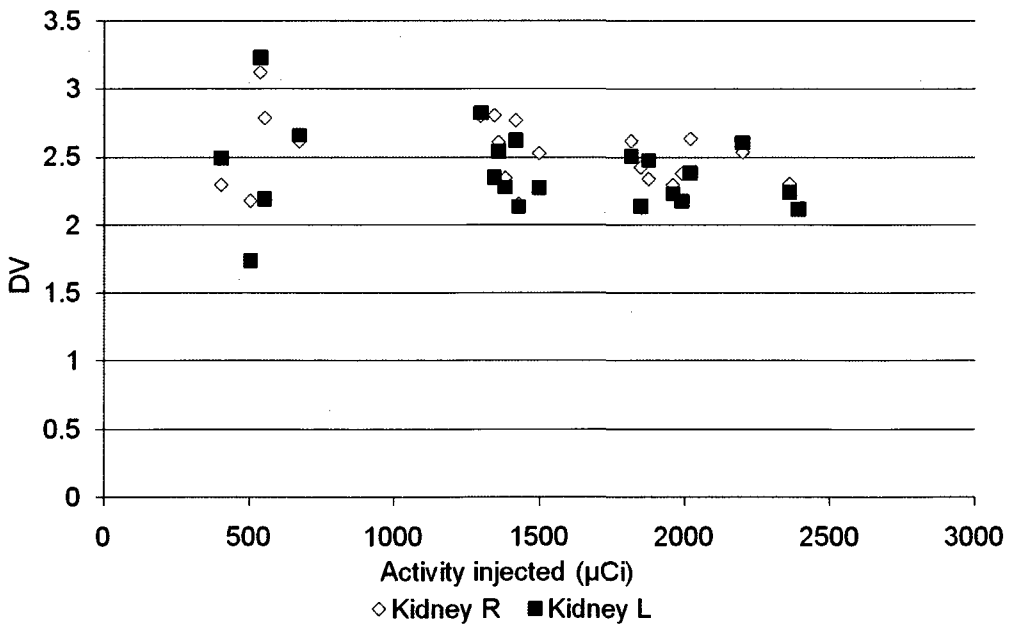

Figure 3.22. Calculated DV values in the right and left kidney over activity (µCi) injected. The LA region was considered the 'whole blood' input. No corrections for plasma to blood activity were applied for the initial analyses. No effect of injected activity on DV value was observed.

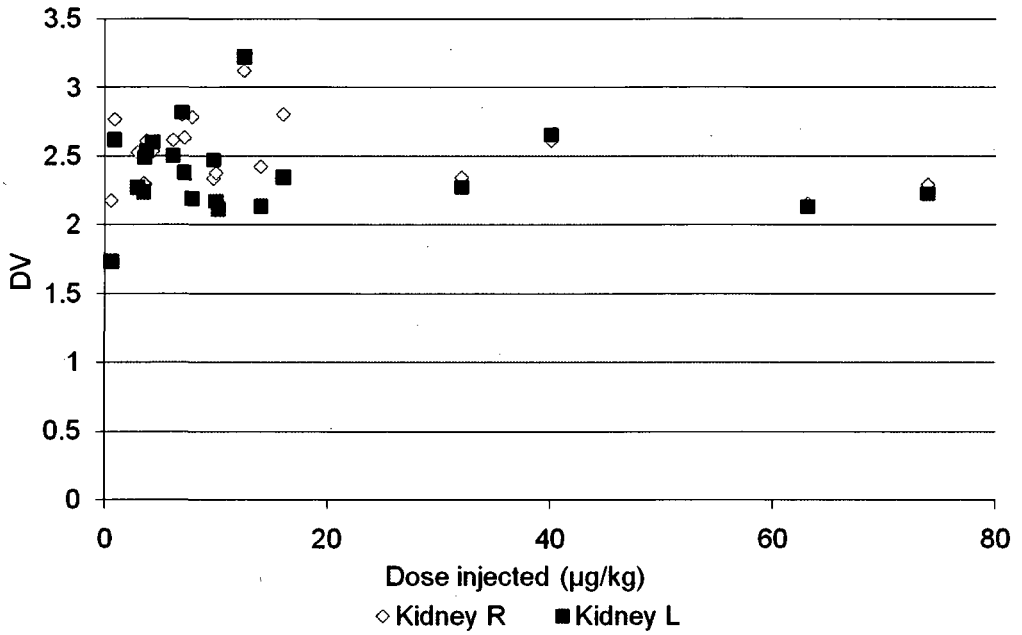

Figure 3.23. Calculated DV values in the right and left kidney over dose (µg/kg) of methyl-candesartan injected. The LA region was considered the 'whole blood' input. No corrections for plasma to blood activity were applied for the initial analyses. No effect of injected dose on DV value was observed.

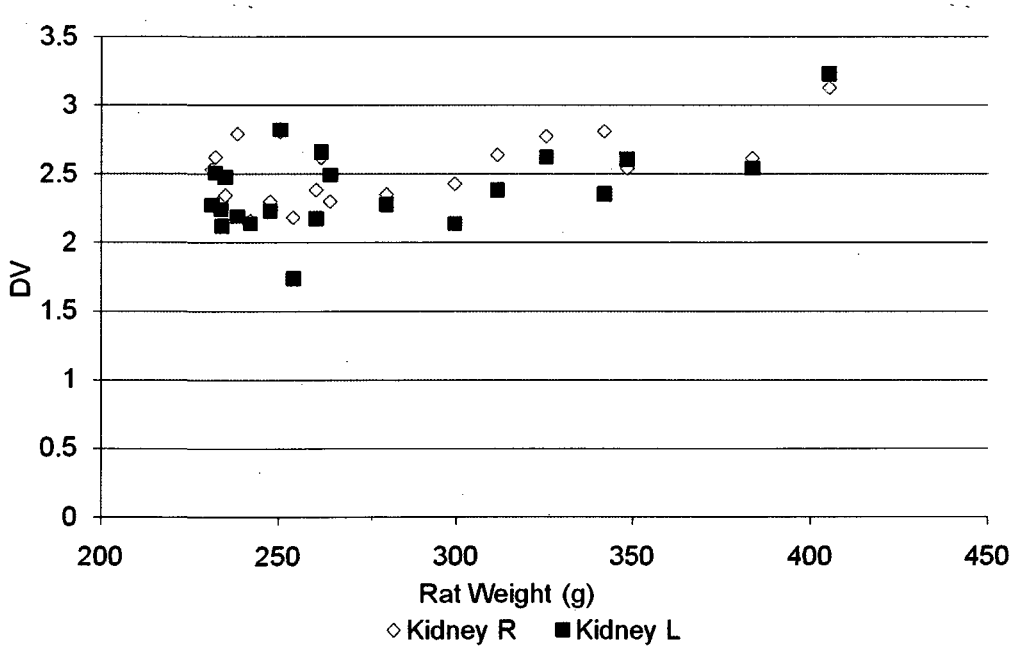

Figure 3.24. Calculated DV values in the right and left kidney over rat weight (g). The LA region was considered the 'whole blood' input. No corrections for plasma to blood activity were applied for the initial analyses. No effect of rat mass on DV value was observed.

Table 3.13. Mean DV values of the left kidney of serially scanned rats and the overall control group.

	All Controls DV	Control Scan 1 DV	Control Scan 2 DV	Absolute Difference Scan 1-2
Mean	2.32	2.04	2.12	0.28
Standard Deviation	0.27	0.25	0.30	0.21

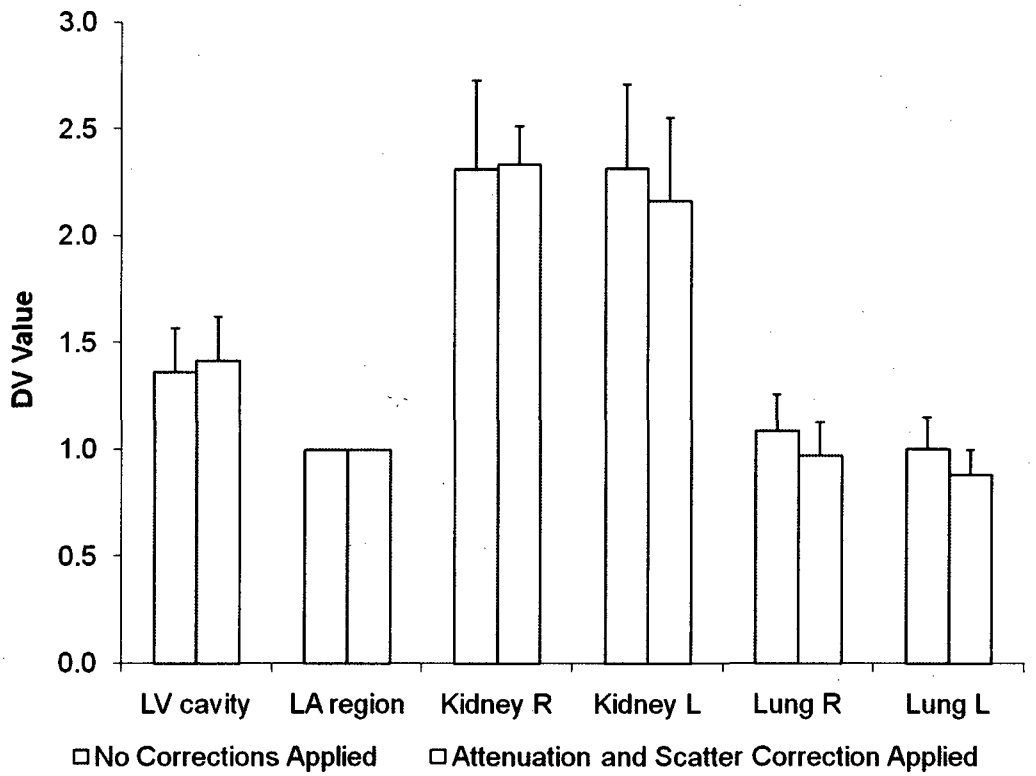

Figure 3.25. Mean calculated DV values (± standard deviation) of 3 control scan images with and without corrections for attenuation and scatter applied to the reconstructions.

Table 3.14. R-squared values for correlations between scan parameters and the generated DV value. Correlations were analyzed by simple linear regression.

DV vs.	Injected activity	Specific activity	Injected mass	Injected dose	Rat weight
R^2	8.04×10^{-4}	0.271	9.02×10^{-5}	5.74×10^{-4}	0.0167
p-value	0.923	0.057	0.974	0.935	0.660

values from images with applied corrections for scatter and attenuation were generally less than those of the uncorrected images (to a maximum of 15%) but overall variation was dampened (Figure 3.25). Application of attenuation and scatter correction in small animal imaging is used frequently (Kim et al., 1996; Zober et al., 2006) and in light of the overall decrease in variability these corrections were applied for all scans.

3.6.2. Plasma Activity Correction

Five rats were injected with [^{11}C]methyl-candesartan and blood was collected. Of those five rats, one rat was excluded due to an interstitial injection. When plotted over time, the blood and plasma activity per mg curves had very similar shapes for the four remaining rats (Figure 3.26). The ratio of the activity per mg in plasma to that of the blood remained unchanged over time and between rats (Figure 3.27). Based on this constant trend, an average ratio was calculated from all time points. The mean ratio of 1.58 was applied as a correction factor for the plasma input in calculation of DV values from scan images in control and treated groups.

3.6.3. Time Course and Biodistribution

Time activity curves of the control scans (Figure 3.18-3.19) show similar trends to those of the *ex vivo* time course studies (section 3.1): the liver showed highest retention at all time points followed by the kidney and lungs. In the initial time frames (0-120s) vasculature, heart cavities, lungs, liver and kidneys were visualized (Figure 3.18). Uptake in later frames was only maintained however in the kidneys and liver. Time activity curves in treatment groups (candesartan and PD123,319; Figures 3.28-3.32) were very similar to the control group in the blood, lungs, and liver. In rats treated with

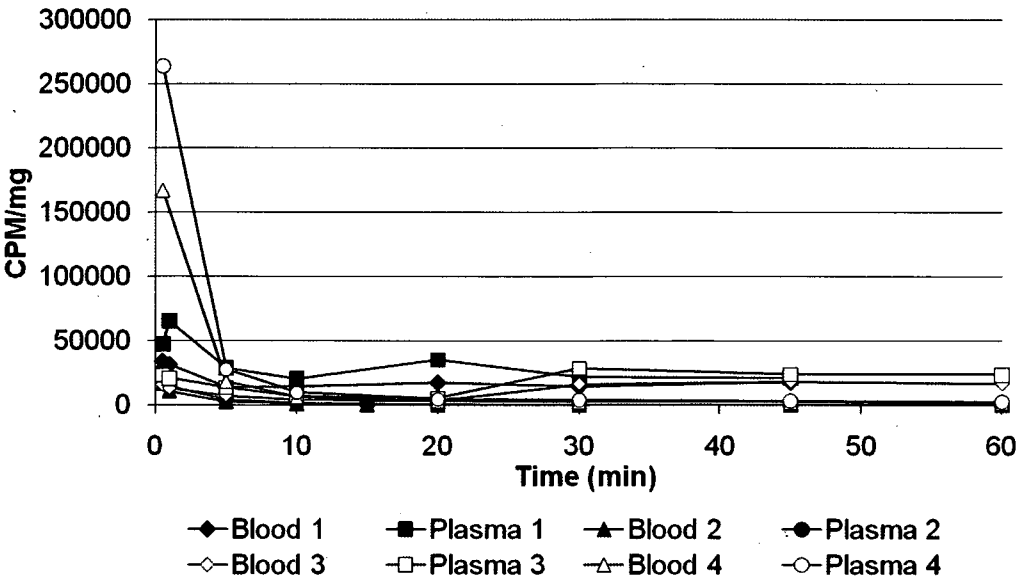

Figure 3.26. Activity (CPM/mg) over 60 minutes for the whole blood and the plasma fraction from rats receiving 2 mCi of [^{11}C]methyl-candesartan immediately prior to sampling.

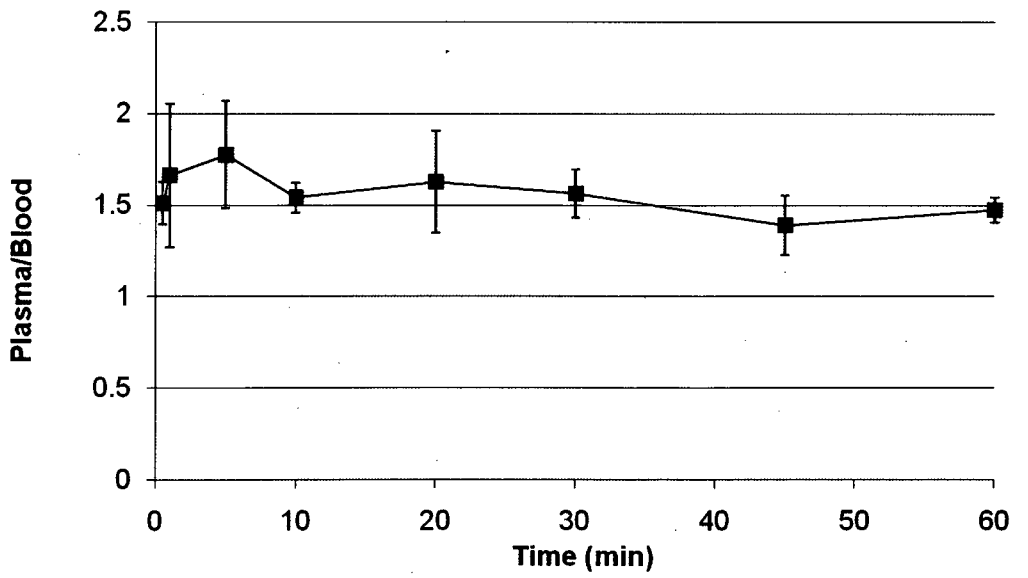

Figure 3.27. Mean ratio for plasma to blood activity per mg (± standard deviation) for the full 60 minutes of sampling. At each time point n≥3.

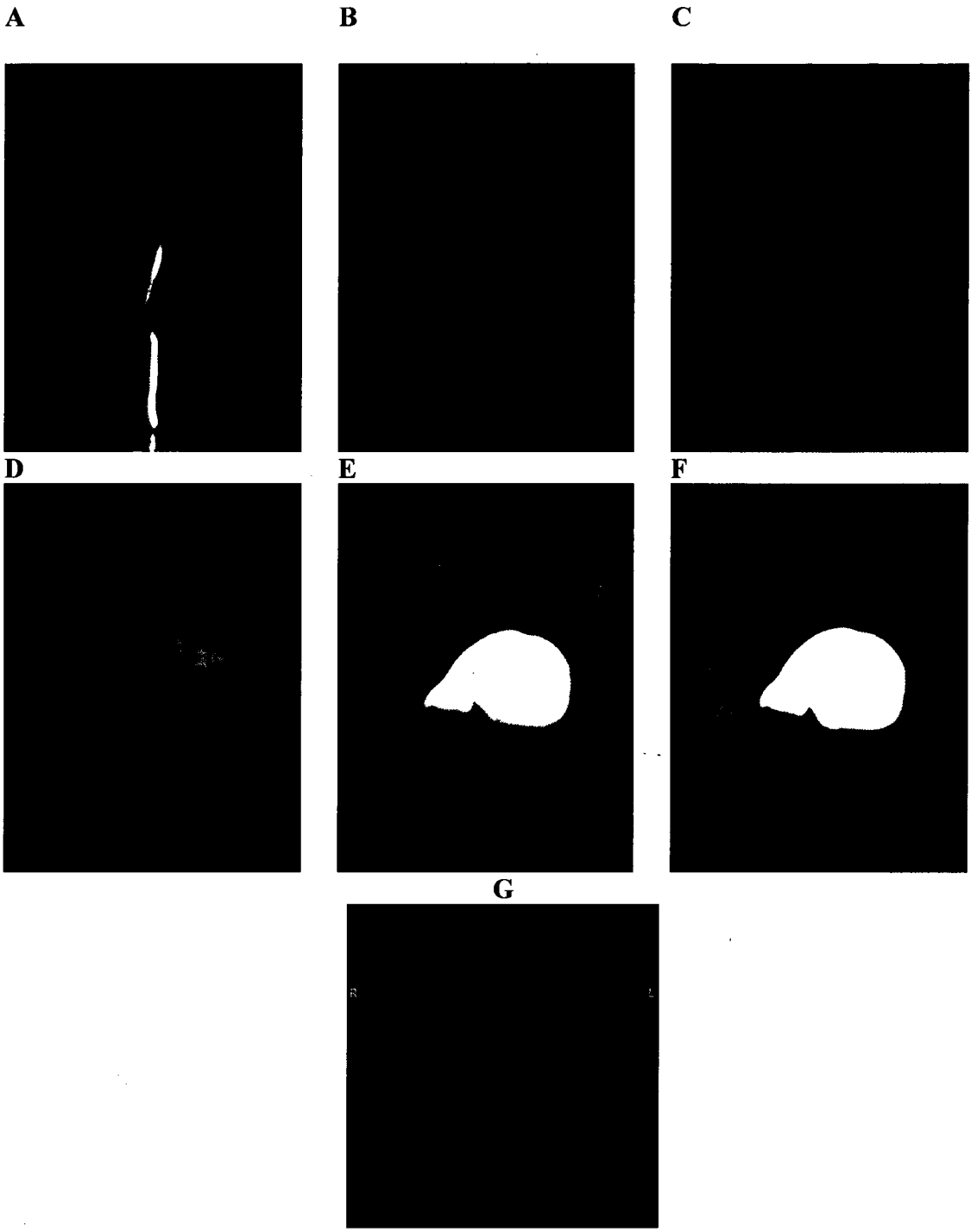

Figure 3.28. (A-F) Sample images from a candesartan (5 mg/kg) co-injection scan at (A) 20-30 seconds, (B) 50-60 seconds, (C) 80-90 seconds, (D) 2-3 minutes, (E) 5-10 minutes, and (F) 55-60 minutes post-injection. (G) A coronal slice of a candesartan co-injection scan image at 2-3 minutes post-injection showing liver and kidney uptake.

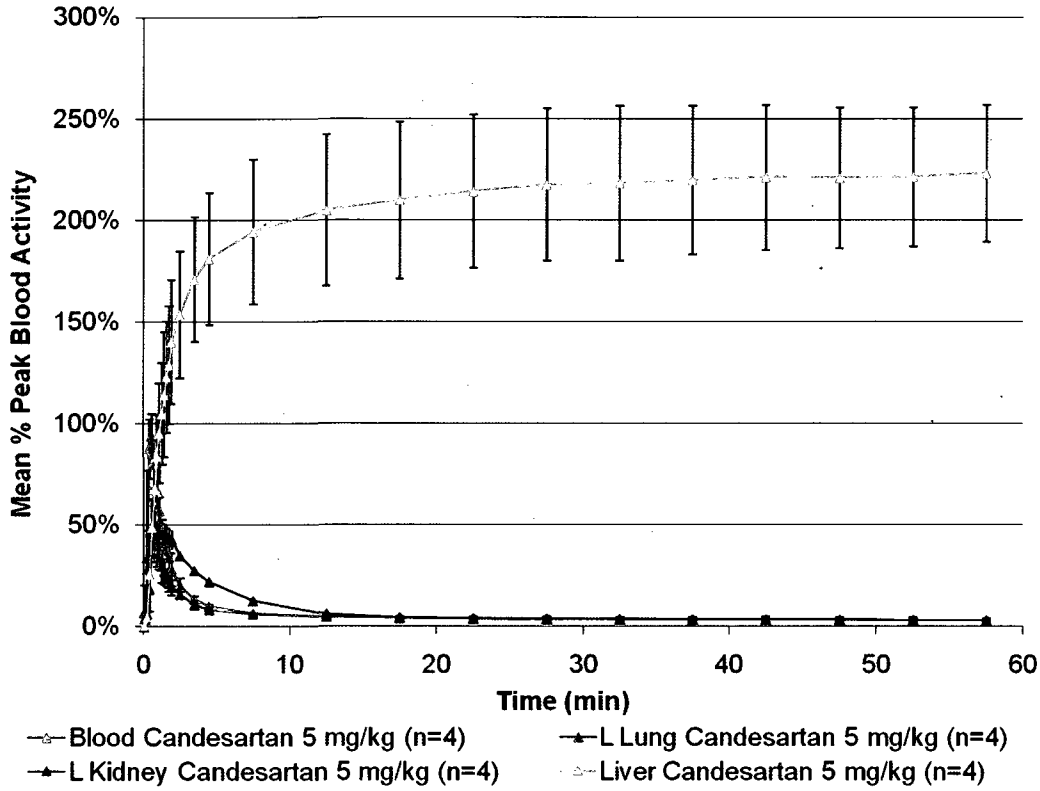

Figure 3.29. Mean percent of peak blood activity over time (± standard deviation) in rats receiving candesartan (5 mg/kg) co-injected with [^{11}C]methyl-candesartan (n=4) in blood, left kidney, left lung, and liver.

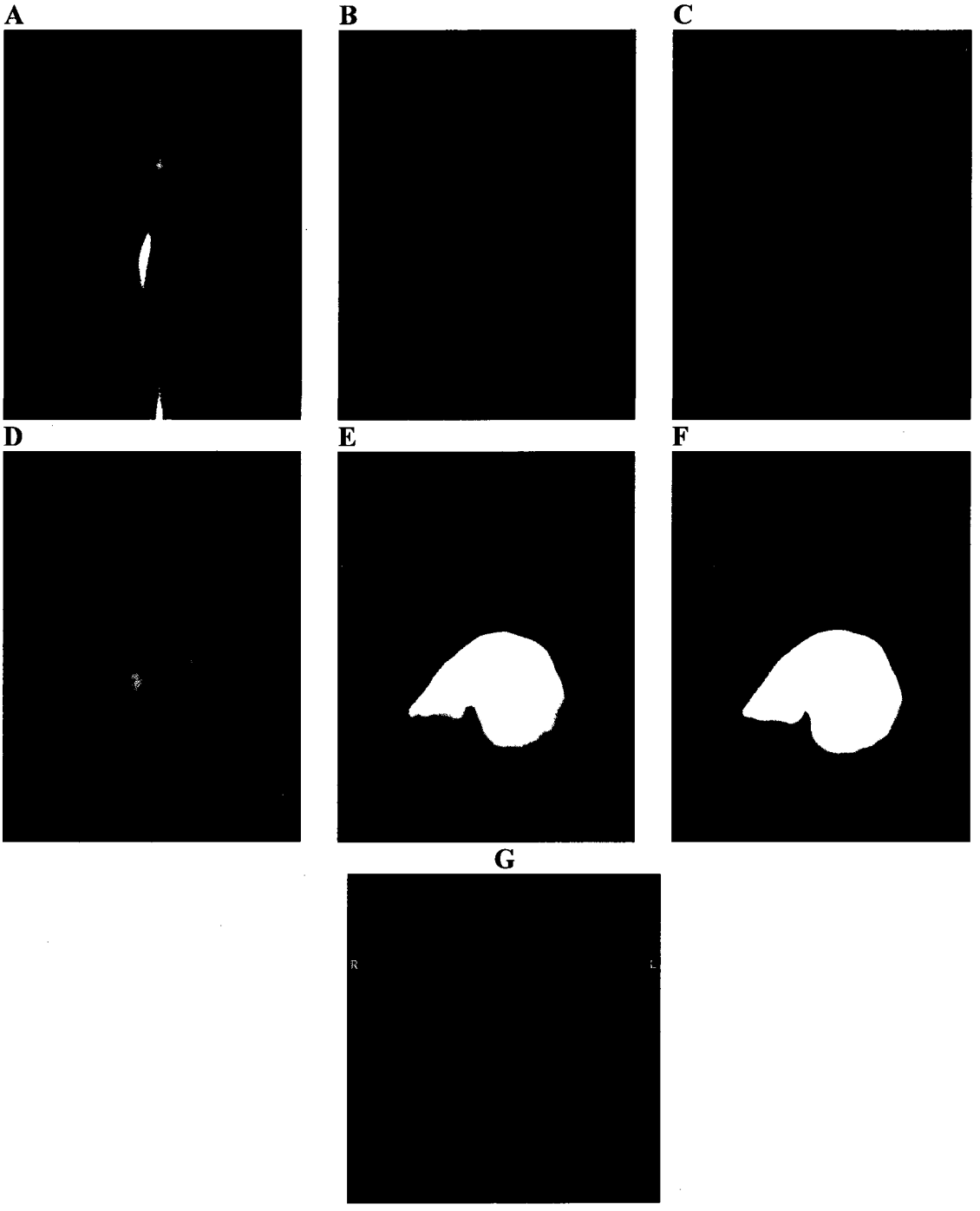

Figure 3.30. (A-F) Sample images from a PD123,319 (5 mg/kg) treatment scan at (A) 20-30 seconds, (B) 50-60 seconds, (C) 80-90 seconds, (D) 2-3 minutes, (E) 5-10 minutes, and (F) 55-60 minutes post-injection. (G) A coronal slice of a PD123,319 treatment scan image at 2-3 minutes post-injection showing liver and kidney uptake.

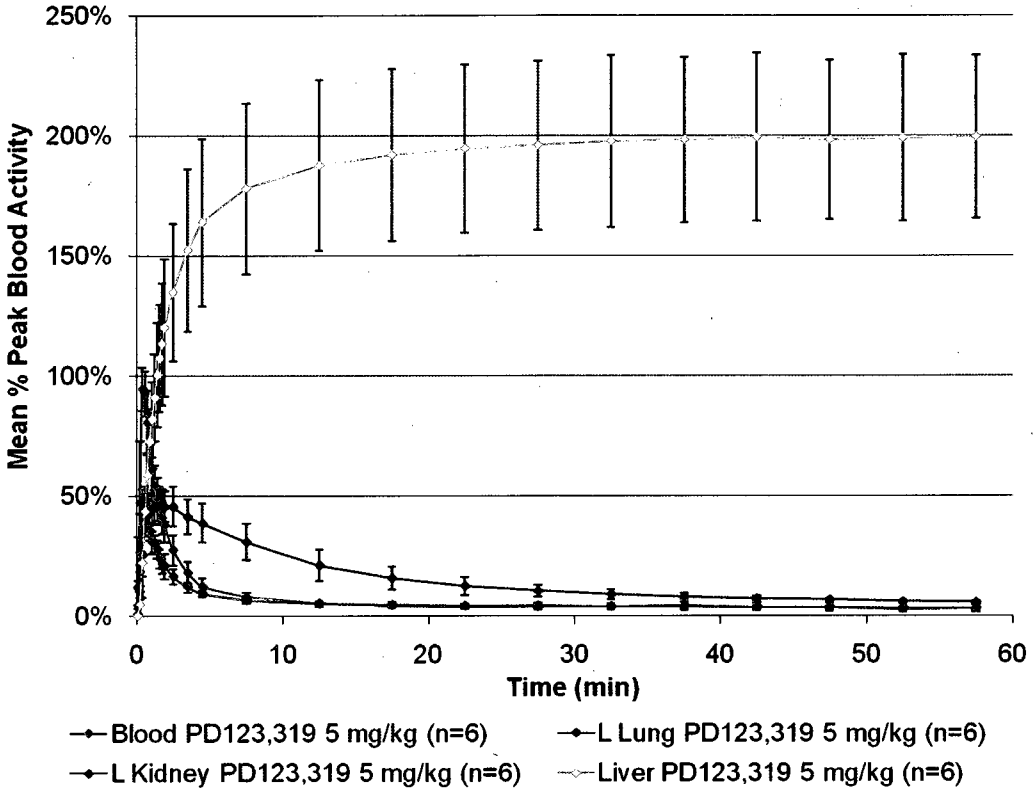

Figure 3.31. Mean percent of peak blood activity over time (± standard deviation) in rats receiving PD123,319 (5 mg/kg) 5 minutes prior to [^{11}C]methyl-candesartan (n=6) in blood, left kidney, left lung, and liver.

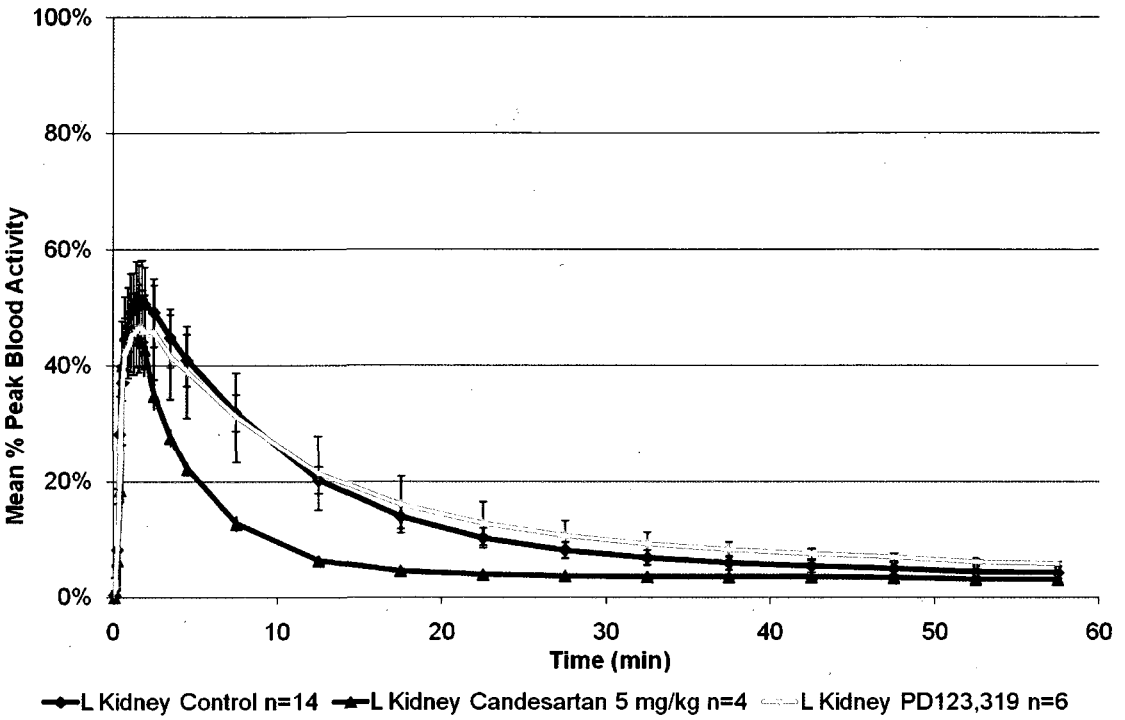

Figure 3.32. Mean percent of peak blood activity over time (± standard deviation) in control rats (n=14) and rats receiving candesartan (5 mg/kg) as a co-injection (n=4) or PD123,319 (5 mg/kg) 5 minutes prior to [^{11}C]methyl-candesartan (n=6) in the left kidney.

PD123,319, kidney activity over time was also very similar to the control group. Rats co-injected with candesartan however displayed differences relative to the other group in the kidney time activity curves. The peak kidney activity was similar between all groups (approximately 42-50%) but in candesartan-treated rats we observed a sharp decline approaching baseline by 15 minutes. In control and PD123,319-treated rats this washout was prolonged to 30 minutes.

3.6.4. Competition

Time activity data were used to calculate DV values for all ROIs (Figure 3.33). Calculated DV values for [^{11}C]methyl-candesartan images, were fit to the left atrium region as the blood pool and from frames 17-26. Overall DV value trends fit with previous data (*ex vivo* time course section 3.1): high uptake in liver (not shown) and kidney. No significant effect of treatment was observed in the LV cavity, lungs or liver. In the kidney, PD123,319 pretreatment had no effect, but co-injection with candesartan produced a decrease in DV relative to controls of 39 and 51% in the right and left kidney respectively (Table 3.15).

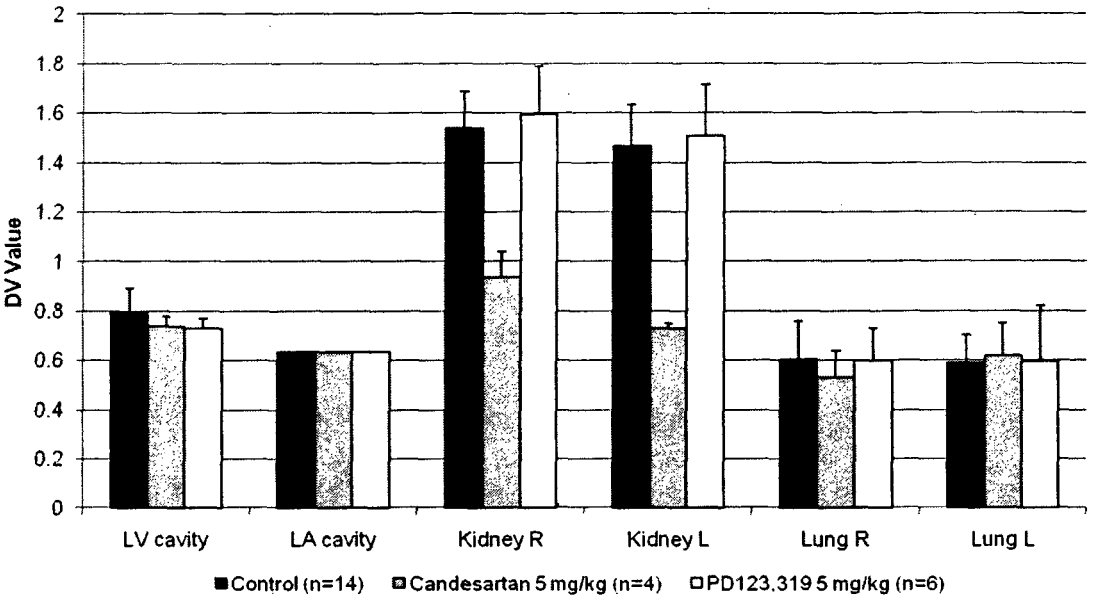

Figure 3.33. Comparison of DV values in control (n=14), candesartan co-injected (n=4), and PD123,319 (n=6) treated rats. Antagonists were administered at 5 mg/kg either as a co-injection (candesartan) or as a 5 minute pretreatment (PD123,319).

Table 3.15. Percent change in mean DV as compared to controls with 5 mg/kg treatment of candesartan or PD123,319. *corresponds to a significant difference from controls ($p<0.05$)

Treatment	LV Cavity	R Kidney	L Kidney	Liver	R Lung	L Lung
PD123,319	-8	4	2	-20	-1	0
Candesartan	-7	-39*	-50*	-11	-12	4

4. DISCUSSION

4.1. Ex Vivo Tracer Uptake and Time Course

Radioligand retention for both [^{11}C]methyl-candesartan and [^{11}C]TH4 was highest in AT_1 receptor rich tissues except the adrenals and correlates with published *in vitro* studies of receptor densities in rat kidney, heart, and aorta (Chang et al., 1991). In these studies, the density of AT_1 was highest in the adrenals (Table 1.1), and then kidney, brain, aorta, and heart (Chang et al., 1991). Although kidney, heart and aorta uptake of [^{11}C]methyl-candesartan and [^{11}C]TH4 correlate with the findings of Chang and Lotti (1991), the adrenal uptake of the tracers was much lower than would be expected based on their work (Table 1.1). In rats, the adrenal AT_1 receptor density is more than 3-fold that of renal tissue (Chang et al., 1991) but the tracer adrenal uptake observed was much less than that of the kidney. The AT_1 radioligands described in the literature also investigated tissue uptake by a similar method to that used to study [^{11}C]methyl-candesartan and [^{11}C]TH4 (section 2.3).

Adrenal uptake was not investigated in [^{11}C]L-159,884 studies (Kim et al., 1996). In [^{11}C]KR31173 *ex vivo* biodistribution experiments in mice, adrenal uptake was shown to be lower than the kidney initially at 5 and 15 minutes post-injection, about 50% greater than the kidney 30 minutes post-injection and just less than double the renal uptake at the final time point, 90 minutes post-injection (Mathews et al., 2004). Adrenal and renal AT_1 receptor density would be expected to show similar proportions in mice as in rats, given the trend across species observed (Chang et al., 1991). Adrenal uptake however in our studies was much lower relative to other tissues than that observed in the literature.

A possible contributor to this difference in tissue activity compared to receptor density is tissue blood flow. Studies in rats demonstrated renal blood flow was greater than that of the adrenals, but statistical comparisons between tissues were not made (Nishiyama et al., 2001). The contribution of this difference in flow cannot be conclusively determined as blood flow was not investigated in our studies, but it does provide insight as to a possible contributing factor, through which adrenal uptake could be lower than expected based solely on receptor density. The increased clearance observed with [^{11}C]methyl-candesartan or [^{11}C]TH4 may also contribute to the reduced activity measured. Also, adrenal AT_1 receptor density is much higher in the adrenal cortex (more than 5-fold) than the adrenal medulla (Balla et al., 1991) and this inner region may be reducing the activity per mass detected for both tracers. The two regions of the adrenal were not investigated separately in [^{11}C]methyl-candesartan or [^{11}C]TH4 experiments, thus confirmation of this would require further study.

Although AT_1 receptors are expressed in the brain, no uptake was observed in this tissue with either tracer. Neither radioligand appeared to cross the BBB to any significant extent, contrary to what was hypothesized for methyl or des-ethyl derivatives of candesartan. Previous research has shown that candesartan administered peripherally (0.1-10 mg/kg) has the ability to antagonize central effects of Ang II and therefore crosses the BBB (Gohlke et al., 2002a). The dose at which this occurred was much greater than the injected dose of the tracer (2.4-10.8 μg/kg). In these studies, it was not indicated what proportion of the dose penetrates the BBB.

Cardiac uptake was low for both [^{11}C]methyl-candesartan and [^{11}C]TH4. Receptor saturation with the unlabeled compound in tracer formulations ([^{11}C]methyl-

candesartan total mass 0.77-2.19 μg; [^{11}C]TH4 total mass 0.80-1.83 μg) may lower the measurable signal (Jagoda et al., 2004; Ma et al., 2004) in tissues expressing low receptor densities such as the heart (Chang et al., 1991). Cardiac uptake may therefore increase with improved specific activity of the tracer formulations. Other groups however have observed similar low radioligand uptake in normal hearts (Zober et al., 2006) and these studies used specific activities much higher than those produced for [^{11}C]methyl-candesartan or [^{11}C]TH4. Normal cardiac tissue AT_1 receptor density may in fact be too low to image by PET. Nevertheless, in models in which cardiac AT_1 receptor expression is increased such as myocardial infarction (Tan et al., 2004), it may become possible to visualize the increased signal *in vivo* using [^{11}C]methyl-candesartan or [^{11}C]TH4. Recently, preliminary PET work with [^{11}C]KR31173 suggested that in a post-MI rat model cardiac uptake was sufficient to visualize and quantify (Fukushima et al., 2009). Further study into the potential for [^{11}C]methyl-candesartan application in AT_1 upregulated states will be necessary.

In comparison to existing AT_1 PET radioligands in the literature, the clearance of [^{11}C]methyl-candesartan and [^{11}C]TH4 activity was more pronounced. Tracers developed at Johns Hopkins University, [^{11}C]KR31173 and [^{11}C]L-159,884, were tested up to 90 minutes post-injection. Even at these late time points, the radioligand activity in tissues remained relatively high. [^{11}C]KR31173 renal activity at 90 minutes post-injection was 28% of the peak kidney signal at 5 minutes post-injection (Mathews et al., 2004). At 90 minutes post-injection, another tracer by the same group, [^{11}C]L-159,884, displayed 69% of the peak renal activity at 5 minutes post-injection (Kim et al., 1996). The clearance of activity in [^{11}C]methyl-candesartan and [^{11}C]TH4 studies was much

greater than the other tracers. At the latest time point tested, 60 minutes post-injection, [^{11}C]methyl-candesartan retention was reduced to only 6% of the peak kidney activity whereas [^{11}C]TH4 was reduced to 5% of the peak kidney activity.

4.2. Ex Vivo Competition

Ex vivo competition studies were completed at 15 minutes post-injection based on the *ex vivo* time course study results. Increases observed in blood activity produced predominantly in the losartan treatment group coincide with a decrease in the liver activity, the likely cause of this increase is available activity in the blood. At 15 minutes post-injection, tracer accumulation in the tissue displayed the maximum contrast with the blood. [^{11}C]Methyl-candesartan bound specifically to AT_1 in a high proportion and this was shown with two different ARBs. [^{11}C]Methyl-candesartan binding selectivity for AT_1 over AT_2, Mas, β-adrenergic and α_2-adrenergic receptors was also demonstrated at tracer doses (2.4-10.8 μg/kg). Although significant reductions occurred in the renal cortex and outer medulla regions at a higher dose (5 mg/kg) of PD123,319, at 2 mg/kg this was not observed. In the literature the 2 mg/kg dose of PD123,319 and similar methods have been employed for characterization of previous AT_1 radioligands (Zober et al., 2006). Moreover, doses reported to block the AT_2 receptor were less than the 2 mg/kg dose used here (Barber et al., 1999; Duke et al., 2005). Additionally, studies administering a high dose of PD123,319 (10 mg/kg) have proposed a loss of functional selectivity to the AT_2 receptor at this dose (Widdop et al., 1992). Ex vivo competition studies for [^{11}C]methyl-candesartan and [^{11}C]TH4 were completed at both 5 and 10 mg/kg (not shown) and no significant difference between these groups was observed. The 5 mg/kg dose in our studies may then also be demonstrating some antagonistic

activity that is not specific to AT_2. [^{11}C]Methyl-candesartan selectivity for AT_1 over AT_2, Mas, β-adrenergic and α_2-adrenergic receptors is therefore not expected to be impacted at tracer doses (2.4-10.8 μg/kg).

[^{11}C]TH4 displayed less specific binding for AT_1 than [^{11}C]methyl-candesartan. Binding selectivity, at 15 minutes post-injection, for AT_1 over AT_2, β-adrenergic and α_2-adrenergic receptors was shown. Selectivity for AT_1 over Mas receptors however was not demonstrated. Significant reductions in [^{11}C]TH4 retention were observed in the renal medulla with A-779 pretreatment and a trend to reduction in the renal cortex. Moreover, this reduction occurred at a dose (100 μg/kg) that approached the tracer dose range tested for [^{11}C]TH4. These results suggest that [^{11}C]TH4 bound specifically to the Mas receptor at tracer doses. Hetero-dimerization of AT_1 with Mas receptors (Kostenis et al., 2005) has been demonstrated *in vitro* and could contribute to this interaction. The extent of this interaction *in vivo* in the kidney at physiological levels is not defined in the literature so the impact this finding may have on these results at present is unclear. The Mas receptor has been shown to be expressed in the myocardium (Ferreira et al., 2007), brain (Bunnemann et al., 1990; Young et al., 1988), and kidney (Young et al., 1986), all of which are regions of interest for further study. In light of this interaction (either through specific binding of the radioligand to the Mas receptor alone or through interaction with a hetero-dimer) and the lower specific binding proportion in comparison to [^{11}C]methyl-candesartan [^{11}C]TH4 was not further characterized, as [^{11}C]methyl-candesartan displayed better kinetics and a better pharmacological profile for imaging AT_1 receptors.

Reduction in tracer retention was expected to be greater in candesartan than losartan treated rats based on the structural similarity to the radioligands and higher affinity of candesartan. The ID_{50} of candesartan cilexitil (the esterified prodrug of candesartan; 0.069 mg/kg), determined in male Sprague-Dawley rats, was reported to be much less than that of losartan (3.027 mg/kg; Shibouta et al., 1993). There are two factors however that may be reducing the measured antagonism of candesartan: the time of onset of antagonistic activity and the metabolism of the compound. A delayed onset of antagonistic activity of candesartan relative to losartan has been reported (Morsing, 1999). This may be contributing to the slight difference in the reductions in tracer uptake between the two antagonists, particularly given the relatively short time point tested and the co-injection protocol.

The primary metabolite of candesartan is CV-15959 is considered inactive (Schmidt et al., 2003) therefore the affinity of CV-15959 for AT_1 is likely to be much less than that of candesartan although it is not specifically tested. Conversely, losartan has been shown to be converted to an active metabolite, EXP3174 (Vanderheyden et al., 1999). Shibouta et al (1993) report similar IC_{50} values in two different systems for candesartan ($2.86x10^{-8}$ M in rabbit aortic strips and $1.12x10^{-7}$ M in bovine adrenal cortex) and EXP3174 ($1.99x10^{-8}$ M in rabbit aortic strips and $2.22x10^{-7}$ M in bovine adrenal cortex). Enhanced blocking with losartan was observed to the greatest extent in the liver where losartan reduces retention by 91%. This reduction was not observed with candesartan (12%). The active metabolite, EXP3174, may play a role in this reduction, as the conversion from losartan occurs in the liver (Taavitsainen et al., 2000).

4.3. Dosimetry

[^{11}C]Methyl-candesartan tissue uptake at 5, 15, 30, and 60 minutes post-injection correlated with the time course data for those tissues in common between the two studies. The liver, kidney and gastrointestinal contents contributed most significantly to the overall effective dose and this is consistent with the expected excretion pathways of the radioligand (van Lier et al., 1997). The effective doses calculated for [^{11}C]methyl-candesartan were within the range of those reported in the literature for other carbon-11 labeled PET tracers (Ribeiro et al., 2007; Wilson et al., 2002) and are well below the regulatory limits reported by the Radioactive Drug Research Committee guidelines. [^{11}C]Methyl-candesartan would therefore be within safe limits for use in human studies. The parent molecule is approved for clinical use, facilitating human use of its analogue [^{11}C]methyl-candesartan.

4.4. Metabolism

Authentic [^{11}C]methyl-candesartan injections demonstrated a 100% capture of the radioligand during the initial phase of the run (pre-switch), indicating an appropriate selection of the capture sorbent. Injections of biological samples spiked with [^{11}C]methyl-candesartan showed significant elution of radioactivity in the initial phase. Authentic [^{11}C]methyl-candesartan was fully captured, therefore some component of the biological samples was preventing trapping by the capture sorbent. The unretained radioactivity in samples of plasma and kidney processed with authentic [^{11}C]methyl-candesartan or in injected rat samples was most likely the compounds of the other peaks not captured due to the high extent of plasma protein binding. The extent of plasma protein binding of methyl-candesartan has not been investigated previously, but studies

on the parent compound candesartan were available. Candesartan was greater than 99% plasma protein bound (Gleiter et al., 2004; Israili, 2000). Our results display similar findings for [^{11}C]methyl-candesartan (section 3.4). Hilton et al (2000) demonstrated disruption of plasma protein binding in this protocol by addition of urea to samples prior to injection on the apparatus. Indeed in these injections, adding urea to plasma disrupted this binding and reduced eluted radioactivity in the initial phase to less than 2% in control samples and less than 5% in injected rat samples. Further reductions were not possible due to the limit of the solubility of urea. When reconstituted with urea in the solution in both control and injected rat kidney samples, unretained radioactivity was less than 2%.

The rapid reduction in activity, described in section 4.1, is in contrast to the known kinetics of the parent compound candesartan. Candesartan has been reported to have a prolonged association (dissociation time of 120 minutes) with the AT_1 receptor in membrane binding studies (Vauquelin et al., 2006). As the parent compound of both tracers, a longer residence time at the receptor, and thus greater tissue retention over time, was expected. The unexpectedly low uptake and rapid washout is likely due to the metabolism of the carbon-11 label through hydrolysis of the [^{11}C]methoxy group. Yoshimura et al (1994) demonstrated that rapidly after iv administration of methyl-candesartan (4.8 minutes), the plasma concentration of candesartan (its metabolite) was more than 9-fold higher than methyl-candesartan. The results of this study suggested rapid hydrolysis of methyl-candesartan when administered iv (Yoshimura, 1994). This same hydrolysis is likely occurring in the [^{11}C]methyl-candesartan and [^{11}C]TH4 studies.

Hydrolysis of the ester group would remove the carbon-11 label and reduce the overall detectable signal for both radioligands. Hydrolysis of the ester group would

likely produce [^{11}C]methanol which has been shown to be eliminated primarily through the lungs and liver in rats (Roe, 1955). *In vivo,* methanol was converted to formic acid in the liver and studies in primates demonstrated that this occurred without appreciable release into the blood within the time period of our studies (Makar et al., 1976). Production of [^{11}C]methanol or a metabolite thereof, would be exhaled or sequestered in liver respectively. These proposed metabolic reactions are a possible explanation for the reduced signal. Despite the reduction in signal, this mechanism can have a positive effect as the hydrolysis of the label would not produce a radioactive metabolite that would impact PET quantification due to the low mass in the formulation.

Although some investigations of unlabeled methyl-candesartan are found in the literature, little is found for [^{11}C]TH4 or similar structures. The primary metabolite of candesartan is CV-15959 (Schmidt et al., 2003) which has a chemical structure similar to that of [^{11}C]TH4 (Figure 1.10). Structurally, [^{11}C]methyl-candesartan and [^{11}C]TH4 are quite similar to each other and could be considered the *O*-methyl ester derivatives of candesartan and the *O*-methyl derivative of its primary metabolite respectively. It is therefore possible that similar mechanisms that impact [^{11}C]methyl-candesartan also impact [^{11}C]TH4, although clear evidence for this is not available at present. The hydrolysis mechanism described above however suggests a possible mechanism through which the overall signal could be reduced for both [^{11}C]methyl-candesartan and [^{11}C]TH4.

Metabolites (peaks 2 and 3) in plasma were less than 5% even at 20 minutes post-injection indicating that metabolite levels were neither changing over time nor collecting in the plasma. In the kidney, labeled metabolites did accumulate over time, particularly

peak 3. The accumulation suggests the production of metabolites within the tissue or the trapping of them from the plasma over time. Trapping of the metabolites produced elsewhere (the plasma or liver for example) would be accompanied by an increased proportion in the plasma, or a change in proportion over time. The lack of appreciable metabolites or change in the levels present in plasma suggest the former mechanism (*in situ* production of metabolites) is more likely.

Metabolism studies of methyl-candesartan were not found in the literature but information on candesartan is available. A cytochrome P450, CYP2C9, has been demonstrated to be expressed in human liver and kidney tissue (Enayetallah et al., 2004; Klose et al., 1999) and be involved in the metabolism of candesartan (Hanatani et al., 2001). This isoform is not expressed in the rat (Kobayashi et al., 2008) but another expressed in rat tissues has been considered a functional substitute, CYP2C23 (Imaoka et al., 2005). Imaoka et al (2005) demonstrated expression of CYP2C23 mRNA and catalytic activity in the rat kidney. Furthermore, studies in rats using a CYP2C9 inhibitor, bucolome, demonstrated significant reduction in substrate production using this inhibitor (Kobayashi et al., 2008). Although studies have not confirmed it, this enzyme may therefore also play a role in the metabolism of [^{11}C]methyl-candesartan.

Data for methyl-candesartan excretion is not available but excretion of candesartan occurred through hepatic and renal routes (van Lier et al., 1997) and methyl-candesartan may be eliminated in a similar fashion. When [^{14}C]candesartan was administered iv, approximately 60 % of the radioactivity was excreted via renal mechanisms (van Lier et al., 1997). The renal *in situ* metabolism mechanism proposed here without transfer to the plasma might therefore be possible. Metabolites may be

formed within the tissue and excreted without returning to the plasma, although further study would be required to support or refute the contribution of this mechanism.

The column-switch HPLC methods in these studies can detect presence or absence of radiolabeled metabolites but cannot determine the identity of the metabolites detected. Samples injected with authentic [^{11}C]TH4 demonstrated co-retention of the [^{11}C]TH4 peak and the major metabolite peak (peak 3). This strongly suggests that the major metabolite is likely to be [^{11}C]TH4. As described previously, the structure of [^{11}C]TH4 is similar to the primary metabolite of candesartan (Figure 1.10). The results of the [^{11}C]TH4 competition studies suggests that the major metabolite peak observed in the kidney (putatively [^{11}C]TH4) would interact with AT_1 receptors ([^{11}C]TH4 retention is reduced by ARB treatment). Co-injection of candesartan (5 mg/kg) with [^{11}C]methyl-candesartan was used to determine any interaction between metabolites and the AT_1 receptor. Saturation of the renal AT_1 receptors with blocking doses (5 mg/kg; Nossaman et al., 2007) of candesartan would disrupt interactions between compounds and the AT_1 receptor. If interactions occur, blocking the receptors would decrease the retention of the compound and change the *proportion* of the radioactivity signal associated with its peak on the HPLC chromatogram. If there is no interaction, the signal associated with a compound does not change. This procedure was recently reported by our group in the characterization of another carbon-11 labeled radioligand, [^{11}C]rolipram (Kenk et al., 2008). In the case of [^{11}C]methyl-candesartan, no difference in the relative proportions of both peaks was observed in either the unchanged tracer or major metabolite peak when a blocking dose of candesartan co-injected with the tracer was administered. The maintained proportions of the radioactivity signal in both peaks suggest one of two

possible situations: 1) neither compound interacts with AT_1; or 2) the major metabolite and the unchanged tracer interact with the AT_1 receptor to a similar extent. That neither compound interacts is not possible, given the known properties of [^{11}C]methyl-candesartan and other results presented here (section 3.2.1). The possible interaction of the metabolite observed in these studies fits with its proposed identity, [^{11}C]TH4, and with previous data (section 3.2.2) demonstrating [^{11}C]TH4 specific binding to AT_1 receptors.

4.5. Small Animal PET Studies

4.5.1. Initial Condition Optimization

A maximum receptor occupancy of 1-5% is important to accurately image receptors using PET for kinetic modelling and to prevent any physiological effect or receptor saturation (Hume et al., 1998; Jagoda et al., 2004). This is particularly important for tissues where receptor density is low, as the absolute number of receptors would be smaller relative to tissues where a receptor is moderately or highly expressed. In the kidney, receptor density is reported as the second highest next to the adrenals and more than 350-fold higher than the heart (Chang et al., 1991). In PET studies of [^{11}C]raclopride, a dopamine receptor radioligand, increased receptor occupancy beyond the ideal range (as a result of lowered specific activity) reduced measured DV values (Alexoff et al., 2003). In these studies the range of injected doses of raclopride was 0.5-3.8 nmol/kg and increasing dose displayed decreases in the DV values generated (Alexoff et al., 2003). In the studies presented here, investigations of the [^{11}C]methyl-candesartan scan parameters of injected mass, dose, activity, or specific activity did not have an effect on kidney DV values. If receptor occupancy was outside the ideal range quoted by Hume

et al (1998) a decrease in DV values with increasing injected mass or decreasing specific activity would be expected, as was observed in the Alexoff et al (2003) studies. Furthermore, a much wider range of doses (0.5-74 μg/kg) and specific activities (29-1796 mCi/μmol) were tested as compared to the studies of Alexoff and colleagues (2003) and 5 mg/kg candesartan was able to reduce the renal DV by 39-50%. Based on the high AT_1 receptor density in the kidney, the lack of effect of injected mass, and the reduction observed in candesartan co-injection scans, it was assumed the AT_1 receptor occupancy in the kidney with [^{11}C]methyl-candesartan likely fell within the 1-5% threshold described by Hume et al (1998) and Jagoda et al (2004). To fully establish the extent of receptor occupancy, further scans would be needed with decreasing specific activity until changes in the DV are observed. This would require modifications to the current protocols, as the maximal injected dose was obtained using the current methods.

4.5.2. Time Course and Biodistribution

The tissues displaying activity in control scans also displayed tissue retention in the *ex vivo* time course studies. Tissue uptake observed in the PET images (lungs, heart, liver, kidneys) corresponds to tissues known to express AT_1 receptors (Allen et al., 2000; Chang et al., 1991). Rapid clearance was observed, as in the *ex vivo* studies (refer to section 4.1 and 4.2). Candesartan co-injection scans demonstrated increased renal washout compared to the renal time course of the control scans, indicating specific binding in this tissue. Blood, liver and lung activity was similar over time to that of the control scans suggesting that specific binding was not observed in these tissues using this methodology. PET imaging studies were carried out after and included more time points than the *ex vivo* biodistribution studies. From the PET data it became evident that the

time point for optimal tissue to blood ratio was earlier than the 15 minutes time point selected from the *ex vivo* data. Future characterization of radioligands utilizing similar methodologies should therefore use PET data to determine appropriate time points for *ex vivo* biodistribution studies.

4.5.3. Competition

Candesartan treated rats showed similar reductions in renal DV values as were observed with renal tissue retention trends in the *ex vivo* competition studies (section 4.2). The magnitude of the reductions was smaller (39-50%) than that of the *ex vivo* competition studies (76%) using the same dose of candesartan. This disparity was likely, at least in part, a factor of the two different methods to measure tissue uptake. Receptor radioligand measurements in PET imaging are reported to exhibit less sensitivity than *ex vivo* biodistribution methods with a more than 2-fold increase in variance in the PET studies (Jagoda et al., 2004; Ma et al., 2004). *Ex vivo* biodistribution methods involve removing the organ or tissue of interest from the animal and counting the activity in a gamma counter (up to CPM), such that no other tissue or background activity interferes. In PET imaging adjacent organs and tissues can interfere with the activity detected in the ROI, a concept called 'spillover' (Fang et al., 2008). In the case of the kidney as an ROI in the rat, there are other adjacent tissues and blood within the kidney that may impact the measured tissue activity level. The liver is in close proximity to both kidneys and has high tracer uptake. The high levels of activity can impact that detected for the renal ROI, particularly for the right kidney. The liver 'spillover' would increase the activity measured in the ROI and therefore result in a smaller reduction when compared to the *ex vivo* results. The blood activity within the kidneys would impact the tissue activity in the

same fashion as the liver, increasing the measured tissue activity in the ROI. In the ex vivo studies kidney tissue is separated and blotted removing some of this blood activity. In the PET studies, spillover from the liver was minimized as much as possible in the ROI generation (2.8.2). Spillover effects of blood activity within the kidney could not be removed from the kidney activity measured in these studies. The impact of renal blood activity is likely to be small, as the blood activity for the time duration selected for analysis was at baseline.

Animals treated with PD123,319 confirmed the binding selectivity of [^{11}C]methyl-candesartan for AT_1 over AT_2 receptors observed in the *ex vivo* competition studies. No reductions were observed in the mean DV values of control or AT_2 antagonized rats, but in *ex vivo* competition studies, reductions were observed (0-38%). The varied effect of the drug in these studies is likely at least partially to be impacted by the loss of sensitivity in PET imaging as compared to *ex vivo* biodistribution methods (described above).

Logan graphical analysis is most appropriate when the analysis includes a corrected arterial plasma input function (plasma time activity curve), and is a common method applied in the literature (e.g. Zober et al., 2006). The plasma input curve of [^{11}C]methyl-candesartan scans was corrected for two factors: any differences in plasma and whole blood activity and the presence and time course of plasma metabolites. A correction for whole blood activity to plasma activity was applied to all scans. Serial samples from arterial cannulations showed that plasma activity comprised a similar proportion of the total blood activity over time. The correction was therefore applied as a

scalar factor of 1.58. In plasma, the levels of all metabolites were less than 10% at all time points tested; therefore no corrections were made for plasma metabolites.

Logan DV values are dependent on the plasma input and the tissue activities, thus changes in blood flow within the tissue would impact these values. Changes in flow would potentially alter the tissue activity without a subsequent change in the plasma input function, artificially shifting the DV. Renal tissue flow was not measured as part of the imaging studies but information on the effects of the drug treatments on renal blood flow can be obtained from the literature. Rats injected with PD123,319 displayed renal blood flow similar to control animals (Lo et al., 1995; Macari et al., 1994). The DV data from PD123,319-treated rats could therefore be considered appropriate for comparison to controls.

The effects of candesartan on renal plasma flow are less clear. At doses similar to those used in this study (1 mg/kg + 50 μg/kg/minute for 60 minutes) and those slightly lower decreased renal blood flow in control rats (Cervenka et al., 1998; Hiranyachattada et al., 2005). Conversely, similar studies at slightly lower doses (0.2 and 1 mg/kg) observed increased renal blood flow (Kanagawa et al., 1997; Takishita et al., 1994). There is a lack of data at the dose injected in these studies (5 mg/kg) and clearly a controversy in the literature. It is therefore unclear exactly what effect candesartan would have (if any) on renal blood flow and what impact (if any) this would have on the measured DV data.

Increases in flow would overestimate the DV value-possibly generated by increasing tissue activity without changes in plasma input. Underestimation of the DV would result from decreases in flow-decreasing tissue activity without changes in plasma

input. Of these two possible effects, underestimation is the most problematic as the 'true' value may indicate that there is less specific binding. No measurements of renal plasma flow were made during the blocking experiments, therefore the candesartan DV data should be considered in conjunction with the other results when making comparisons to the control and PD123,319 treated groups.

Although renal flow was not measured, it is possible however to make general comparisons across groups. From those studies which demonstrated a decrease in renal flow, the maximum decrease observed was less than 25% (Cervenka et al., 1998; Hiranyachattada et al., 2005). Assuming that renal blood flow was reduced in this way, the reductions we observe (39-50%) are much greater than the 25% decrease reported by Cervenka et al (1998). It is therefore very likely that reductions indicating specific binding are present. In the case of an increase in renal blood flow demonstrated by Kanagawa et al (1997) and Takishita et al (1994) the difference between controls and candesartan treated rats would only be augmented, strengthening our results. When the DV values are considered with the previous *ex vivo* competition data showing 57-81% reductions in the renal cortex with candesartan treatment at 15 minutes post-injection, it becomes clear that the reductions must at least in part have resulted from specific binding. This effect is not seen with PD123,319. This conclusion is strengthened by the losartan data from the *ex vivo* studies. Reductions of up to 90% were observed with losartan, an ARB with a different chemical structure than that of candesartan. Moreover, losartan has been demonstrated to have no effect on (Lo et al., 1995; Macari et al., 1994) or to increase renal blood flow (Lo et al., 1995; Macari et al., 1994). Despite the lack of renal flow data in the drug treatment group, it was demonstrated from these data that

[^{11}C]methyl-candesartan displays AT_1-specific binding and selectivity for AT_1 over AT_2 receptors *in vivo*. Future studies could incorporate flow measurements through [^{13}N]ammonia PET or by Doppler flow studies.

4.6. Overall Impact, Applications and Future Work

The ultimate goal of this research was to characterize a novel AT_1 radioligand in hopes of improving upon those radioligands currently described in the literature for translational research from rats to humans such that clinical use of an AT_1 radioligand is possible. Previously published AT_1 radioligands have been demonstrated to have 3 main disadvantages: little cardiac uptake in the normal condition and minimal brain uptake; technical difficulties in radiosynthesis and metabolism; and an unknown safety profile for human use. The three AT_1 radioligands currently published, [^{11}C]MK-996, [^{11}C]L-159,884, and [^{11}C]KR31173, have minimal brain uptake and low cardiac uptake in the baseline condition. [^{11}C]KR31173 has recently however been demonstrated to display appreciable cardiac uptake in an AT_1 upregulated state, a rodent model of MI (Fukushima et al., 2009). [^{11}C]MK-996 and [^{11}C]L-159,884 have technical barriers to clinical use – Hamill et al (1996) reported these compounds to have difficult syntheses. Although [^{11}C]L-159,884 has been studied in humans, the tracer is readily metabolized (Hamill et al., 1996), necessitating more complex kinetic modelling (van den Hoff, 2005) and reducing the feasibility of its application in a clinical setting. Although [^{11}C]KR31173, the more recent radioligand from the literature, does not have the difficult synthesis described for [^{11}C]MK-996 and [^{11}C]L-159,884, the metabolism profile in humans is currently unknown as this radioligand has yet to be characterized in human studies. The translation to human study may be prolonged because the radioligand would require

approval through the appropriate regulatory bodies for use in humans. [^{11}C]Methyl-candesartan and [^{11}C]TH4 are the *O*-methyl analogues of the parent compound, candesartan, which is widely used as a clinical ARB. The safety data of the parent compound has already received approval and could then facilitate approval of its derivatives.

Use of AT_1 radioligands and PET in human studies would provide a wealth of information in the study of disease, such as the two examples described here, heart failure and diabetic nephropathy (sections 1.1.8 and 1.1.9). Current knowledge of the expression changes occurring during the progression of these diseases in humans is limited technically and practically. Expression data is collected only at discrete time points because current techniques are limited to *in vitro* determination of receptor expression which require tissue samples from biopsies or explanted tissue (Mezzano et al., 2003; Regitz-Zagrosek et al., 1997; Regitz-Zagrosek et al., 1998; Wagner et al., 1999). PET imaging could provide the means to longitudinally study patients non-invasively. In this way PET could be used to monitor changes in receptor expression with progression of disease, or regression of the disease in response to therapy. To reach clinical application, the radioligands must be well characterized, thus the rationale for this research.

The results of the *ex vivo* studies were able to highlight the limitations of using [^{11}C]TH4 as a radioligand. [^{11}C]TH4 demonstrated a lower specific binding proportion compared to [^{11}C]methyl-candesartan, and an unfavourable selectivity profile in that specific binding to the Mas receptor was established. This receptor has been shown to be expressed in several tissues, including myocardium (Ferreira et al., 2007), brain (Bunnemann et al., 1990; Young et al., 1988), and kidney (Young et al., 1986). This

binding may also be due to hetero-dimerization of AT_1 with Mas receptors (Kostenis et al., 2005) as this occurrence has been demonstrated *in vitro*. Whether the formation of this complex occurs *in vivo* in the kidney and heart at physiological levels is unknown. In light of this, [^{11}C]TH4 was not further characterized.

[^{11}C]Methyl-candesartan demonstrated a high specific-binding component and selectivity to AT_1 receptors, suggesting potential for imaging these receptors *in vivo*. The [^{11}C]methyl-candesartan tissue signal displays similar biodistribution trends to other AT_1 radioligands currently published. Cardiac and brain uptake were not improved over other published radioligands but [^{11}C]methyl-candesartan is specific and selective to AT_1 and therefore comparable. Additionally renal AT_1 receptor imaging using [^{11}C]methyl-candesartan in small animal PET is possible in rodents, and specificity and selectivity were confirmed in these studies. Specific and selective binding to AT_1, both in *ex vivo* and imaging studies, and the ability to image renal AT_1 receptors demonstrate the potential of [^{11}C]methyl-candesartan as a radioligand for future use.

Further study would however be necessary for translation to clinical studies. One such avenue would be the investigation of cardiac uptake in an animal model which has increased AT_1 receptor expression to assess the ability of [^{11}C]methyl-candesartan to image cardiac AT_1 receptors in an upregulated state. The studies presented were completed in normal rats, so further investigation in disease models would be necessary to assess the ability of [^{11}C]methyl-candesartan to detect changes AT_1 expression with disease (such as heart failure and diabetic nephropathy).

Additionally, characterization of [^{11}C]methyl-candesartan in humans would be necessary, including biodistribution of the tracer using PET and investigation of the tracer

metabolism. The labeled metabolite of [^{11}C]methyl-candesartan detected in rats (possibly [^{11}C]TH4) necessitates the assessment of [^{11}C]methyl-candesartan metabolism in humans. Species differences in metabolism of the parent compound candesartan exist. The human P450 isoform responsible for candesartan metabolism (and presumably [^{11}C]methyl-candesartan) is not expressed in rats (Kobayashi et al., 2008). Although a functional substitute exists (Imaoka et al., 2005), the metabolism profile presented here could be much different than that observed in humans. This characterization is therefore required to describe kinetics of metabolite formation and accumulation and adequately model the binding kinetics of [^{11}C]methyl-candesartan in humans. Presence of this labeled metabolite does not impede AT_1 receptor quantification by Logan graphical analysis as the plasma input function can be modified to model for the changes in tracer metabolism.

5. CONCLUSIONS

Several conclusions can be drawn from the results of the [^{11}C]methyl-candesartan and [^{11}C]TH4 studies in this thesis. [^{11}C]Methyl-candesartan and [^{11}C]TH4 tracer accumulation occurred to the greatest degree in certain tissues reported previously to express AT_1 receptors, such as the kidney, heart and aorta. The brain uptake was minimal as neither [^{11}C]methyl-candesartan nor [^{11}C]TH4 crossed the BBB to an appreciable extent. [^{11}C]Methyl-candesartan was considered to perform better than [^{11}C]TH4 in *ex vivo* studies in three aspects: 1) [^{11}C]methyl-candesartan displayed specific binding to AT_1 receptors in the kidney, as well as the adrenals and lung; 2) [^{11}C]methyl-candesartan binds selectively to AT_1 over AT_2, Mas, β-adrenergic or α_2-adrenergic receptors at tracer doses in the renal cortex and outer medulla regions; and 3)

[^{11}C]TH4 did not bind selectively, in the renal outer medulla region, to AT_1 over Mas (Ang(1-7)) receptors.

[^{11}C]Methyl-candesartan produces a labeled metabolite in rats that accounts for approximately 26% of the total radioactivity at 20 minutes post-injection and that interacts with the AT_1 receptor in the kidney. Further study is required to determine the presence or absence of this metabolite in humans, and if present the contribution of this metabolite over time.

[^{11}C]Methyl-candesartan has potential as a possible clinical PET imaging radioligand, as the effective dose and effective dose equivalent for [^{11}C]methyl-candesartan is well below the safe limits reported for clinically used radioligands. Renal small animal PET studies are possible with [^{11}C]methyl-candesartan in rats and warrants further use as an AT_1 radioligand in human PET scans. [^{11}C]Methyl-candesartan was able to reproducibly image renal AT_1 receptors. The small animal PET quantification data also supported *ex vivo* results of selective binding to AT_1 over AT_2 receptors in the kidney. Additional work is necessary to determine the ability of [^{11}C]methyl-candesartan to image AT_1 receptors in disease states.

6. REFERENCES

Aksnes, T.A., Reims, H.M., Guptha, S., Moan, A., Os, I., Kjeldsen, S.E. 2006. Improved insulin sensitivity with the angiotensin II-receptor blocker losartan in patients with hypertension and other cardiovascular risk factors. J Hum Hypertens 20, 860-866.

Alexoff, D.L., Vaska, P., Marsteller, D., Gerasimov, T., Li, J., Logan, J., Fowler, J.S., Taintor, N.B., Thanos, P.K., Volkow, N.D. 2003. Reproducibility of 11C-raclopride binding in the rat brain measured with the microPET R4: effects of scatter correction and tracer specific activity. J Nucl Med 44, 815-822.

Ali, M.S., Sayeski, P.P., Dirksen, L.B., Hayzer, D.J., Marrero, M.B., Bernstein, K.E. 1997. Dependence on the motif YIPP for the physical association of Jak2 kinase with the intracellular carboxyl tail of the angiotensin II AT1 receptor. J Biol Chem 272, 23382-23388.

Allen, A.M., Zhuo, J., Mendelsohn, F.A. 2000. Localization and function of angiotensin AT1 receptors. Am J Hypertens 13, 31S-38S.

Allen, T.J., Cao, Z., Youssef, S., Hulthen, U.L., Cooper, M.E. 1997. Role of angiotensin II and bradykinin in experimental diabetic nephropathy. Functional and structural studies. Diabetes 46, 1612-1618.

Amiri, F., Garcia, R. 1999a. Regulation of angiotensin II receptors and PKC isoforms by glucose in rat mesangial cells. Am J Physiol 276, F691-699.

Amiri, F., Garcia, R. 2000. Renal angiotensin II receptors and protein kinase C in diabetic rats: effects of insulin and ACE inhibition. Am J Physiol Renal Physiol 278, F603-612.

Amiri, F., Venema, V.J., Wang, X., Ju, H., Venema, R.C., Marrero, M.B. 1999b. Hyperglycemia enhances angiotensin II-induced janus-activated kinase/STAT signaling in vascular smooth muscle cells. J Biol Chem 274, 32382-32386.

Anderson, K.M., Murahashi, T., Dostal, D.E., Peach, M.J. 1993. Morphological and biochemical analysis of angiotensin II internalization in cultured rat aortic smooth muscle cells. Am J Physiol 264, C179-188.

Anderson, R.J., Ray, C.J., Popoff, M.R. 2000. Evidence for Rho protein regulation of renal tubular epithelial cell function. Kidney Int 58, 1996-2006.

Ardaillou, R. 1999. Angiotensin II receptors. J Am Soc Nephrol 10 Suppl 11, S30-39.

Asano, K., Dutcher, D.L., Port, J.D., Minobe, W.A., Tremmel, K.D., Roden, R.L., Bohlmeyer, T.J., Bush, E.W., Jenkin, M.J., Abraham, W.T., Raynolds, M.V., Zisman, L.S., Perryman, M.B., Bristow, M.R. 1997. Selective downregulation of the angiotensin II AT1-receptor subtype in failing human ventricular myocardium. Circulation 95, 1193-1200.

Balla, T., Baukal, A.J., Eng, S., Catt, K.J. 1991. Angiotensin II receptor subtypes and biological responses in the adrenal cortex and medulla. Mol Pharmacol 40, 401-406.

Balmforth, A.J., Shepherd, F.H., Warburton, P., Ball, S.G. 1997. Evidence of an important and direct role for protein kinase C in agonist-induced phosphorylation leading to desensitization of the angiotensin AT1A receptor. Br J Pharmacol 122, 1469-1477.

Barber, M.N., Sampey, D.B., Widdop, R.E. 1999. AT(2) receptor stimulation enhances antihypertensive effect of AT(1) receptor antagonist in hypertensive rats. Hypertension 34, 1112-1116.

Bayorh, M.A., Eatman, D., Walton, M., Socci, R.R., Thierry-Palmer, M., Emmett, N. 2002. 1A-779 attenuates angiotensin-(1-7) depressor response in salt-induced hypertensive rats. Peptides 23, 57-64.

Bernobich, E., de Angelis, L., Lerin, C., Bellini, G. 2002. The role of the angiotensin system in cardiac glucose homeostasis: therapeutic implications. Drugs 62, 1295-1314.

Berridge, M.J. 1987. Inositol trisphosphate and diacylglycerol: two interacting second messengers. Annu Rev Biochem 56, 159-193.

Bhat, G.J., Thekkumkara, T.J., Thomas, W.G., Conrad, K.M., Baker, K.M. 1994. Angiotensin II stimulates sis-inducing factor-like DNA binding activity. Evidence that the AT1A receptor activates transcription factor-Stat91 and/or a related protein. J Biol Chem 269, 31443-31449.

Bhat, G.J., Thekkumkara, T.J., Thomas, W.G., Conrad, K.M., Baker, K.M. 1995. Activation of the STAT pathway by angiotensin II in T3CHO/AT1A cells. Cross-talk between angiotensin II and interleukin-6 nuclear signaling. J Biol Chem 270, 19059-19065.

Brenner, B.M., Cooper, M.E., de Zeeuw, D., Keane, W.F., Mitch, W.E., Parving, H.H., Remuzzi, G., Snapinn, S.M., Zhang, Z., Shahinfar, S. 2001. Effects of losartan on renal and cardiovascular outcomes in patients with type 2 diabetes and nephropathy. N Engl J Med 345, 861-869.

Brooks, V.L. 1995. Chronic infusion of angiotensin II resets baroreflex control of heart rate by an arterial pressure-independent mechanism. Hypertension 26, 420-424.

Brooks, V.L., Hatton, D.C. 1997. Chronic ANG II infusion and reflex control of norepinephrine and corticosterone in conscious rabbits. Am J Physiol 272, R487-496.

Bunnemann, B., Fuxe, K., Metzger, R., Mullins, J., Jackson, T.R., Hanley, M.R., Ganten, D. 1990. Autoradiographic localization of mas proto-oncogene mRNA in adult rat brain using in situ hybridization. Neurosci Lett 114, 147-153.

Bunnemann, B., Iwai, N., Metzger, R., Fuxe, K., Inagami, T., Ganten, D. 1992. The distribution of angiotensin II AT1 receptor subtype mRNA in the rat brain. Neurosci Lett 142, 155-158.

Burson, J.M., Aguilera, G., Gross, K.W., Sigmund, C.D. 1994. Differential expression of angiotensin receptor 1A and 1B in mouse. Am J Physiol 267, E260-267.

Campbell, D.J., Habener, J.F. 1986. Angiotensinogen gene is expressed and differentially regulated in multiple tissues of the rat. J Clin Invest 78, 31-39.

Cervenka, L., Wang, C.T., Navar, L.G. 1998. Effects of acute AT1 receptor blockade by candesartan on arterial pressure and renal function in rats. Am J Physiol 274, F940-945.

Chang, R.S., Lotti, V.J. 1991. Angiotensin receptor subtypes in rat, rabbit and monkey tissues: relative distribution and species dependency. Life Sci 49, 1485-1490.
Cherry, S.R., Gambhir, S.S. 2001. Use of positron emission tomography in animal research. ILAR J 42, 219-232.
Chiu, A.T., Dunscomb, J., Kosierowski, J., Burton, C.R., Santomenna, L.D., Corjay, M.H., Benfield, P. 1993. The ligand binding signatures of the rat AT1A, AT1B and the human AT1 receptors are essentially identical. Biochem Biophys Res Commun 197, 440-449.
Clark, A.J., Balla, T., Jones, M.R., Catt, K.J. 1992. Stimulation of early gene expression by angiotensin II in bovine adrenal glomerulosa cells: roles of calcium and protein kinase C. Mol Endocrinol 6, 1889-1898.
Cline, W.H., Jr. 1985. Enhanced in vivo responsiveness of presynaptic angiotensin II receptor-mediated facilitation of vascular adrenergic neurotransmission in spontaneously hypertensive rats. J Pharmacol Exp Ther 232, 661-669.
Collis, M.G., Keddie, J.R. 1981. Captopril attenuates adrenergic vasoconstriction in rat mesenteric arteries by angiotensin-dependent and -independent mechanisms. Clin Sci (Lond) 61, 281-286.
Danser, A.H., van Kats, J.P., Admiraal, P.J., Derkx, F.H., Lamers, J.M., Verdouw, P.D., Saxena, P.R., Schalekamp, M.A. 1994. Cardiac renin and angiotensins. Uptake from plasma versus in situ synthesis. Hypertension 24, 37-48.
Darnell, J.E., Jr., Kerr, I.M., Stark, G.R. 1994. Jak-STAT pathways and transcriptional activation in response to IFNs and other extracellular signaling proteins. Science 264, 1415-1421.
de Gasparo, M., Catt, K.J., Inagami, T., Wright, J.W., Unger, T. 2000. International union of pharmacology. XXIII. The angiotensin II receptors. Pharmacol Rev 52, 415-472.
DiBona, G.F. 2000. Nervous kidney. Interaction between renal sympathetic nerves and the renin-angiotensin system in the control of renal function. Hypertension 36, 1083-1088.
Dinh, D.T., Frauman, A.G., Johnston, C.I., Fabiani, M.E. 2001. Angiotensin receptors: distribution, signalling and function. Clin Sci (Lond) 100, 481-492.
Dostal, D.E. 2000. The cardiac renin-angiotensin system: novel signaling mechanisms related to cardiac growth and function. Regul Pept 91, 1-11.
Duke, L.M., Evans, R.G., Widdop, R.E. 2005. AT2 receptors contribute to acute blood pressure-lowering and vasodilator effects of AT1 receptor antagonism in conscious normotensive but not hypertensive rats. Am J Physiol Heart Circ Physiol 288, H2289-2297.
Dzau, V.J., Burt, D.W., Pratt, R.E. 1988. Molecular biology of the renin-angiotensin system. Am J Physiol 255, F563-573.
Dzau, V.J., Ingelfinger, J., Pratt, R.E., Ellison, K.E. 1986. Identification of renin and angiotensinogen messenger RNA sequences in mouse and rat brains. Hypertension 8, 544-548.
Dzau, V.J., Ingelfinger, J.R. 1989. Molecular biology and pathophysiology of the intrarenal renin-angiotensin system. J Hypertens Suppl 7, S3-8.
Eguchi, S., Matsumoto, T., Motley, E.D., Utsunomiya, H., Inagami, T. 1996. Identification of an essential signaling cascade for mitogen-activated protein

kinase activation by angiotensin II in cultured rat vascular smooth muscle cells. Possible requirement of Gq-mediated p21ras activation coupled to a Ca2+/calmodulin-sensitive tyrosine kinase. J Biol Chem 271, 14169-14175.

Eguchi, S., Numaguchi, K., Iwasaki, H., Matsumoto, T., Yamakawa, T., Utsunomiya, H., Motley, E.D., Kawakatsu, H., Owada, K.M., Hirata, Y., Marumo, F., Inagami, T. 1998. Calcium-dependent epidermal growth factor receptor transactivation mediates the angiotensin II-induced mitogen-activated protein kinase activation in vascular smooth muscle cells. J Biol Chem 273, 8890-8896.

Enayetallah, A.E., French, R.A., Thibodeau, M.S., Grant, D.F. 2004. Distribution of soluble epoxide hydrolase and of cytochrome P450 2C8, 2C9, and 2J2 in human tissues. J Histochem Cytochem 52, 447-454.

Fang, Y.H., Muzic, R.F., Jr. 2008. Spillover and partial-volume correction for image-derived input functions for small-animal 18F-FDG PET studies. J Nucl Med 49, 606-614.

Feller, P.A., Sodd, V.J. 1975. Dosimetry of four heart-imaging radionuclides: 43K, 81Rb, 129Cs, and 201Ti. J Nucl Med 16, 1070-1075.

Feng, Y.H., Noda, K., Saad, Y., Liu, X.P., Husain, A., Karnik, S.S. 1995. The docking of Arg2 of angiotensin II with Asp281 of AT1 receptor is essential for full agonism. J Biol Chem 270, 12846-12850.

Ferreira, A.J., Jacoby, B.A., Araujo, C.A., Macedo, F.A., Silva, G.A., Almeida, A.P., Caliari, M.V., Santos, R.A. 2007. The nonpeptide angiotensin-(1-7) receptor Mas agonist AVE-0991 attenuates heart failure induced by myocardial infarction. Am J Physiol Heart Circ Physiol 292, H1113-1119.

Fierens, F., Vanderheyden, P.M., De Backer, J.P., Vauquelin, G. 1999. Binding of the antagonist [3H]candesartan to angiotensin II AT1 receptor-transfected [correction of tranfected] Chinese hamster ovary cells. Eur J Pharmacol 367, 413-422.

Fierens, F.L., Vanderheyden, P.M., Gaborik, Z., Minh, T.L., Backer, J.P., Hunyady, L., Ijzerman, A., Vauquelin, G. 2000. Lys(199) mutation of the human angiotensin type 1 receptor differentially affects the binding of surmountable and insurmountable non-peptide antagonists. J Renin Angiotensin Aldosterone Syst 1, 283-288.

Fierens, F.L., Vanderheyden, P.M., Roggeman, C., Vande Gucht, P., De Backer, J.P., Vauquelin, G. 2002. Distinct binding properties of the AT(1) receptor antagonist [(3)H]candesartan to intact cells and membrane preparations. Biochem Pharmacol 63, 1273-1279.

Francis, J., Weiss, R.M., Wei, S.G., Johnson, A.K., Felder, R.B. 2001. Progression of heart failure after myocardial infarction in the rat. Am J Physiol Regul Integr Comp Physiol 281, R1734-1745.

Frank, G.D., Saito, S., Motley, E.D., Sasaki, T., Ohba, M., Kuroki, T., Inagami, T., Eguchi, S. 2002. Requirement of Ca(2+) and PKCdelta for Janus kinase 2 activation by angiotensin II: involvement of PYK2. Mol Endocrinol 16, 367-377.

Friedman, E.M., Irwin, M. 2001. Central CRH suppresses specific antibody responses: effects of beta-adrenoceptor antagonism and adrenalectomy. Brain Behav Immun 15, 65-77.

Fukushima, K., Xia, J., Lautamaki, R., Fox, J., Mathews, W.B., Szabo, Z., Bengel, F. 2009. Assessment of regional myocardial angiotensin II receptor upregulation

after myocardial infarction by PET. Abstract. Journal of Nuclear Medicine 50, 48P.

Gasc, J.M., Shanmugam, S., Sibony, M., Corvol, P. 1994. Tissue-specific expression of type 1 angiotensin II receptor subtypes. An in situ hybridization study. Hypertension 24, 531-537.

Gleiter, C.H., Jagle, C., Gresser, U., Morike, K. 2004. Candesartan. Cardiovasc Drug Rev 22, 263-284.

Gohlke, P., Kox, T., Jurgensen, T., von Kugelgen, S., Rascher, W., Unger, T., Culman, J. 2002a. Peripherally applied candesartan inhibits central responses to angiotensin II in conscious rats. Naunyn Schmiedebergs Arch Pharmacol 365, 477-483.

Gohlke, P., Von Kugelgen, S., Jurgensen, T., Kox, T., Rascher, W., Culman, J., Unger, T. 2002b. Effects of orally applied candesartan cilexetil on central responses to angiotensin II in conscious rats. J Hypertens 20, 909-918.

Gohlke, P., Weiss, S., Jansen, A., Wienen, W., Stangier, J., Rascher, W., Culman, J., Unger, T. 2001. AT1 receptor antagonist telmisartan administered peripherally inhibits central responses to angiotensin II in conscious rats. J Pharmacol Exp Ther 298, 62-70.

Griendling, K.K., Delafontaine, P., Rittenhouse, S.E., Gimbrone, M.A., Jr., Alexander, R.W. 1987. Correlation of receptor sequestration with sustained diacylglycerol accumulation in angiotensin II-stimulated cultured vascular smooth muscle cells. J Biol Chem 262, 14555-14562.

Griendling, K.K., Ushio-Fukai, M., Lassegue, B., Alexander, R.W. 1997. Angiotensin II signaling in vascular smooth muscle. New concepts. Hypertension 29, 366-373.

Gruden, G., Perin, P.C., Camussi, G. 2005. Insight on the pathogenesis of diabetic nephropathy from the study of podocyte and mesangial cell biology. Curr Diabetes Rev 1, 27-40.

Gunther, S., Gimbrone, M.A., Jr., Alexander, R.W. 1980. Regulation by angiotensin II of its receptors in resistance blood vessels. Nature 287, 230-232.

Guo, D.F., Inagami, T. 1994. Epidermal growth factor-enhanced human angiotensin II type 1 receptor. Hypertension 23, 1032-1035.

Gupta, S., Das, B., Sen, S. 2007. Cardiac hypertrophy: mechanisms and therapeutic opportunities. Antioxid Redox Signal 9, 623-652.

Hadizad, T., Kirkpatrick, S.A., Mason, S., Burns, K.D., Beanlands, R.S., DaSilva, J.N. in press. Novel O-[11C]Methylated Derivatives of Candesartan as Angiotensin II AT1 Receptor Imaging Ligands: Radiosynthesis and Ex Vivo Evaluation in Rats. Bioorganic and Medicinal Chemistry.

Hamill, T.G., Burns, H.D., Dannals, R.F., Mathews, W.B., Musachio, J.L., Ravert, H.T., Naylor, E.M. 1996. Development of [^{11}C]L-159,884: A Radiolabelled, Nonpeptide Angiotensin II Antagonist that is Useful for Angiotensin II, AT_1 Receptor Imaging. Appl. Radiat. Isot. 47, 221-218.

Hanatani, T., Fukuda, T., Ikeda, M., Imaoka, S., Hiroi, T., Funae, Y., Azuma, J. 2001. CYP2C9*3 influences the metabolism and the drug-interaction of candesartan in vitro. Pharmacogenomics J 1, 288-292.

Harrison-Bernard, L.M., Imig, J.D., Carmines, P.K. 2002. Renal AT1 receptor protein expression during the early stage of diabetes mellitus. Int J Exp Diabetes Res 3, 97-108.

Haywood, G.A., Gullestad, L., Katsuya, T., Hutchinson, H.G., Pratt, R.E., Horiuchi, M., Fowler, M.B. 1997. AT1 and AT2 angiotensin receptor gene expression in human heart failure. Circulation 95, 1201-1206.

Henriksen, E.J., Jacob, S., Kinnick, T.R., Teachey, M.K., Krekler, M. 2001. Selective angiotensin II receptor receptor antagonism reduces insulin resistance in obese Zucker rats. Hypertension 38, 884-890.

Hilton, J., Yokoi, F., Dannals, R.F., Ravert, H.T., Szabo, Z., Wong, D.F. 2000. Column-switching HPLC for the analysis of plasma in PET imaging studies. Nucl Med Biol 27, 627-630.

Hiranyachattada, S., Saetew, S., Harris, P.J. 2005. Acute effects of candesartan on rat renal haemodynamics and proximal tubular reabsorption. Clin Exp Pharmacol Physiol 32, 714-720.

Hjorth, S.A., Schambye, H.T., Greenlee, W.J., Schwartz, T.W. 1994. Identification of peptide binding residues in the extracellular domains of the AT1 receptor. J Biol Chem 269, 30953-30959.

Hume, S.P., Gunn, R.N., Jones, T. 1998. Pharmacological constraints associated with positron emission tomographic scanning of small laboratory animals. Eur J Nucl Med 25, 173-176.

Hunyady, L., Bor, M., Balla, T., Catt, K.J. 1994. Identification of a cytoplasmic Ser-Thr-Leu motif that determines agonist-induced internalization of the AT1 angiotensin receptor. J Biol Chem 269, 31378-31382.

Ichikawi, I., Harris, R.C. 1991. Angiotensin actions in the kidney: renewed insight into the old hormone. Kidney Int 40, 583-596.

ICRP. 1975. Report on the task group on reference man. Ann ICRP 4, iii.

ICRP. 1987. Radiation dose to patients from radiopharmaceuticals. A report of a Task Group of Committee 2 of the International Commission on Radiological Protection. Ann ICRP 18, 1-377.

ICRP. 1998. Radiation dose to patients from radiopharmaceuticals (addendum 2 to ICRP publication 53). Ann ICRP 28, 1-126.

Imaoka, S., Hashizume, T., Funae, Y. 2005. Localization of rat cytochrome P450 in various tissues and comparison of arachidonic acid metabolism by rat P450 with that by human P450 orthologs. Drug Metab Pharmacokinet 20, 478-484.

Israili, Z.H. 2000. Clinical pharmacokinetics of angiotensin II (AT1) receptor blockers in hypertension. J Hum Hypertens 14 Suppl 1, S73-86.

Jagoda, E.M., Vaquero, J.J., Seidel, J., Green, M.V., Eckelman, W.C. 2004. Experiment assessment of mass effects in the rat: implications for small animal PET imaging. Nucl Med Biol 31, 771-779.

Jessup, J.A., Brosnihan, K.B., Gallagher, P.E., Chappell, M.C., Ferrario, C.M. 2008. Differential Effect of Low Dose Thiazides on the Renin Angiotensin System in Genetically Hypertensive and Normotensive Rats. J Am Soc Hypertens 2, 106-115.

Kanagawa, R., Wada, T., Sanada, T., Ojima, M., Inada, Y. 1997. Regional hemodynamic effects of candesartan cilexetil (TCV-116), an angiotensin II AT1-receptor antagonist, in conscious spontaneously hypertensive rats. Jpn J Pharmacol 73, 185-190.

Kaufman, L.J., Vollmer, R.R. 1985. Endogenous angiotensin II facilitates sympathetically mediated hemodynamic responses in pithed rats. J Pharmacol Exp Ther 235, 128-134.

Kelly, M.P., Kahr, O., Aalkjaer, C., Cumin, F., Samani, N.J. 1997. Tissue expression of components of the renin-angiotensin system in experimental post-infarction heart failure in rats: effects of heart failure and angiotensin-converting enzyme inhibitor treatment. Clin. Sci. 92, 455-465.

Kenk, M., Greene, M., Lortie, M., Dekemp, R.A., Beanlands, R.S., Dasilva, J.N. 2008. Use of a column-switching high-performance liquid chromatography method to assess the presence of specific binding of (R)- and (S)-[(11)C]rolipram and their labeled metabolites to the phosphodiesterase-4 enzyme in rat plasma and tissues. Nucl Med Biol 35, 515-521.

Kenk, M., Greene, M., Thackeray, J., deKemp, R.A., Lortie, M., Thorn, S., Beanlands, R.S., DaSilva, J.N. 2007. In vivo selective binding of (R)-[11C]rolipram to phosphodiesterase-4 provides the basis for studying intracellular cAMP signaling in the myocardium and other peripheral tissues. Nucl Med Biol 34, 71-77.

Kifor, I., Dzau, V.J. 1987. Endothelial renin-angiotensin pathway: evidence for intracellular synthesis and secretion of angiotensins. Circ Res 60, 422-428.

Kim, S.E., Scheffel, U., Szabo, Z., Burns, H.D., Gibson, R.E., Ravert, H.T., Mathews, W.B., Hamill, T.G., Dannals, R.F. 1996. In vivo labeling of angiotensin II receptors with a carbon-11-labeled selective nonpeptide antagonist. J Nucl Med 37, 307-311.

Klose, T.S., Blaisdell, J.A., Goldstein, J.A. 1999. Gene structure of CYP2C8 and extrahepatic distribution of the human CYP2Cs. J Biochem Mol Toxicol 13, 289-295.

Kobayashi, M., Takagi, M., Fukumoto, K., Kato, R., Tanaka, K., Ueno, K. 2008. The effect of bucolome, a CYP2C9 inhibitor, on the pharmacokinetics of losartan. Drug Metab Pharmacokinet 23, 115-119.

Kostenis, E., Milligan, G., Christopoulos, A., Sanchez-Ferrer, C.F., Heringer-Walther, S., Sexton, P.M., Gembardt, F., Kellett, E., Martini, L., Vanderheyden, P., Schultheiss, H.P., Walther, T. 2005. G-protein-coupled receptor Mas is a physiological antagonist of the angiotensin II type 1 receptor. Circulation 111, 1806-1813.

Kubo, K., Kohara, Y., Imamiya, E., Sugiura, Y., Inada, Y., Furukawa, Y., Nishikawa, K., Naka, T. 1993a. Nonpeptide angiotensin II receptor antagonists. Synthesis and biological activity of benzimidazolecarboxylic acids. J Med Chem 36, 2182-2195.

Kubo, K., Kohara, Y., Yoshimura, Y., Inada, Y., Shibouta, Y., Furukawa, Y., Kato, T., Nishikawa, K., Naka, T. 1993b. Nonpeptide angiotensin II receptor antagonists. Synthesis and biological activity of potential prodrugs of benzimidazole-7-carboxylic acids. J Med Chem 36, 2343-2349.

Kudoh, A., Matsuki, A. 2000. Effects of angiotensin-converting enzyme inhibitors on glucose uptake. Hypertension 36, 239-244.

Lassegue, B., Alexander, R.W., Nickenig, G., Clark, M., Murphy, T.J., Griendling, K.K. 1995. Angiotensin II down-regulates the vascular smooth muscle AT1 receptor by transcriptional and post-transcriptional mechanisms: evidence for homologous and heterologous regulation. Mol Pharmacol 48, 601-609.

Lee, J., Kim, S., Jung, M., Oh, Y., Kim, S.W. 2002a. Altered expression of vascular natriuretic peptide receptors in experimental hypertensive rats. Clin Exp Pharmacol Physiol 29, 299-303.

Lee, J., Kim, S., Oh, Y., Ryu, S.Y., Kim, S.W. 2002b. Upregulation of vascular renin-angiotensin and endothelin systems in rats inhibited of nitric oxide synthesis. Pharmacol Res 46, 383-387.

Leenen, F.H.H., Skarda, V., Yuan, B., White, R. 1999. Changes in cardiac ANG II postmyocardial infarction in rats: effects of nephrectomy and ACE inhibitors. Am J Physiol Heart Circ Physiol 276, H317-325.

Lewis, E.J., Hunsicker, L.G., Bain, R.P., Rohde, R.D. 1993. The effect of angiotensin-converting-enzyme inhibition on diabetic nephropathy. The Collaborative Study Group. N Engl J Med 329, 1456-1462.

Liu, Y., Leri, A., Li, B., Wang, X., Cheng, W., Kajstura, J., Anversa, P. 1998. Angiotensin II stimulation in vitro induces hypertrophy of normal and postinfarcted ventricular myocytes. Circ Res 82, 1145-1159.

Lo, M., Liu, K.L., Lantelme, P., Sassard, J. 1995. Subtype 2 of angiotensin II receptors controls pressure-natriuresis in rats. J Clin Invest 95, 1394-1397.

Lohmeier, T.E. 2001. The sympathetic nervous system and long-term blood pressure regulation. Am J Hypertens 14, 147S-154S.

Lourenco, C.M., Houle, S., Wilson, A.A., DaSilva, J.N. 2001. Characterization of r-(11)C]rolipram for PET imaging of phosphodieterase-4: in vito binding, metabolism, and dosimetry studies in rats. Nucl Med Biol 28, 347-358.

Luigi Zinzani, P., Stefoni, V., Tani, M., Fanti, S., Musuraca, G., Castellucci, P., Marchi, E., Fina, M., Ambrosini, V., Pellegrini, C., Alinari, L., Derenzini, E., Montini, G., Broccoli, A., Bacci, F., Pileri, S., Baccarani, M. 2009. Role of [18F]Fluorodeoxyglucose Positron Emission Tomography Scan in the Follow-Up of Lymphoma. J Clin Oncol 27, 1781-1787.

Ma, B., Sherman, P.S., Moskwa, J.E., Koeppe, R.A., Kilbourn, M.R. 2004. Sensitivity of [11C]N-methylpyrrolidinyl benzilate ([11C]NMPYB) to endogenous acetylcholine: PET imaging vs tissue sampling methods. Nucl Med Biol 31, 393-397.

Macari, D., Whitebread, S., Cumin, F., De Gasparo, M., Levens, N. 1994. Renal actions of the angiotensin AT2 receptor ligands CGP 42112 and PD 123319 after blockade of the renin-angiotensin system. Eur J Pharmacol 259, 27-36.

Macrez, N., Morel, J.L., Kalkbrenner, F., Viard, P., Schultz, G., Mironneau, J. 1997. A betagamma dimer derived from G13 transduces the angiotensin AT1 receptor signal to stimulation of Ca2+ channels in rat portal vein myocytes. J Biol Chem 272, 23180-23185.

Makar, A.B., Tephly, T.R. 1976. Methanol poisoning in the folate-deficient rat. Nature 261, 715-716.

Marrero, M.B., Fulton, D., Stepp, D., Stern, D.M. 2004. Angiotensin II-induced insulin resistance and protein tyrosine phosphatases. Arterioscler Thromb Vasc Biol 24, 2009-2013.

Mathews, W.B., Yoo, S.E., Lee, S.H., Scheffel, U., Rauseo, P.A., Zober, T.G., Gocco, G., Sandberg, K., Ravert, H.T., Dannals, R.F., Szabo, Z. 2004. A novel

radioligand for imaging the AT(1) angiotensin receptor with PET. Nucl Med Biol 31, 571-574.

Matsoukas, J.M., Hondrelis, J., Keramida, M., Mavromoustakos, T., Makriyannis, A., Yamdagni, R., Wu, Q., Moore, G.J. 1994. Role of the NH2-terminal domain of angiotensin II (ANG II) and [Sar1]angiotensin II on conformation and activity. NMR evidence for aromatic ring clustering and peptide backbone folding compared with [des-1,2,3]angiotensin II. J Biol Chem 269, 5303-5312.

McWhinney, C.D., Dostal, D., Baker, K. 1998. Angiotensin II activates Stat5 through Jak2 kinase in cardiac myocytes. J Mol Cell Cardiol 30, 751-761.

Mento, P.F., Pica, M.E., Hilepo, J., Chang, J., Hirsch, L., Wilkes, B.M. 1998. Increased expression of glomerular AT1 receptors in rats with myocardial infarction. Am J Physiol 275, H1247-1253.

Mercure, C., Ramla, D., Garcia, R., Thibault, G., Deschepper, C.F., Reudelhuber, T.L. 1998. Evidence for intracellular generation of angiotensin II in rat juxtaglomerular cells. FEBS Lett 422, 395-399.

Mezzano, S., Droguett, A., Burgos, M.E., Ardiles, L.G., Flores, C.A., Aros, C.A., Caorsi, I., Vio, C.P., Ruiz-Ortega, M., Egido, J. 2003. Renin-angiotensin system activation and interstitial inflammation in human diabetic nephropathy. Kidney Int Suppl, S64-70.

Mimran, A., Alfaro, V. 2003. Candesartan: nephroprotective effects and treatment of diabetic nephropathy. Drugs Today (Barc) 39, 439-450.

Morsing, P. 1999. Candesartan: a new-generation angiotensin II AT1 receptor blocker: pharmacology, antihypertensive efficacy, renal function, and renoprotection. J Am Soc Nephrol 10 Suppl 11, S248-254.

Munzar, P., Goldberg, S.R. 1999. Noradrenergic modulation of the discriminative-stimulus effects of methamphetamine in rats. Psychopharmacology (Berl) 143, 293-301.

Murasawa, S., Matsubara, H., Urakami, M., Inada, M. 1993. Regulatory elements that mediate expression of the gene for the angiotensin II type 1a receptor for the rat. J Biol Chem 268, 26996-27003.

Naruse, M., Tanabe, A., Sato, A., Takagi, S., Tsuchiya, K., Imaki, T., Takano, K. 2002. Aldosterone breakthrough during angiotensin II receptor antagonist therapy in stroke-prone spontaneously hypertensive rats. Hypertension 40, 28-33.

Nickenig, G., Michaelsen, F., Muller, C., Berger, A., Vogel, T., Sachinidis, A., Vetter, H., Bohm, M. 2002. Destabilization of AT(1) receptor mRNA by calreticulin. Circ Res 90, 53-58.

Nickenig, G., Michaelsen, F., Muller, C., Vogel, T., Strehlow, K., Bohm, M. 2001. Post-transcriptional regulation of the AT1 receptor mRNA. Identification of the mRNA binding motif and functional characterization. FASEB J 15, 1490-1492.

Nickenig, G., Murphy, T.J. 1994. Down-regulation by growth factors of vascular smooth muscle angiotensin receptor gene expression. Mol Pharmacol 46, 653-659.

Nickenig, G., Murphy, T.J. 1996. Enhanced angiotensin receptor type 1 mRNA degradation and induction of polyribosomal mRNA binding proteins by angiotensin II in vascular smooth muscle cells. Mol Pharmacol 50, 743-751.

Nickenig, G., Roling, J., Strehlow, K., Schnabel, P., Bohm, M. 1998. Insulin induces upregulation of vascular AT1 receptor gene expression by posttranscriptional mechanisms. Circulation 98, 2453-2460.

Nickenig, G., Sachinidis, A., Michaelsen, F., Bohm, M., Seewald, S., Vetter, H. 1997. Upregulation of Vascular Angiotensin II Receptor Gene Expression by Low-Density Lipoprotein in Vascular Smooth Muscle Cells. Circulation 95, 473-478.

Nickenig, G., Strehlow, K., Wassmann, S., Baumer, A.T., Albory, K., Sauer, H., Bohm, M. 2000a. Differential effects of estrogen and progesterone on AT(1) receptor gene expression in vascular smooth muscle cells. Circulation 102, 1828-1833.

Nickenig, G., Wassmann, S., Bohm, M. 2000b. Regulation of the angiotensin AT1 receptor by hypercholesterolaemia. Diabetes Obes Metab 2, 223-228.

Nikiforovich, G.V., Kao, J.L., Plucinska, K., Zhang, W.J., Marshall, G.R. 1994. Conformational analysis of two cyclic analogs of angiotensin: implications for the biologically active conformation. Biochemistry 33, 3591-3598.

Nikiforovich, G.V., Marshall, G.R. 1993. Three-dimensional recognition requirements for angiotensin agonists: a novel solution for an old problem. Biochem Biophys Res Commun 195, 222-228.

Nishiyama, A., Fujisawa, Y., Fukui, T., Rahman, M., Kondo, N., Ogawa, Y., Fanzhu, L., Guoxing, Z., Kimura, S., Abe, Y. 2001. Role of Nitric Oxide in Regional Blood Flow in Angiotensin II-Induced Hypertensive Rats. Hypertension Research 24, 421-427.

Noda, K., Feng, Y.H., Liu, X.P., Saad, Y., Husain, A., Karnik, S.S. 1996. The active state of the AT1 angiotensin receptor is generated by angiotensin II induction. Biochemistry 35, 16435-16442.

Noda, K., Saad, Y., Karnik, S.S. 1995. Interaction of Phe8 of angiotensin II with Lys199 and His256 of AT1 receptor in agonist activation. J Biol Chem 270, 28511-28514.

Nossaman, B.D., Baber, S.R., Nazim, M.M., Detrolio, J.D., Kadowitz, P.J. 2007. Differential effects of losartan and candesartan on vasoconstrictor responses in the rat. Can J Physiol Pharmacol 85, 360-371.

Ogihara, T., Asano, T., Ando, K., Chiba, Y., Sakoda, H., Anai, M., Shojima, N., Ono, H., Onishi, Y., Fujishiro, M., Katagiri, H., Fukushima, Y., Kikuchi, M., Noguchi, N., Aburatani, H., Komuro, I., Fujita, T. 2002. Angiotensin II-induced insulin resistance is associated with enhanced insulin signaling. Hypertension 40, 872-879.

Okamura, T., Clemens, D.L., Inagami, T. 1981. Renin, angiotensins, and angiotensin-converting enzyme in neuroblastoma cells: evidence for intracellular formation of angiotensins. Proc Natl Acad Sci U S A 78, 6940-6943.

Okamura, T., Miyazaki, M., Inagami, T., Toda, N. 1986. Vascular renin-angiotensin system in two-kidney, one clip hypertensive rats. Hypertension 8, 560-565.

Oliveira, L., Costa-Neto, C.M., Nakaie, C.R., Schreier, S., Shimuta, S.I., Paiva, A.C. 2007. The angiotensin II AT1 receptor structure-activity correlations in the light of rhodopsin structure. Physiol Rev 87, 565-592.

Opie, L.H., Sack, M.N. 2001. Enhanced angiotensin II activity in heart failure: reevaluation of the counterregulatory hypothesis of receptor subtypes. Circ Res 88, 654-658.

Oppermann, M., Freedman, N.J., Alexander, R.W., Lefkowitz, R.J. 1996. Phosphorylation of the type 1A angiotensin II receptor by G protein-coupled receptor kinases and protein kinase C. J Biol Chem 271, 13266-13272.

Osborn, J.L., Camara, A.K. 1997. Renal neurogenic mediation of intracerebroventricular angiotensin II hypertension in rats raised on high sodium chloride diet. Hypertension 30, 331-336.

Otsuka, S., Sugano, M., Makino, N., Sawada, S., Hata, T., Niho, Y. 1998. Interaction of mRNAs for angiotensin II type 1 and type 2 receptors to vascular remodeling in spontaneously hypertensive rats. Hypertension 32, 467-472.

Ouali, R., Berthelon, M.C., Begeot, M., Saez, J.M. 1997. Angiotensin II receptor subtypes AT1 and AT2 are down-regulated by angiotensin II through AT1 receptor by different mechanisms. Endocrinology 138, 725-733.

Panisset, J.C., Bourdois, P. 1968. Effect of angiotensin on the response to noradrenaline and sympathetic nerve stimulation, and on 3H-noradrenaline uptake in cat mesenteric blood vessels. Can J Physiol Pharmacol 46, 125-131.

Perin, P.C., Maule, S., Quadri, R. 2001. Sympathetic nervous system, diabetes, and hypertension. Clin Exp Hypertens 23, 45-55.

Pfeffer, M.A., McMurray, J.J., Velazquez, E.J., Rouleau, J.L., Kober, L., Maggioni, A.P., Solomon, S.D., Swedberg, K., Van de Werf, F., White, H., Leimberger, J.D., Henis, M., Edwards, S., Zelenkofske, S., Sellers, M.A., Califf, R.M. 2003a. Valsartan, captopril, or both in myocardial infarction complicated by heart failure, left ventricular dysfunction, or both. N Engl J Med 349, 1893-1906.

Pfeffer, M.A., Swedberg, K., Granger, C.B., Held, P., McMurray, J.J., Michelson, E.L., Olofsson, B., Ostergren, J., Yusuf, S., Pocock, S. 2003b. Effects of candesartan on mortality and morbidity in patients with chronic heart failure: the CHARM-Overall programme. Lancet 362, 759-766.

Phillips, M.I., Speakman, E.A., Kimura, B. 1993. Levels of angiotensin and molecular biology of the tissue renin angiotensin systems. Regul Pept 43, 1-20.

Pierson, M.E., Freer, R.J. 1992. Analysis of the active conformation of angiotensin II: a comparison of AII and non-peptide AII antagonists. Pept Res 5, 102-105.

Re, R.N. 1987. Cellular mechanisms of growth in cardiovascular tissue. Am J Cardiol 60, 104I-109I.

Regitz-Zagrosek, V., Fielitz, J., Dreysse, R., Hildebrandt, A.G., Fleck, E. 1997. Angiotensin receptor type 1 mRNA in human right ventricular endomyocardial biopsies: downregulation in heart failure. Cardiovasc Res 35, 99-105.

Regitz-Zagrosek, V., Fielitz, J., Fleck, E. 1998. Myocardial angiotensin receptors in human hearts. Basic Res Cardiol 93 Suppl 2, 37-42.

Reid, I.A. 1992. Interactions between ANG II, sympathetic nervous system, and baroreceptor reflexes in regulation of blood pressure. Am J Physiol 262, E763-778.

Reja, V., Goodchild, A.K., Phillips, J.K., Pilowsky, P.M. 2006. Upregulation of angiotensin AT1 receptor and intracellular kinase gene expression in hypertensive rats. Clin Exp Pharmacol Physiol 33, 690-695.

Remuzzi, A., Perico, N., Amuchastegui, C.S., Malanchini, B., Mazerska, M., Battaglia, C., Bertani, T., Remuzzi, G. 1993. Short- and long-term effect of angiotensin II receptor blockade in rats with experimental diabetes. J Am Soc Nephrol 4, 40-49.

Reuter, H., Adam, C., Gronke, S., Zobel, C., Frank, K.F., Muller-Ehmsen, J., Brabender, J., Schwinger, R.H. 2006. The increased angiotensin II (type 1) receptor density in myocardium of type 2 diabetic patients is prevented by blockade of the renin-angiotensin system. Diabetologia 49, 3067-3074.

Ribeiro, M.J., Ricard, M., Lievre, M.A., Bourgeois, S., Emond, P., Gervais, P., Dolle, F., Syrota, A. 2007. Whole-body distribution and radiation dosimetry of the dopamine transporter radioligand [(11)C]PE2I in healthy volunteers. Nucl Med Biol 34, 465-470.

Richer, C., Fornes, P., Cazaubon, C., Domergue, V., Nisato, D., Giudicelli, J.F. 1999a. Effects of long-term angiotensin II AT1 receptor blockade on survival, hemodynamics and cardiac remodeling in chronic heart failure in rats. Cardiovasc Res 41, 100-108.

Richer, C., Fornes, P., Domergue, V., De Gasparo, M., Giudicelli, J.F. 2001. Combined angiotensin II AT1-receptor blockade and angiotensin I-converting enzyme inhibition on survival and cardiac remodeling in chronic heart failure in rats. J Card Fail 7, 269-276.

Richer, C., Gervais, M., Fornes, P., Giudicelli, J.F. 1999b. Combined selective angiotensin II AT1-receptor blockade and angiotensin I-converting enzyme inhibition on coronary flow reserve in postischemic heart failure in rats. J Cardiovasc Pharmacol 34, 772-781.

Robertson, J.I.S., Nicholls, M.G. 1992. Renin-Angiotensin System Gower Medical Publishing, London, 2 v. ([1200] p.).

Roe, O. 1955. The metabolism and toxicity of methanol. Pharmacol Rev 7, 399-412.

Sadoshima, J., Qiu, Z., Morgan, J.P., Izumo, S. 1995. Angiotensin II and other hypertrophic stimuli mediated by G protein-coupled receptors activate tyrosine kinase, mitogen-activated protein kinase, and 90-kD S6 kinase in cardiac myocytes. The critical role of Ca(2+)-dependent signaling. Circ Res 76, 1-15.

Sandberg, K. 1994. Structural analysis and regulation of angiotensin II receptors. Trends Endocrinol Metab 5, 28-35.

Sayeski, P.P., Ali, M.S., Semeniuk, D.J., Doan, T.N., Bernstein, K.E. 1998. Angiotensin II signal transduction pathways. Regul Pept 78, 19-29.

Schindler, C., Darnell, J.E., Jr. 1995. Transcriptional responses to polypeptide ligands: the JAK-STAT pathway. Annu Rev Biochem 64, 621-651.

Schlaepfer, D.D., Jones, K.C., Hunter, T. 1998. Multiple Grb2-mediated integrin-stimulated signaling pathways to ERK2/mitogen-activated protein kinase: summation of both c-Src- and focal adhesion kinase-initiated tyrosine phosphorylation events. Mol Cell Biol 18, 2571-2585.

Schmidt, B., Schieffer, B. 2003. Angiotensin II AT1 receptor antagonists. Clinical implications of active metabolites. J Med Chem 46, 2261-2270.

Seeland, U., Kouchi, I., Zolk, O., Jockenhovel, F., Itter, G., Linz, W., Bohm, M. 2003. Effects of diuretic treatment on cardiac and circulating RAS in chronic heart failure post-myocardial infarction in rats. Eur J Heart Fail 5, 241-246.

Shepherd, J.T., Vanhoutte, P.M. 1981. George E. Brown memorial lecture. Local modulation of adrenergic neurotransmission. Circulation 64, 655-666.

Shibouta, Y., Inada, Y., Ojima, M., Wada, T., Noda, M., Sanada, T., Kubo, K., Kohara, Y., Naka, T., Nishikawa, K. 1993. Pharmacological profile of a highly potent and

long-acting angiotensin II receptor antagonist, 2-ethoxy-1-[[2'-(1H-tetrazol-5-yl)biphenyl-4- yl]methyl]-1H-benzimidazole-7-carboxylic acid (CV-11974), and its prodrug, (+/-)-1-(cyclohexyloxycarbonyloxy)-ethyl 2-ethoxy-1-[[2'-(1H-tetrazol-5- yl)biphenyl-4-yl]methyl]-1H-benzimidazole-7-carboxylate (TCV-116). J Pharmacol Exp Ther 266, 114-120.

Singh, R., Singh, A.K., Alavi, N., Leehey, D.J. 2003. Mechanism of increased angiotensin II levels in glomerular mesangial cells cultured in high glucose. J Am Soc Nephrol 14, 873-880.

Solomon, S.D., Skali, H., Bourgoun, M., Fang, J., Ghali, J.K., Martelet, M., Wojciechowski, D., Ansmite, B., Skards, J., Laks, T., Henry, D., Packer, M., Pfeffer, M.A. 2005. Effect of angiotensin-converting enzyme or vasopeptidase inhibition on ventricular size and function in patients with heart failure: the Omapatrilat Versus Enalapril Randomized Trial of Utility in Reducing Events (OVERTURE) echocardiographic study. Am Heart J 150, 257-262.

Song, K., Kurobe, Y., Kanehara, H., Wada, T., Inada, Y., Nishikawa, K., Miyazaki, M. 1995. Mapping of angiotensin II receptor subtypes in peripheral tissues of spontaneously hypertensive rats by in vitro autoradiography. Clin Exp Pharmacol Physiol Suppl 22, S17-19.

Stabin, M.G., Tagesson, M., Thomas, S.R., Ljungberg, M., Strand, S.E. 1999. Radiation dosimetry in nuclear medicine. Appl Radiat Isot 50, 73-87.

Starke, K., Werner, U., Hellerforth, R., Schumann, H.J. 1970. Influence of peptides on the output of noradrenaline from isolated rabbit hearts. Eur J Pharmacol 9, 136-140.

Staufenberger, S., Jacobs, M., Brandstatter, K., Hafner, M., Regitz-Zagrosek, V., Ertl, G., Schorb, W. 2001. Angiotensin II type 1 receptor regulation and differential trophic effects on rat cardiac myofibroblasts after acute myocardial infarction. J Cell Physiol 187, 326-335.

Stornetta, R.L., Hawelu-Johnson, C.L., Guyenet, P.G., Lynch, K.R. 1988. Astrocytes synthesize angiotensinogen in brain. Science 242, 1444-1446.

Sun, C.K., Chang, L.T., Sheu, J.J., Wang, C.Y., Youssef, A.A., Wu, C.J., Chua, S., Yip, H.K. 2007. Losartan Preserves Integrity of Cardiac Gap Junctions and PGC-1 alpha Gene Expression and Prevents Cellular Apoptosis in Remote Area of Left Ventricular Myocardium Following Acute Myocardial Infarction. Int Heart J 48, 533-546.

Suzuki, H., Motley, E.D., Frank, G.D., Utsunomiya, H., Eguchi, S. 2005. Recent progress in signal transduction research of the angiotensin II type-1 receptor: protein kinases, vascular dysfunction and structural requirement. Curr Med Chem Cardiovasc Hematol Agents 3, 305-322.

Taavitsainen, P., Kiukaanniemi, K., Pelkonen, O. 2000. In vitro inhibition screening of human hepatic P450 enzymes by five angiotensin-II receptor antagonists. Eur J Clin Pharmacol 56, 135-140.

Takayanagi, R., Ohnaka, K., Sakai, Y., Nakao, R., Yanase, T., Haji, M., Inagami, T., Furuta, H., Gou, D.F., Nakamuta, M., et al. 1992. Molecular cloning, sequence analysis and expression of a cDNA encoding human type-1 angiotensin II receptor. Biochem Biophys Res Commun 183, 910-916.

Takishita, S., Muratani, H., Sesoko, S., Teruya, H., Tozawa, M., Fukiyama, K., Inada, Y. 1994. Short-term effects of angiotensin II blockade on renal blood flow and sympathetic activity in awake rats. Hypertension 24, 445-450.

Tan, J., Wang, H., Leenen, F.H. 2004. Increases in brain and cardiac AT1 receptor and ACE densities after myocardial infarct in rats. Am J Physiol Heart Circ Physiol 286, H1665-1671.

Thomas, W.G. 1999. Regulation of angiotensin II type 1 (AT1) receptor function. Regul Pept 79, 9-23.

Thomas, W.G., Motel, T.J., Kule, C.E., Karoor, V., Baker, K.M. 1998. Phosphorylation of the angiotensin II (AT1A) receptor carboxyl terminus: a role in receptor endocytosis. Mol Endocrinol 12, 1513-1524.

Thomas, W.G., Thekkumkara, T.J., Motel, T.J., Baker, K.M. 1995. Stable expression of a truncated AT1A receptor in CHO-K1 cells. The carboxyl-terminal region directs agonist-induced internalization but not receptor signaling or desensitization. J Biol Chem 270, 207-213.

Turu, G., Szidonya, L., Gaborik, Z., Buday, L., Spat, A., Clark, A.J., Hunyady, L. 2006. Differential beta-arrestin binding of AT1 and AT2 angiotensin receptors. FEBS Lett 580, 41-45.

Ullian, M.E., Linas, S.L. 1989. Role of receptor cycling in the regulation of angiotensin II surface receptor number and angiotensin II uptake in rat vascular smooth muscle cells. J Clin Invest 84, 840-846.

Ullian, M.E., Webb, J.G., Chen, R., Paul, R.V., Morinelli, T.A. 2004. Mechanisms of vascular angiotensin II surface receptor regulation by epidermal growth factor. J Cell Physiol 200, 451-457.

Unger, T., Gohlke, P., Paul, M., Rettig, R. 1991. Tissue renin-angiotensin systems: fact or fiction? J Cardiovasc Pharmacol 18 Suppl 2, S20-25.

Ushio-Fukai, M., Alexander, R.W., Akers, M., Lyons, P.R., Lassegue, B., Griendling, K.K. 1999. Angiotensin II receptor coupling to phospholipase D is mediated by the betagamma subunits of heterotrimeric G proteins in vascular smooth muscle cells. Mol Pharmacol 55, 142-149.

Ushio-Fukai, M., Griendling, K.K., Akers, M., Lyons, P.R., Alexander, R.W. 1998. Temporal dispersion of activation of phospholipase C-beta1 and -gamma isoforms by angiotensin II in vascular smooth muscle cells. Role of alphaq/11, alpha12, and beta gamma G protein subunits. J Biol Chem 273, 19772-19777.

Vallega, G.A., Canessa, M.L., Berk, B.C., Brock, T.A., Alexander, R.W. 1988. Vascular smooth muscle Na+-H+ exchanger kinetics and its activation by angiotensin II. Am J Physiol 254, C751-758.

van den Hoff, J. 2005. Principles of quantitative positron emission tomography. Amino Acids 29, 341-353.

van Kats, J.P., de Lannoy, L.M., Jan Danser, A.H., van Meegen, J.R., Verdouw, P.D., Schalekamp, M.A. 1997. Angiotensin II type 1 (AT1) receptor-mediated accumulation of angiotensin II in tissues and its intracellular half-life in vivo. Hypertension 30, 42-49.

van Lier, J.J., van Heiningen, P.N., Sunzel, M. 1997. Absorption, metabolism and excretion of 14C-candesartan and 14C-candesartan cilexetil in healthy volunteers. J Hum Hypertens 11 Suppl 2, S27-28.

Vanderheyden, P.M., Fierens, F.L., De Backer, J.P., Fraeyman, N., Vauquelin, G. 1999. Distinction between surmountable and insurmountable selective AT1 receptor antagonists by use of CHO-K1 cells expressing human angiotensin II AT1 receptors. Br J Pharmacol 126, 1057-1065.

Vauquelin, G., Fierens, F., Van Liefde, I. 2006. Long-lasting angiotensin type 1 receptor binding and protection by candesartan: comparison with other biphenyl-tetrazole sartans. J Hypertens Suppl 24, S23-30.

Venema, R.C., Ju, H., Venema, V.J., Schieffer, B., Harp, J.B., Ling, B.N., Eaton, D.C., Marrero, M.B. 1998. Angiotensin II-induced association of phospholipase Cgamma1 with the G-protein-coupled AT1 receptor. J Biol Chem 273, 7703-7708.

Vidotti, D.B., Casarini, D.E., Cristovam, P.C., Leite, C.A., Schor, N., Boim, M.A. 2004. High glucose concentration stimulates intracellular renin activity and angiotensin II generation in rat mesangial cells. Am J Physiol Renal Physiol 286, F1039-1045.

von Bohlen und Halbach, O., Albrecht, D. 2006. The CNS renin-angiotensin system. Cell Tissue Res 326, 599-616.

Wagner, J., Gehlen, F., Ciechanowicz, A., Ritz, E. 1999. Angiotensin II receptor type 1 gene expression in human glomerulonephritis and diabetes mellitus. J Am Soc Nephrol 10, 545-551.

Wehbi, G.J., Zimpelmann, J., Carey, R.M., Levine, D.Z., Burns, K.D. 2001. Early streptozotocin-diabetes mellitus downregulates rat kidney AT2 receptors. Am J Physiol Renal Physiol 280, F254-265.

Wei, H., Ahn, S., Shenoy, S.K., Karnik, S.S., Hunyady, L., Luttrell, L.M., Lefkowitz, R.J. 2003. Independent beta-arrestin 2 and G protein-mediated pathways for angiotensin II activation of extracellular signal-regulated kinases 1 and 2. Proc Natl Acad Sci U S A 100, 10782-10787.

Wei, Y., Sowers, J.R., Nistala, R., Gong, H., Uptergrove, G.M., Clark, S.E., Morris, E.M., Szary, N., Manrique, C., Stump, C.S. 2006. Angiotensin II-induced NADPH oxidase activation impairs insulin signaling in skeletal muscle cells. J Biol Chem 281, 35137-35146.

Whiting, P., Nava, S., Mozley, L., Eastham, H., Poat, J. 1991. Expression of angiotensin converting enzyme mRNA in rat brain. Brain Res Mol Brain Res 11, 93-96.

Widdop, R.E., Gardiner, S.M., Kemp, P.A., Bennett, T. 1992. Inhibition of the haemodynamic effects of angiotensin II in conscious rats by AT2-receptor antagonists given after the AT1-receptor antagonist, EXP 3174. Br J Pharmacol 107, 873-880.

Wilson, A.A., Ginovart, N., Hussey, D., Meyer, J., Houle, S. 2002. In vitro and in vivo characterisation of [11C]-DASB: a probe for in vivo measurements of the serotonin transporter by positron emission tomography. Nucl Med Biol 29, 509-515.

Wolf, G., Chen, S., Ziyadeh, F.N. 2005. From the periphery of the glomerular capillary wall toward the center of disease: podocyte injury comes of age in diabetic nephropathy. Diabetes 54, 1626-1634.

Yamano, Y., Ohyama, K., Kikyo, M., Sano, T., Nakagomi, Y., Inoue, Y., Nakamura, N., Morishima, I., Guo, D.F., Hamakubo, T., et al. 1995. Mutagenesis and the

molecular modeling of the rat angiotensin II receptor (AT1). J Biol Chem 270, 14024-14030.

Yoshimura, Y., N. Tada, K. Kubo, M. Miyamoto, Y. Inada, K. Nishikawa, and T. Naka. 1994. Evaluation and improvement of bioavailability of a new angiotensin II receptor antagonist, 2-butyl-1-[2'-(1H-tetrazol-5-yl)biphenyl-4-yl]methyl-1H-benzimidazole-7-carboxylic acid by making prodrug. International Journal of Pharmaceutics 103, 1-7.

Young, D., O'Neill, K., Jessell, T., Wigler, M. 1988. Characterization of the rat mas oncogene and its high-level expression in the hippocampus and cerebral cortex of rat brain. Proc Natl Acad Sci U S A 85, 5339-5342.

Young, D., Waitches, G., Birchmeier, C., Fasano, O., Wigler, M. 1986. Isolation and characterization of a new cellular oncogene encoding a protein with multiple potential transmembrane domains. Cell 45, 711-719.

Zober, T.G., Mathews, W.B., Seckin, E., Yoo, S.E., Hilton, J., Xia, J., Sandberg, K., Ravert, H.T., Dannals, R.F., Szabo, Z. 2006. PET Imaging of the AT1 receptor with [11C]KR31173. Nucl Med Biol 33, 5-13.